IntechOpen

Flame Retardants

Edited by Fahmina Zafar and Eram Sharmin

FLAME RETARDANTS

Edited by **Fahmina Zafar** and **Eram Sharmin**

Flame Retardants
http://dx.doi.org/10.5772/intechopen.73636
Edited by Fahmina Zafar and Eram Sharmin

Contributors

Yichen Guo, Yuan Xue, Miriam Rafailovich, Layla Al-Omran, Fahmina Zafar, Eram Sharmin, Pierre Mertiny, Hamidreza Ahmadi Moghaddam

Notice

First published in London, United Kingdom, 2019 by IntechOpen
IntechOpen is the global imprint of INTECHOPEN LIMITED, registered in England and Wales, registration number: 11086078, The Shard, 25th floor, 32 London Bridge Street
London, SE19SG – United Kingdom
Printed in Croatia

British Library Cataloguing-in-Publication Data
A catalogue record for this book is available from the British Library

Additional hard and PDF copies can be obtained from orders@intechopen.com

Flame Retardants, Edited by Fahmina Zafar and Eram Sharmin
p. cm.
Print ISBN 978-1-78985-879-2
Online ISBN 978-1-78985-880-8
eBook (PDF) ISBN 978-1-83881-139-6

Meet the editors

Dr. Fahmina Zafar is a senior researcher working at the Department of Chemistry, Jamia Millia Islamia (JMI), New Delhi, India, under the Women Scientists Scheme for Research in Basic/Applied Sciences, DST, India. Dr. Zafar received her PhD and MSc degrees in Chemistry from JMI in 2006. She has worked as a postdoctoral fellow under UGC Kothari Postdoctoral Fellowship, as well as a scientist , research associate, and senior research fellow (Council of Scientific and Industrial Research) at the same department. She has more than 50 publications in peer-reviewed journals and books, and has presented over 40 research papers at national and international conferences. Her research work involves the development of bio-based polymers, metallopolymers, organic/inorganic hybrids, coordination polymers, and nanocomposites for the green environment in different fields, including adsorption, antimicrobials, and corrosion-protective applications.

Dr. Eram Sharmin is an assistant professor in the Department of Pharmaceutical Chemistry, College of Pharmacy, Umm Al-Qura University, Makkah, Saudi Arabia. She obtained her PhD degree in Chemistry from Jamia Millia Islamia (JMI) - A Central University, New Delhi, India, in 2007. She has previously worked as a senior research associate [Council of Scientific and Industrial Research (CSIR), New Delhi, India], a research associate (CSIR, New Delhi), and as a senior research fellow (CSIR, New Delhi) at the Materials Research Laboratory, Department of Chemistry, JMI. Dr. Sharmin has more than 50 publications in peer-reviewed journals and books, and has presented more than 30 research papers at national and international conferences. Her research interests include the development of “green” materials with applications such as antimicrobials and corrosion-resistant films, coatings, and packaging materials.

Contents

Preface XI

Section 1 Introduction 1

Chapter 1 **Introductory Chapter: Flame Retardants 3**
Eram Sharmin and Fahmina Zafar

Section 2 Properties 17

Chapter 2 **Physiochemical Properties and Environmental Levels of Legacy and Novel Brominated Flame Retardants 19**
Layla Salih Al-Omran

Section 3 Fire Retardant Polymer Nanocomposite 39

Chapter 3 **Flame Retardant Polymer Nanocomposites and Interfaces 41**
Yuan Xue, Yichen Guo* and Miriam H. Rafailovich

Section 4 Computational analysis 63

Chapter 4 **Stochastic Finite Element Modelling of Char Forming Filler Addition and Alignment – Effects on Heat Conduction into Polymer Condensed Phase 65**
Hamidreza Ahmadi Moghaddam and Pierre Mertiny

Preface

Flame Retardants has a significant meaning since flame retardants are one of the most important properties of materials for fire resistance and characterization of materials. The prevention and control of fire in different fields is a hot topic of research. Flame-retardant materials are used to reduce the risk of fire by decreasing the combustion rate and flame propagation in the presence of fire. Phosphorus, silicone, boron, nitrogen, and other miscellaneous elements containing materials or reactive monomers (petroleum or bio-based) possess inherent flame-retarding characteristics and they are used as halogen-free and green flame-retardant materials. They can be used on their own or added to develop materials to enhance flame retardancy. Moreover, nanoadditives/fillers such as graphite, carbon nanotubes, organoclay, and others have gained interest in improving the flammability of materials because of their small size when forming nanocomposites.

The book is divided into four sections. Section 1 consists of an introduction that focuses on the basic aspects of flame-retardant materials, types of fillers, and additives used. The introduction also discusses briefly bio-based flame retardants, while particular emphasis is given to the development of vegetable oil-based flame retardants and their applications. Section 2 is dedicated to physiochemical properties such as molecular weight, vapor pressure, octanol/air partitioning coefficient, octanol/water partition coefficient, water solubility, and organic carbon/water partitioning coefficient, all of which influence the distribution pattern of these contaminants in the environment. In addition, this section also provides an evaluation of the concentrations of these chemicals in various environmental media, such as indoor and outdoor air, indoor dust, soil and sediment, sewage sludge, biota and food, and human tissues. Section 3 focuses on thermoplastic polymers and their interactions with the surfaces of flame-retardant fillers; physical properties of nanocomposites such as mechanical properties, gas permeability, rheological performance, and thermal conductivity are also briefly reviewed along with flame retardancy. Section 4 includes computational analysis. The book will be useful for scientists and researchers interested in the field of fire control.

It has been a rewarding process for us to learn from all the contributing authors throughout the editing process and we would like to express appreciation to all them. Their dedication and enriching expertise have added value to this book and will definitely be appreciated by readers.

I would like to acknowledge the technical staff and Ms. Romina Skomersic, author service manager of Intech Open Access Publisher, for their remarkable efforts and coordination

with the editors and contributors. Many thanks to Professor Nahid Nishat and also to the Department of Science and Technology, New Delhi, India, for the Women Scientist Scheme (WOS) for Research in Basic/Applied Sciences.

Dr. Fahmina Zafar, PhD
Inorganic Materials Research Laboratory
Department of Chemistry
Jamia Millia Islamia
New Delhi, India

Dr. Eram Sharmin, PhD
Department of Pharmaceutical Chemistry
College of Pharmacy
Umm Al-Qura University
Makkah Al-Mukarramah, Saudi Arabia

Introduction

Chapter 1

Introductory Chapter: Flame Retardants

Eram Sharmin and Fahmina Zafar

Additional information is available at the end of the chapter

http://dx.doi.org/10.5772/intechopen.82783

1. Introduction

Fire is one of the greatest inventions of human beings, no doubt. However, if not managed cautiously, it may be deadly hazardous causing inestimable harm to life and property. Polymeric materials comprising of hydrocarbon chains are prone to burning when exposed to fire, releasing enormous heat, flame and smoke. With polymers all around us today, the great significance of fire/flame retardant materials [FiRs] in our lives can be judiciously realized. Polymers can be made fire/flame retardant [FiR] by the inclusion of micro- and nano- FiR fillers or by the incorporation of FiR compounds in their backbone. This review paper focuses on the basic aspects of FiR polymers such as their composition, types of fillers and additives used, and their applications. The review also discusses briefly about bio-based FiRs, while emphasis will be particularly made on the developments in the field of vegetable oil–based FiRs and their applications.

Polymers celebrate prominent place in our daily lives. The extensive uses of polymers also raise our concerns and requirements for fire safety, as the polymers are highly combustible, being mainly made up of carbon and hydrogen. When exposed to fire, polymers burn rapidly, releasing lot of heat and smoke, causing great damage to life and property. Thus, the use of FiRs has become mandatory from viewpoint of safety of life and environment. FiRs stop or inhibit the polymer combustion process, acting physically or chemically, by interfering with heating, pyrolysis, ignition, thermal degradation, i.e., various processes involved in polymer combustion. Thus, to improve FiR properties of polymers, it is very important to understand combustion which requires three main candidates: heat, oxygen and fuel (combusting material). When a substance is heated, its temperature rises to its pyrolysis temperature, and it produces char, liquid condensates and some gases (flammable and non-flammable). At still higher temperature, combustion temperature, these flammable gases produce large amount of light, heat and smoke on combining with oxygen (**Figure 1**).

The combustion cycle thus continues with the help of heat produced by combustion [1]. The disruption in this combustion cycle can cause flame retardancy, and can be achieved by the following mechanisms (**Figure 2**):

- incorporation of such materials in polymers that, on exposure to heat do not allow the temperature of material to rise to pyrolysis temperature,
- incorporation of materials that produce more non-flammable by-products and char during pyrolysis; the latter acts as an obstacle to heat and mass transfer between gas and condensed phase (condensed phase mechanism), and
- using FiRs that cause reduction in O_2 concentration in flame zone, by releasing non-flammable gases (gas phase mechanism).

FiRs comprise of additive FiRs, compounds (mineral fillers, hybrids) that are incorporated in polymers but they react with polymers only at higher temperatures, that is at the onset of fire, and reactive FiRs that are incorporated in polymer chains during synthesis.

There are many types of FiRs based on:

- minerals (oxides and hydroxides of metals, ex: magnesium hydroxide, aluminum hydroxide, calcium carbonate; borates, ex: zinc borates)
- halogens
- phosphorus
- silicon
- nitrogen
- nanoparticles

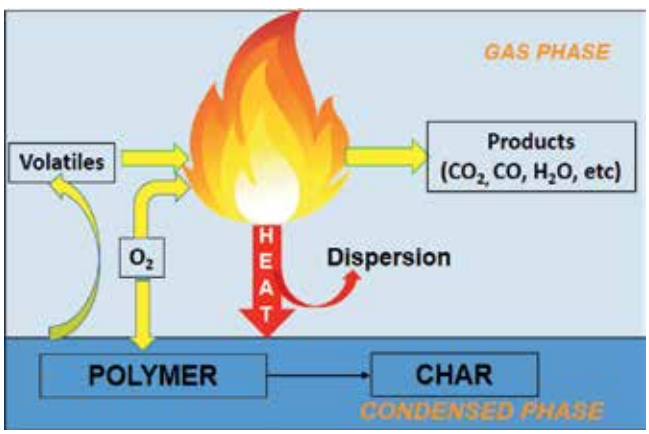

Figure 1. Combustion cycle.

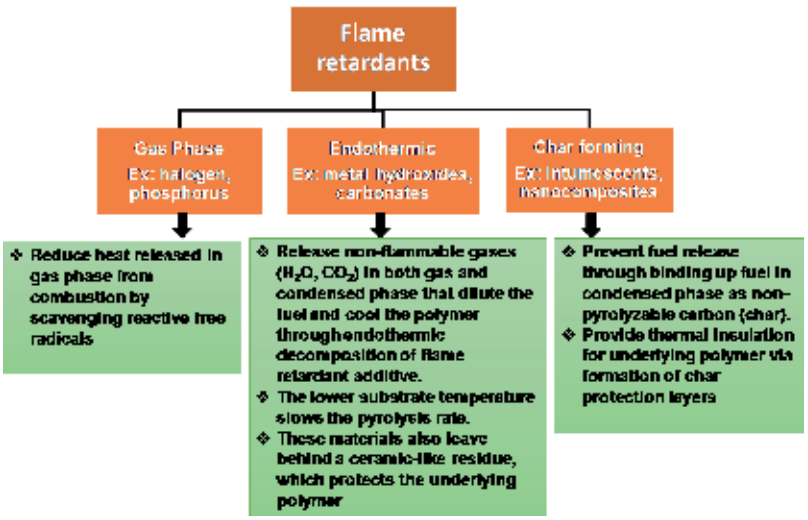

Figure 2. Types of FiRs and their mode of action.

Some examples of FiRs containing bromine and phosphorus are given in **Figures 3** and **4**.

Nanoparticles not only improve mechanical strength but also enhance flame retardance of polymers. These include nanoclays, carbon nanotubes, sepiolites, silsesquioxane, silica and titanium nanoparticles, nano metal oxides and others (**Figure 5**). **Figure 6** provides mechanism of flame retardance by nanoclays in a polymer composite. The selection of a particular nanoparticle as FiR, in polymer composite systems, depends upon its chemical structure and geometry.

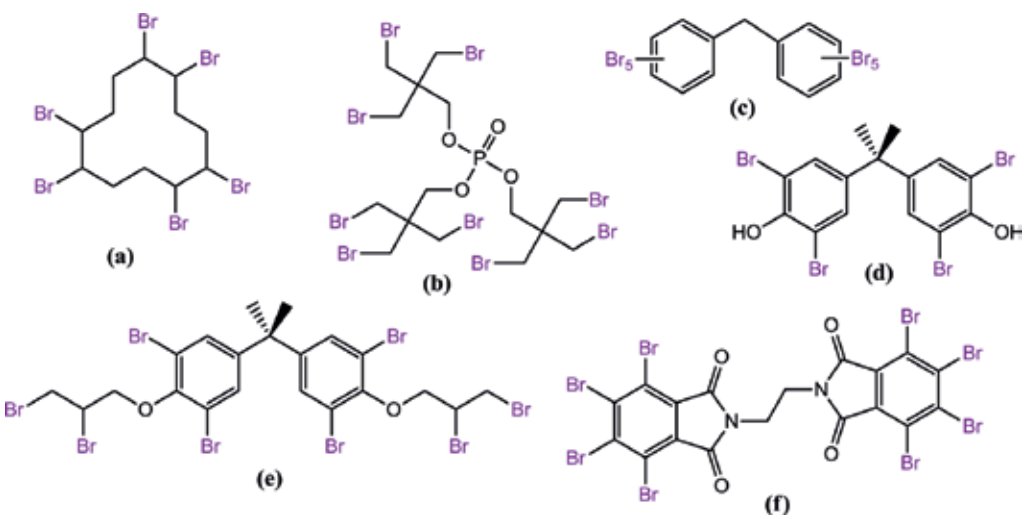

Figure 3. Bromine-based aliphatic and aromatic FiRs (a) hexabromocyclododecane, (b) tris (tribromoneopentyl) phosphate, (c) decabromodiphenyl ether, (d) tetrabromo bisphenol A, (e) bis (2–3-dibromopropylether) tetrabromo bisphenol A and (f) 1,2-ethylene bis (tetrabromophthalimide).

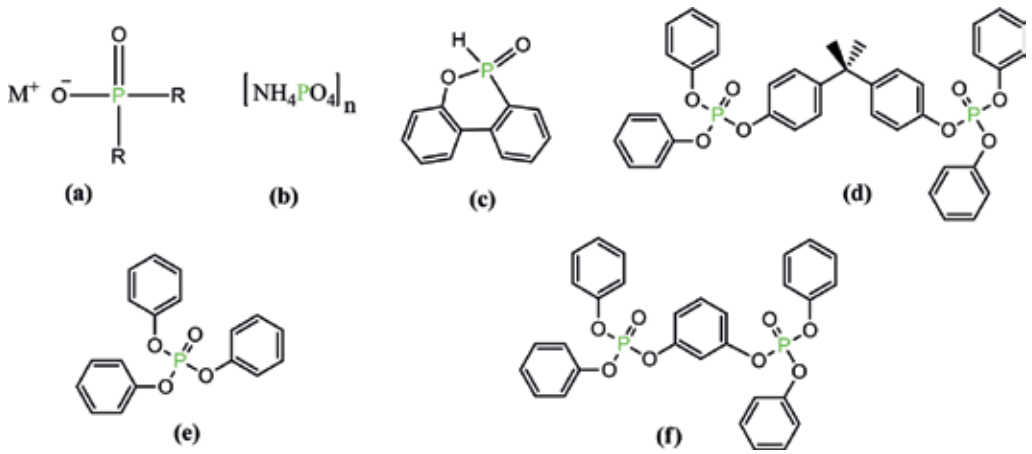

Figure 4. Phosphorus containing FiRs (a) phosphinate salts (M = Al, Zn, R = alkyl), (b) ammonium polyphosphate, (c) 9,10-dihydro-9-oxa-10-phosphaphenanthrene-10-oxide, (d) bisphenol A diphosphate, (e) triphenylphosphate and (f) resorcinol diphosphate.

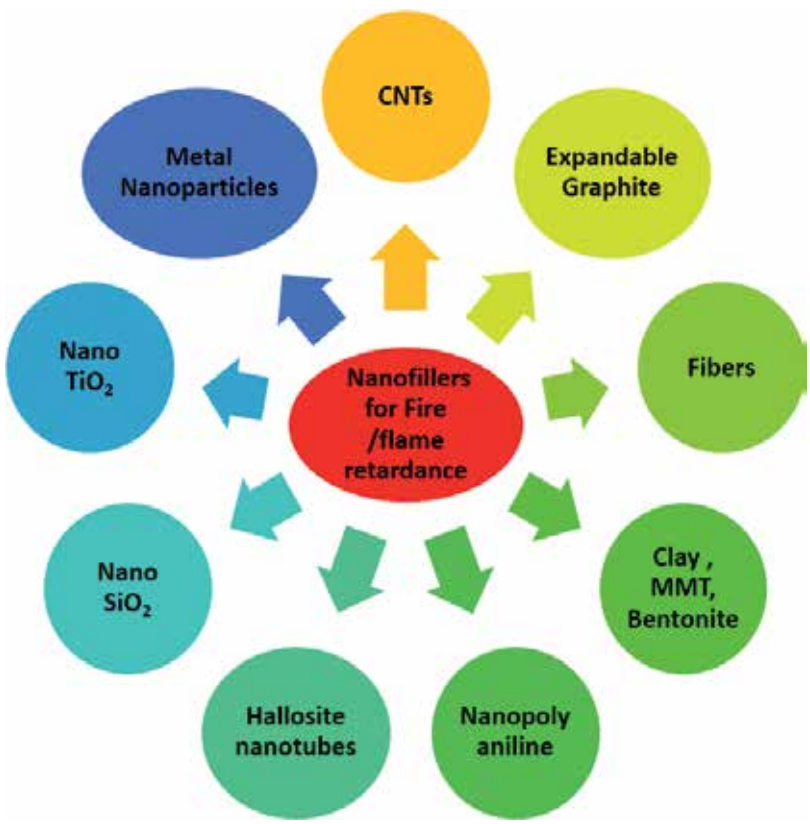

Figure 5. Some nanofillers used for fire/flame retardance.

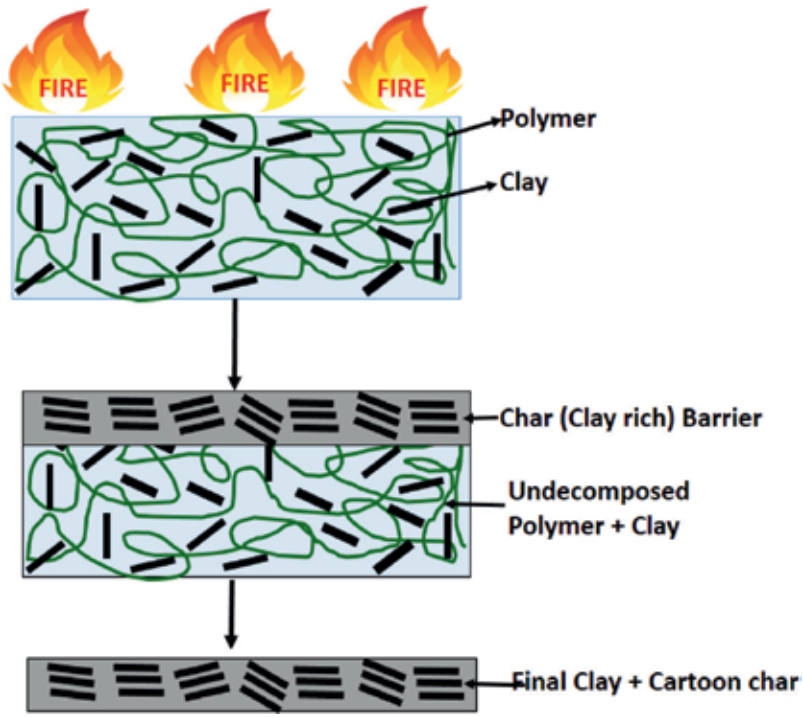

Figure 6. Mechanism of flame retardance by nanoclays.

FiRs are tested by UL 94 V, limited oxygen index, cone calorimeter, and other tests. Several prospects of FiRs have been described in detail in previously published reviews [1–3].

The strategies to improve fire/flame resistance are primarily governed by the nature and chemical structure of polymers, their mode of decomposition, fire safety level required and the performance of the polymer product. Today, our rising concerns towards human health and environment protection, together with the fire safety of life and property, have driven us to develop FiRs that are cost effective, less/non-toxic, environment-friendly and are conducive to optimum fire safety performance. Bio-based FiRs are ideal alternatives in this context, discussed briefly in following section.

2. Bio-based FiRs

Fast depleting petroleum resources, high prices of petro-based chemicals, health and environmental hazards caused by these, worldwide legislations and also ban on the use of some compounds have drastically influenced the world of polymer materials, so also FiRs. Thus it has become imperative to use bio-based resources in the field of FiRs. Biomolecules such as carbohydrates (cellulose, starch, chitosan, alginates), proteins, lipids (vegetable oils, cardanol) and phenolic compounds (lignin, tannin) can be used as such or can be derivatised to obtain bio-based

building blocks. The latter can be further modified to obtain FiRs, based on their chemical structure and inherent thermal properties. To assess the use of bio-based materials as FiRs, it is necessary to inspect their composition and thermal behavior. Apart from this, bio-based materials should meet some other criteria as well, to be used as FiRs, that is, (i) these materials should bear sufficiently high thermal stability in compliance with their processing, (ii) their charring ability should be high, (iii) they should bear functional groups such as hydroxyls, carboxylic acids, amines, double bonds and others, that may undergo chemical transformations, and (iv) there should be inclusion of elements (P, N, Si) that are capable of introducing flame retardancy. Bio-based materials can be used by themselves as an ideal component of FiRs, or in combination with traditional FiRs such as P, N or with melamine, boric acid and also by chemical modifications.

2.1. Why biomolecules mentioned above are used in the field of FiRs?

Lignin is used as an additive to increase the fire retardance of polymers. At high temperatures, it gives the highest char yield. This char residue slows down combustion as it forms a protective layer. Lignin has been used in combination with boric acid, melamine, aluminum phosphate, urea and other FiRs. Proteins and deoxyribonucleic acid [DNA] are used in the field as both contain important elements, N and P, showing flame retardance. Both are capable to form films over textiles. The protein coating increases the burning time and slows down the burning rate. DNA, a natural intumescent FiR, contains C, N and P. Carbohydrates are used as charring agents as they contain oxygen. Starch is used as matrix and also as FiR coating in textiles through layer-by-layer technique. Chitosan as a carbon source is also used as FiR in textile coating by layer-by-layer technique. This technique improves FiR ability of the coated fabrics by declining their thermal decomposition and decreasing their burning time. Lipids such as fatty acids, vegetable oils, cardanol and others are also used as FiRs. Phosphorylation is the most frequently used method to introduce fire retardance in bio-based materials. Chitosan, lignin, vegetable oils, cardanol, and others have successfully undergone phosphorylation.

Past years have witnessed great research and development in this field. Several fire protection solutions have cropped up utilizing bio-based resources and complying with "Green Chemistry" principles. However, even with gigantic number of solutions available, it is not easy to assess which one is the most successful. In this context what should significantly be kept in mind is (i) overall performance of FiRs, (ii) environmental and health hazards associated with their processing, formulation and application, and (iii) cost effectiveness of raw materials used and processes involved. Vegetable oils [VO] are domestically abundant, cost-effective and non-toxic. They contain several functional groups that can be tailor-made by different chemical transformations through "greener" methods for different applications such as FiRs.

3. Vegetable oil based FiRs

VO can be modified by P, Si, halogens such as chlorine and bromine, to be used as FiRs. Such VO derivatives can be used as plasticizers for PVC (**Figure 7**). During thermal degradation, they provide carbon and acid sources that enhance flame retardancy by promoting char residue formation [4].

http://dx.doi.org/10.5772/intechopen.82783

Figure 7. Phosphorus containing VO based derivatives, where (a-c) 9, 10-Dihydro-9-oxa-10-phosphaphenenthrene-10-oxide groups containing soybean oil based derivatives, (d-e) diphenyl phosphine oxide containing sunflower oil based derivatives, (f-g) cashew nut shell liquid based derivatives, and (h-j) diethyl phosphate and chlorinated phosphate derivatives of castor oil [4].

In the synthesis of FiR polymers from VO, the advantage is taken of the presence of functional groups in VO such as double bonds, hydroxyl and ester groups which undergo derivatization reactions such as epoxidation, esterification, urethanation, alcoholysis and others (**Figure 8**). The inserted epoxide, ester, urethane groups or the alcoholyzed products are then modified accordingly by phosphorylation, silylation, boronation, halogenation and others resulting in FiRs [5]. The polymerization on double bonds can also be done by using styrene, divinyl benzene, dicyclopentadiene, and norbornadiene. Soybean and sunflower oils were reacted with acrylic acid and N-bromosuccinimide. The bromoacrylated products were then copolymerized with styrene, and this resulted in the formation of rigid FiR polymer [6, 7]. Bromine containing FiRs release hydrogen bromide during combustion, causing toxicity and corrosion. Therefore, P, Si and B containing polymers are significantly popular relative to those containing halogen because the combustion products they produce are non-toxic, while the latter release corrosives, pollute environment, erode instruments and are hazardous to human health.

VO derivatives have also shown dual behavior as they render flame retardancy and also plasticizing effect to polyvinyl chloride (PVC) materials, which find wide applications in packaging, pipes, toys, wire and cable. PVC materials show excellent mechanical and physical properties, not in neat form, but when combined with plasticizers, such as dioctyl phthalate [DOP] and dibutyl phthalate. However, there are disadvantages associated with the use of these plasticizers with PVC, such as diffusion of these plasticizers into surroundings, deterioration in the performance of PVC materials due to loss of plasticizers, and often being

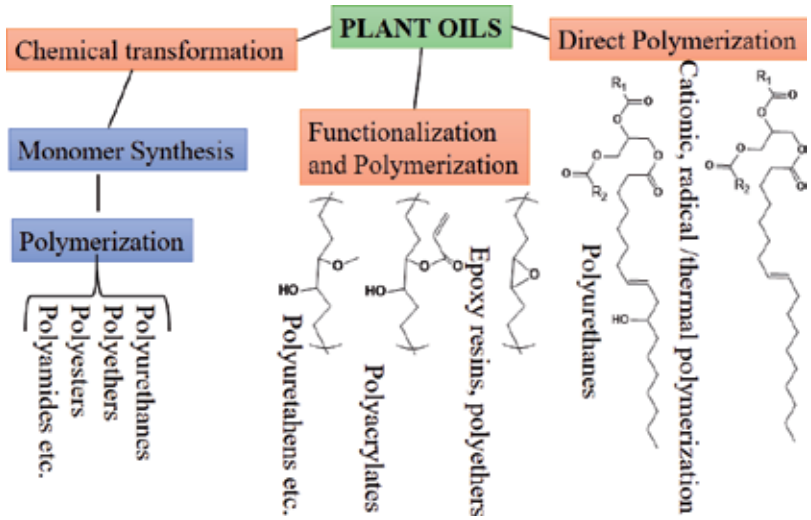

Figure 8. Chemical routes to produce VO derivatives [5].

susceptible to burning easily. The latter restricts their application in wire and cable that demand FiR properties. Thus, bio-based plasticizers that improve mechanical properties and flame retardancy (by supplying acid, carbon and gas source during thermal degradation of PVC materials) are welcomed [8–10].

VO-based FiRs and FiR plasticizers are prepared by different chemical transformations as mentioned above. Some of these have been discussed briefly in following sections:

By epoxidation: Epoxidation is carried out at the double bonds of VO. Epoxidized VO, followed by further derivatization such as ring opening of oxirane forming polyols, and also urethanation, produce FiRs. Castor oil [CO] was esterified at hydroxyl groups and then epoxidized at unsaturation producing epoxidized CO polyol ester, and the latter was treated with phosphorus oxychloride forming chloro phosphate ester of CO [ClPECO]. ClPECO was substituted in place of 50 wt% DOP for plasticizing PVC. ClPECO and DOP were blended with PVC in different ratio producing PVC films that showed high limited oxygen index [LOI] and improved thermal stability. During thermal degradation, the fatty acid chains of CO in ClPECO provided carbon source and the generated phosphorus containing components promoted the formation of char residual. Thus ClPECO improved plasticization and also flame retardancy of PVC (**Figure 9**) [4, 8]. CO was epoxidized at double bond and then the inserted oxirane ring was modified with diethyl phosphate in presence of triphenylphosphine producing phosphate ester, which was blended with PVC. The plasticized PVC showed high Tg, improved thermal stability and high LOI values [11, 12]. Phosphorylated polyol polyurethanes [PU] were prepared by epoxidation of soybean oil followed by epoxide ring opening reaction with phosphoric acid, and the treatment of formed phosphorylated polyols with polymeric diphenylmethane diisocyanate [PMDI]. These PU showed flame retardancy same as commercial PU [13]. In another example, two types of polyols were prepared from rapeseed oil, one through epoxidation followed by ring opening reaction and the other one

http://dx.doi.org/10.5772/intechopen.82783

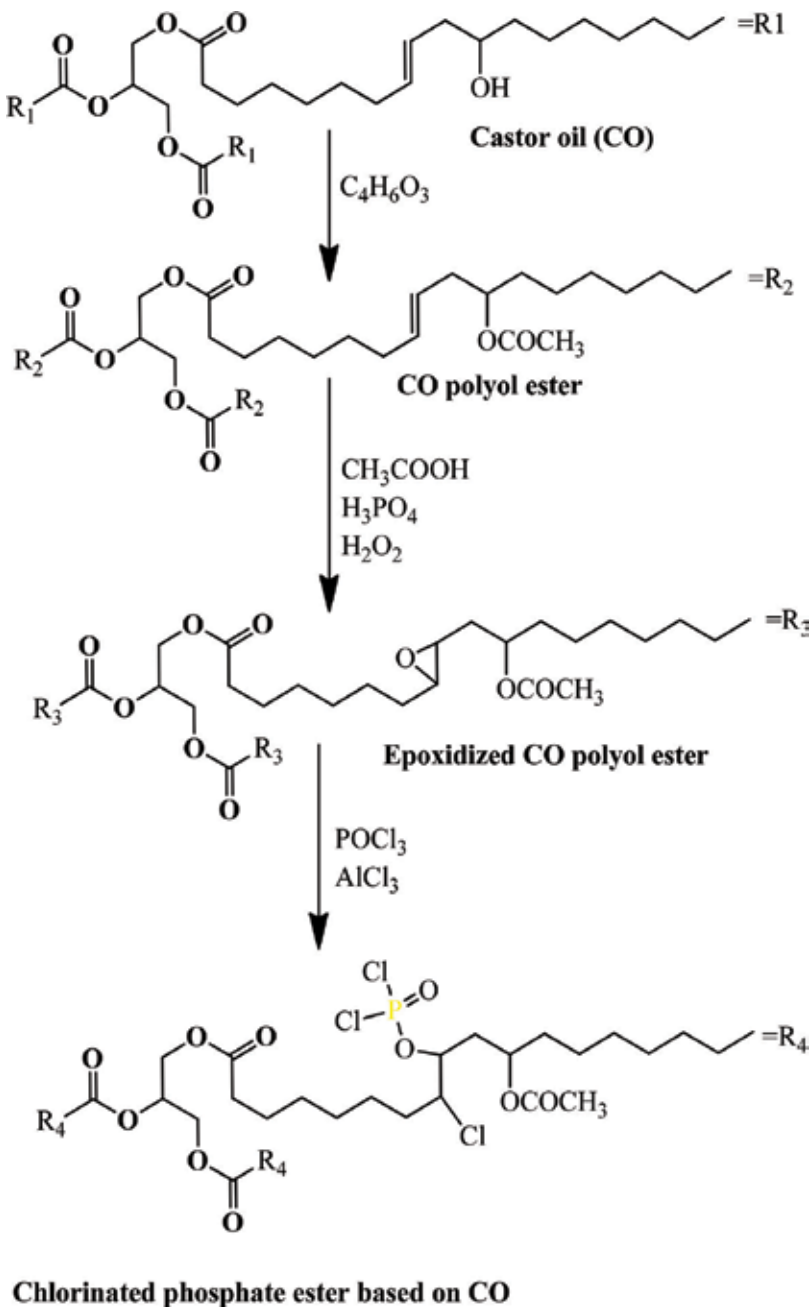

Figure 9. Phosphorus and halogen containing FiRs from castor oil [8].

by transesterification with triethanolamine. PU foams were prepared by replacing 70% of petrochemical polyols by each of these polyols, adding expandable graphite [EG] as filler and then these formulations were treated with PMDI forming two-component PU. EG has stacked layers which are intercalated with acids (sulfuric, nitric, and acetic). Under the influence of

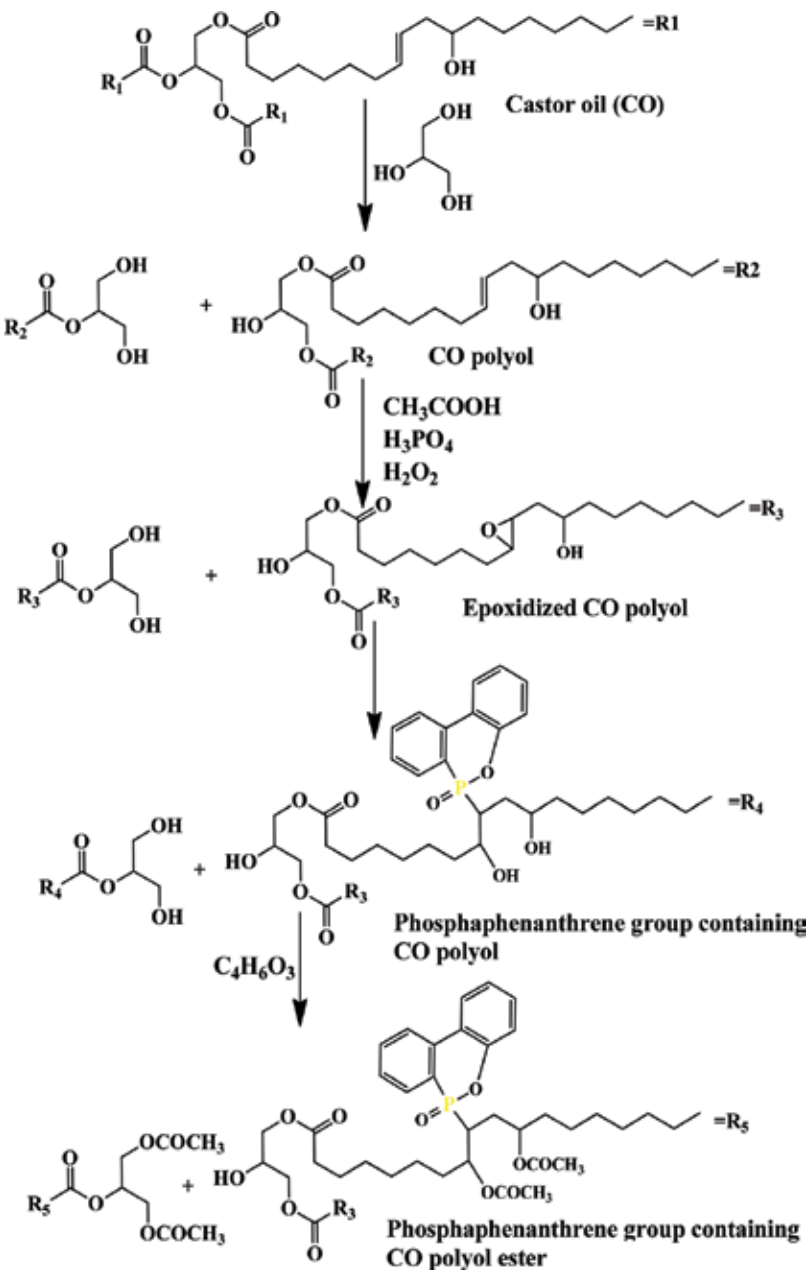

Figure 10. Phosphaphenanthrene containing FiR from castor oil [17].

high temperatures, EG reacts with acids releasing H_2O, CO_2, SO_2 gases that cause expansion of graphite that behaves as physical barrier for heat and mass transfer. EG modified PU foams were characterized by flammability test by cone calorimeter to determine certain parameters (time to ignition, heat release rate, peak of heat release rate, time to peak of heat release

rate, total smoke release, maximum average rate of heat emission), and by combustion and thermal stability analyses. The inclusion of EG into VO-based PU foam reduced flammability, prolonged the combustion time, increased the average burning temperature and rendered overall good thermal properties and flame resistance to VO-based PU foam [7]. In another approach, CO was epoxidized, and phosphaphenanthrene [PPP] groups were inserted on epoxidized CO by oxirane ring opening reaction. The hydroxyl groups of CO and hydroxyl groups formed during oxirane ring opening reaction were esterified in the next step. This CO polyester with PPP groups was blended with PVC (partially replacing DOP). The modified CO polyester improved thermal stability of PVC by promoting the formation of char residue. The thermal degradation of PPP groups produces phosphorus rich layers that prevent oxygen and heat transfer, rendering PVC more thermally stable and flame retardant. Long fatty acid chains of CO form a rigid char skeleton preventing char from collapsing [14].

By glycerolysis: Glycerolysis of CO was accomplished with glycerol, in presence of sodium methoxide and triethanolamine forming monoglyceride and diglyceride of CO [15, 16]. The latter were further epoxidized at double bonds, and the epoxy ring opening reaction with diethylphosphate resulted in the formation of P containing flame retardant polyol. The flame retardant polyol formed PU foams in one shot process with PMDI. Such PU foams were analyzed with thermogravimetric analysis, flammability tests and cone calorimetric measurement, which showed excellent fire resistance performance of these PU, with only 3% P incorporation, compared to pure PU [15]. In another attempt, glycerolyzed products of CO, monoglyceride and diglyceride, were epoxidized and PPP groups were inserted in CO mono- and diglycerides by epoxide ring opening reaction. The hydroxyl groups of CO and those formed by epoxide ring opening were further esterified and these PPP-containing CO polyols were used as plasticizer for PVC, partially replacing with DOP (**Figure 10**). Thus plasticized, PVC showed high LOI (35.95%) values, improved thermal stability and reduced flammability [17]. Monoglyceride obtained by glycerolysis of Nahar seed oil, epichlorohydrin, bisphenol A and tetrabromobisphenol A were reacted together in an alkaline medium and then nanoclay was incorporated in different weight percentages (1, 2.5, and 5 wt%). These nanocomposites showed high LOI values ranging from 40 to 45. Flame retardance of these nanocomposites is related to the incorporation of nanoclay that acts as thermal insulator and mass transport barrier during thermal decomposition of epoxy, and also promotes char formation [18].

Thus, VO can be modified in several ways for their applications as FiRs. With numerous types of nanoparticulate systems and synthesis methods cropping up and the advent of newer techniques of analyses of FiRs, there is immense scope for utilization of VO as "green" FiRs.

4. Summary

With the presence of polymers in every sphere of daily life, the use of FiRs poses greater safety, health and environment concerns, also keeping in mind the demands for non-toxicity, cost effectiveness, level of performance and degree of "greenness" of the final product. The polymer

matrices are extensively diverse, and therefore no strategy claims as an ideal solution of fire/flame retardance. The research still continues on the topic in the quest for better and yet better.

FiRs. To some extent, bio-based FiRs do fill the gap.

Acknowledgements

Dr. Fahmina Zafar is grateful to the Department of Science & Technology, New Delhi, India, for the research project under the Women Scientists' Scheme (WOS) for Research in Basic/Applied Sciences (Ref. No. SR/WOS-A/CS-97/2016). Dr Fahmina Zafar is also thankful to Prof. Nahid Nishat (Mentor), Inorganic Materials Research Lab, Department of Chemistry, Jamia Millia Islamia, for her kind support and the Head, Department of Chemistry, Jamia Millia Islamia, for providing facilities to carry out the research work.

Author details

Eram Sharmin[1] and Fahmina Zafar[2]*

*Address all correspondence to: fahmzafar@gmail.com

1 Department of Pharmaceutical Chemistry, College of Pharmacy, Umm Al-Qura University, Makkah Al-Mukarramah, Saudi Arabia

2 Inorganic Materials Research Laboratory, Department of Chemistry, Jamia Millia Islamia (A Central University), New Delhi, India

References

[1] Bar M, Alagirusamy R, Das A. Flame retardant polymer composites. Fibers and Polymers. 2015;**16**(4):705-717

[2] Laoutid F et al. New prospects in flame retardant polymer materials: From fundamentals to nanocomposites. Materials Science and Engineering: R: Reports. 2009;**63**(3):100-125

[3] Morgan AB, Gilman JW. An overview of flame retardancy of polymeric materials: Application, technology, and future directions. Fire and Materials. 2013;**37**(4):259-279

[4] Jia P et al. Phosphorus containing castor oil based derivatives: Potential non-migratory flame retardant plasticizer. European Polymer Journal. 2017;**87**:209-220

[5] Ronda JC et al. A renewable approach to thermosetting resins. Reactive and Functional Polymers. 2013;**73**(2):381-395

[6] Eren T, Küsefoğlu SH. Synthesis and polymerization of the bromoacrylated plant oil triglycerides to rigid, flame-retardant polymers. Journal of Applied Polymer Science. 2004;**91**(4):2700-2710

[7] Kurańska M et al. Bio-based polyurethane-polyisocyanurate composites with an intumescent flame retardant. Polymer Degradation and Stability. 2016;**127**:11-19

[8] Jia P et al. Effect of chlorinated phosphate ester based on castor oil on thermal degradation of poly (vinyl chloride) blends and its flame retardant mechanism as secondary plasticizer. RSC Advances. 2015;**5**(51):41169-41178

[9] Jia P et al. TG-FTIR and TG-MS analysis applied to study the flame retardancy of PVC–castor oil-based chlorinated phosphate ester blends. Journal of Thermal Analysis and Calorimetry. 2016;**124**(3):1331-1339

[10] Coltro L, Pitta JB, Madaleno E. Performance evaluation of new plasticizers for stretch PVC films. Polymer Testing. 2013;**32**(2):272-278

[11] Jia P et al. Synthesis, application, and flame-retardant mechanism of a novel phosphorus-containing plasticizer based on castor oil for polyvinyl chloride. Journal of Thermal Analysis and Calorimetry. 2015;**120**(3):1731-1740

[12] Jia P-Y et al. Synthesis of castor oil based plasticizers containing flame retarded group and their application in poly (vinyl chloride) as secondary plasticizer. Journal of Industrial and Engineering Chemistry. 2015;**28**:217-224

[13] Heinen M, Gerbase AE, Petzhold CL. Vegetable oil-based rigid polyurethanes and phosphorylated flame-retardants derived from epoxydized soybean oil. Polymer Degradation and Stability. 2014;**108**:76-86

[14] Jia P et al. Development of a vegetable oil based plasticizer for preparing flame retardant poly(vinyl chloride) materials. RSC Advances. 2015;**5**(93):76392-76400

[15] Zhang L et al. Synthesis of rigid polyurethane foams with castor oil-based flame retardant polyols. Industrial Crops and Products. 2014;**52**:380-388

[16] Zhang M et al. Study of the mechanical, thermal properties and flame retardancy of rigid polyurethane foams prepared from modified castor-oil-based polyols. Industrial Crops and Products. 2014;**59**:135-143

[17] Jia P et al. A composition of phosphaphenanthrene groups-containing castor-oil-based phosphate plasticizer for PVC: Synthesis, characterization and property. Journal of Industrial and Engineering Chemistry. 2018;**60**:192-205

[18] Das G, Karak N. Vegetable oil-based flame retardant epoxy/clay nanocomposites. Polymer Degradation and Stability. 2009;**94**(11):1948-1954

Properties

Chapter 2

Physiochemical Properties and Environmental Levels of Legacy and Novel Brominated Flame Retardants

Layla Salih Al-Omran

Additional information is available at the end of the chapter

http://dx.doi.org/10.5772/intechopen.79823

Abstract

Polybrominated diphenyl ethers (PBDEs) and 'novel' brominated flame retardants (NBFRs) are synthetic chemicals widely used in consumer products to enhance their ignition resistance. Since in most applications, these chemicals are used additively, they can transfer from such products into the environment. PBDEs have been classified as significant pollutants in the environment. Knowledge of PBDE and NBFR physicochemical properties provides information about their potential environmental fate and behaviour. This chapter highlights the most important physiochemical properties such as molecular weight, vapour pressure, octanol/air partitioning coefficient, octanol/water partition coefficient, water solubility and organic carbon/water partitioning coefficient that influence the distribution pattern of these contaminants in the environment. In addition, this chapter provides an evaluation of the concentrations of these chemicals in various environmental media such as indoor and outdoor air, indoor dust, soil and sediment, sewage sludge, biota and food, and human tissues.

Keywords: PBDEs, NBFRs, physiochemical properties, environmental levels, fate and behaviour

1. Introduction

Brominated flame retardants (BFRs) are a group of synthetic chemicals added to a wide range of polymers, foam, plastic, textile, and building materials to meet flame retardancy standards set by various jurisdictions worldwide, containing 50–85% bromine by weight [1]. Depending on their mode of incorporation into the polymers to which they are added, they are referred to as either reactive or additive BFRs. Reactive flame retardants, such as tetrabromobisphenol-A

(TBBPA), are chemically bonded to the polymer. Conversely, additive BFRs, such as PBDEs and hexabromocylododecane (HBCD) are simply blended with the polymers and do not become a part of the base polymer. Additive BFRs are the most common because their application in consumer goods is less complicated than for reactive BFRs [2]. An extensive body of research has reported the presence of BFRs in air, dust, soil, sediment and biota samples. Evidence of their persistence and capacity for bioaccumulation, coupled with concerns about their adverse health effects has led to widespread bans and restrictions on the manufacture and use of PBDEs and their listing under the Stockholm Convention on Persistent Organic Pollutants (POPs) [3]. Such bans and restrictions on the use of BFRs without the relaxation of flammability standards has likely resulted in increased production and use of alternatives referred to collectively as 'novel' brominated flame retardants [4]. According to the empirical data, studies suggest that some NBFRs have the same hazard profiles as 'legacy' BFRs [5].

2. PBDEs and NBFRs

PBDEs are a family of chemicals with a common structure of a brominated diphenyl ether and have the chemical formula $C_{12}H_{(0–9)}Br_{(1–10)}O$. Any of the 10 hydrogen atoms of the diphenyl ether moiety can be exchanged with bromine, resulting in 209 possible congeners. Each individual PBDE is distinguished from others by both the number of bromine atoms and the placement of those atoms (**Figure 1**). These congeners are numbered using the International Union of Pure and Applied Chemistry (IUPAC) system [6].

Commercial products of PBDEs have been marketed in three main formulations, namely: pentabromodiphenyl ether (Penta-BDE), octabromodiphenyl ether (Octa-BDE) and decabromodiphenyl ether (Deca-BDE). The leading commercial Penta-BDE mixture is primarily comprised 28% BDE-47 and 43% BDE-99. A commercial Octa-BDE mixture is comprised of 13–42% BDE-183 and 11–22% BDE-197, while Deca-BDE mixture contains primarily >97% BDE-209 [7].

Bans and restrictions on the use of established BFRs have resulted in the production of alternatives to comply with flammability standards. The term NBFRs refer to brominated flame retardants, which 'are new to the market or recently observed in the environment due to the restrictions and bans on the use of some "legacy" BFRs'. Other terms such as 'alternate', 'emerging' or 'non-PBDEs' have also been used to refer to these BFRs [4]. It has been indicated that the NBFRs are urgently required because any non-halogenated substituting chemicals can involve significant costs, as industries must adapt their products for all required

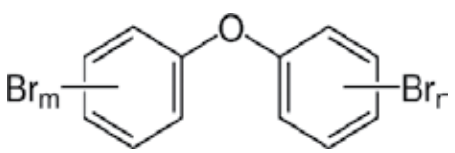

Figure 1. General structure of PBDEs (n + m = 1–10).

http://dx.doi.org/10.5772/intechopen.79823

performances and product standards [1]. The most common NBFRs replacing PBDEs are: a mixture of 2-ethylhexyl-2,3,4,5-tetrabromobenzoate (EH-TBB) and bis (2-ethylhexyl)3,4,5,6-tetrabromophthalate (BEH-TEBP) under the trade name Firemaster 550 as a replacement for Penta-BDEs; 1,2-bis(2,4,6-tribromophenoxy)ethane (BTBPE) as a replacement for Octa-BDE; and decabromodiphenyl ethane (DBDPE) as a replacement for Deca-BDE [8]. **Figure 2** illustrates the chemical structure of selected NBFRs replacing PBDEs.

2.1. Physicochemical properties of PBDEs and NBFRs

PBDE commercial products are solids at room temperature, not flammable, and do not present a physiochemical hazard [7]. They are hydrophobic contaminants (highly water insoluble) and typically have high log octanol-water partition coefficients.

Similar to PBDEs, NBFRs are highly hydrophobic compounds and displaying low volatility. However, differences in molecular structure between PBDEs and their NBFR replacements result in specific differences in physicochemical properties. For example, the ethane bridge between the aromatic rings in the DBDPE molecule makes it more flexible and hydrophobic than BDE-209, with consequences for its environmental fate and behaviour [4]. In general, BTBPE, BEH-TEBP and DBDPE possess lower vapour pressures and higher log octanol-water partition coefficients compared with Octa-, Penta- and Deca-BDE, respectively. **Tables 1** and **2** and **Figure 3** illustrate the most important physiochemical properties: molecular weight (MW), vapour pressure (V_P), octanol/air partitioning coefficient (K_{OA}), octanol/water partition coefficient (K_{OW}), water solubility and organic carbon/water partitioning (K_{OC}) that influences the environmental fate and behaviour of PBDEs and NBFRs.

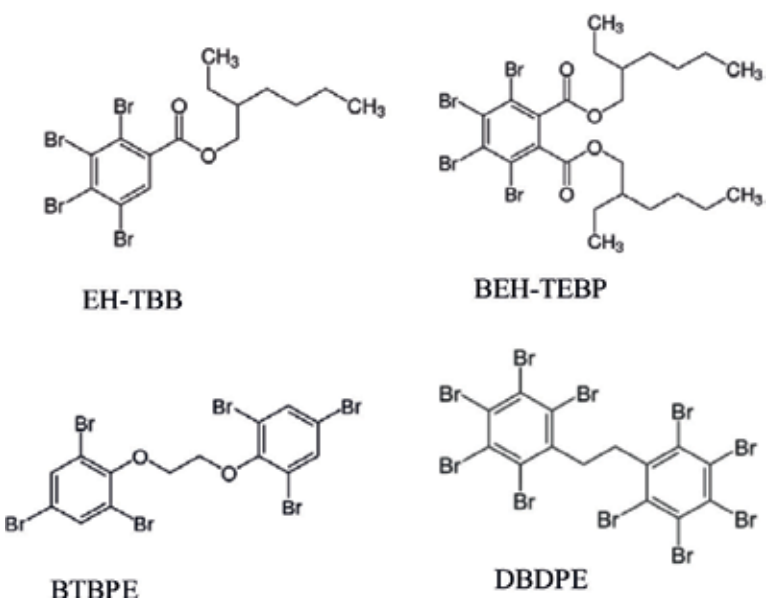

Figure 2. Chemical structure of selected NBFRs replacing PBDEs.

BDE	Molecular weight	Water solubility mg/L (@25°C)	Log K_{OW}	Log K_{OA} (@25°C)	Log K_{OC}	Vapour pressure (Pa) (@25°C)
BDE-28	407.1	0.07	5.94	9.5	3.91	6.51×10^{-4}
BDE-47	485.82	0.001–0.002	6.81	10.53	4.12	5.52×10^{-5}
BDE-99	564.75	0.009	7.32	11.31	4.34	7.94×10^{-6}
BDE-100	564.75	0.04	7.24	11.13	n.a	7.07×10^{-6}
BDE-153	643.62	0.001	7.9	11.82	n.a	5.80×10^{-6}
BDE-154	643.62	0.001	7.82	11.92	n.a	2.64×10^{-7}
BDE-183	722.4	0.002	8.27	11.96	n.a	n.a
BDE-209	959.17	<0.001	6.3–12.6	13.21	6.30	9.28×10^{-9}

Table 1. Physicochemical properties of selected BDEs [1, 7, 9].

NBFR	Molecular weight	Water solubility (mg/L @ 25°C)	Log K_{OW}	Log K_{OA} (@25°C)	Log K_{OC}	Vapour pressure (Pa) (@25°C)
EH-TBB	549.92	1.10×10^{-5}	7.73	12.34	5.59	4.57×10^{-6}
BTBPE	687.64	1.90×10^{-5}	8.31	15.67	5.89	3.88×10^{-10}
BEH-TEBP	706.14	1.60×10^{-6}	9.34	16.86	6.45	1.55×10^{-11}
DBDPE	971.22	2.10×10^{-7}	11.1	19.22	7.00	6.00×10^{-15}

Table 2. Physicochemical properties of selected NBFRs [8, 10, 11].

2.1.1. Impact of physicochemical properties on the environmental behaviour of BFRs

Knowledge of the physicochemical properties of substances provides information about their potential environmental fate and behaviour.

2.1.1.1. Molecular weight (MW)

Depending on their molecular weight, chemicals show diverse behaviour in environmental and biological systems. With specific regard to PBDEs, variations in the degree of bromination drive variations in physicochemical properties such as vapour pressure, hydrophobicity and lipophilicity, which in turn lead to congener-specific variations in environmental fate and behaviour. For example, while those less brominated congeners prevalent in the commercial Penta- and Octa-BDE formulations are more bioaccumulative in aquatic biota; higher brominated congeners, such as BDE-209, predominated in sediments. However, potential degradation of higher brominated compounds could yield lower brominated PBDEs that display stronger bioaccumulation characteristics than BDE-209 itself [12].

2.1.1.2. Vapour pressure (V_p)

V_p is a useful indicator to determine the potential of chemicals to volatilise from surfaces to the atmosphere. Inhalation is less likely to be a substantial pathway of exposure to chemicals

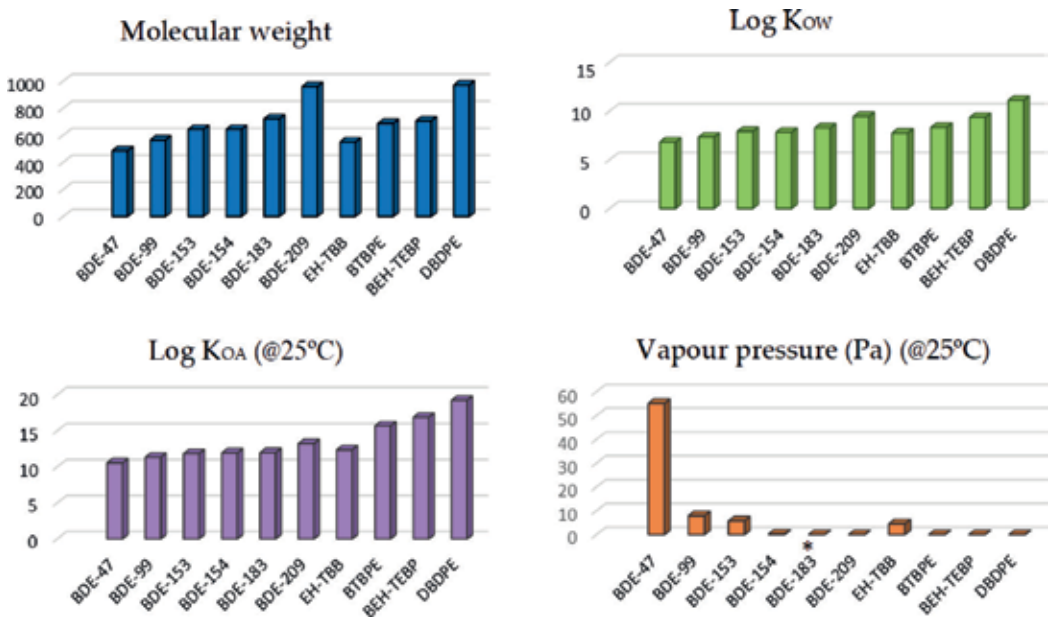

Figure 3. Molecular weight, Log K_{OW} (octanol/water partition coefficient), Log K_{OA} (octanol/air partitioning coefficient) and vapour pressure of selected PBDEs and NBFRs. *Octa-BDE.

with a $V_P < 10^{-6}$ mm Hg (10^{-4} Pa). Conversely, inhalation is likely significant for chemicals with a $V_P > 1 \times 10^{-4}$ mm Hg (10^{-2} Pa) [5]. Chemicals including many BFRs possess a V_P between 1×10^{-8} and 1×10^{-4} mm Hg partition between the gas and particulate phases and are thereby considered semi-volatile. The equilibrium between the two phases is controlled by the V_P, the surrounding air temperature, and the concentration and chemical composition of airborne particulate matter. V_p of PBDEs and NBFRs decrease with increasing molecular weight and degree of bromination [5, 7].

2.1.1.3. Octanol-air partition coefficient (K_{OA})

K_{OA} is a parameter that describes the partition of semi-volatile organic compounds (SVOCs) between the gas phase and organic matter such as that found in airborne particles. Commonly expressed as log $K_{OA,}$ it is the ratio between the concentration of the chemical in air and its concentration in octanol at the equilibrium state. As with V_P, log K_{OA} depends on the temperature. Higher log K_{OA} values imply stronger binding to the organic content of particles [13, 14]. As shown in **Tables 1** and **2**, log K_{OA} values fall between 9.5 and 13.2 for PBDEs and between 12.3 and 19.2 for NBFRs. This indicates that BFRs will deposit readily from the gas phase into indoor dust, soil and vegetative biomass. In addition, the wide range of log K_{OA} values implies a varying abundance of these pollutants in particulate phases [7].

2.1.1.4. Water solubility and octanol/water partition coefficient (K_{OW})

As shown in **Tables 1** and **2** and **Figure 3**, in general, PBDE water solubility values are higher than those of NBFRs. Water solubility is strongly inversely related to the K_{OW}. Commonly expressed as log K_{OW}, this is an important property for assessing the environmental fate and

behaviour of chemicals. Generally, organic chemicals with a log K_{OW} value ≥ 5.0 are very hydrophobic, thereby displaying a high tendency to sorb organic carbon in sediments, soils, and indoor dust and—when combined with a resistance to metabolism—possess a marked capacity for bioaccumulation [7].

2.1.1.5. Organic carbon water partitioning coefficient (K_{OC})

Another important physiochemical property is K_{OC}, which provides an indication of a chemical to leach from soil to groundwater and to partition from the aqueous phase of water bodies to suspended solids and sediments. Chemicals with high K_{OC} values are strongly sorb to soil [5, 7]. In general, as shown in **Tables 1** and **2**, K_{OC} values for PBDEs (3.9–6.3) are slightly lower than by those of their replacements (log K_{OC} of NBFRs 5.8–7).

2.2. Environmental levels of PBDEs and NBFRs

PBDEs and NBFRs as additive flame retardants can be released from treated products and enter the environment via several ways. These include volatilisation and leaching from treated products, partitioning to indoor dust, leaching from landfills and recycling of waste products [15]. As a consequence of their persistence and potential for long-range atmospheric transport, PBDEs and NBFRs have been detected in Arctic media, transported on airborne particulates rather than the gas phase. The first detection of PBDEs was in 1979 in soil, and slug samples from the USA, with the first detection in vertebrates (fish and marine mammals collected from the Baltic Sea) were in the 1980s. By comparison with legacy BFRs, the occurrence of NBFRs in the environment is at lower levels; however, the last few years has seen a rise in contamination with NBFRs [16].

2.2.1. Levels of PBDEs and NBFRs in indoor and outdoor air

Depending on their V_P and K_{OA}, SVOC BFRs can volatilise from treated products and be abundant in both gaseous and particulate phases. The partitioning between the two phases is mainly driven by atmospheric temperature. It is expected that at a given temperature, lower brominated compounds are more abundant in the gas phase, while higher brominated congeners are more prevalent in the particle phase [14].

It is difficult to compare PBDEs levels in air samples between countries, due to the different number of individual congeners, sampling method (passive or active) and the atmospheric phase sampled (vapour, particle or both). PBDEs were detected in indoor air samples from the UK [17], Germany [18], Denmark [19], Sweden [20], USA [21], Canada [22], China [23] Japan [24], and Australia [25]. Concentrations were variable between countries. For the above-mentioned countries, PBDE concentrations were between 17 and 55 pg/m^3 in Japan and 210 and 3980 pg/m^3 in the USA. In Norway, the maximum concentration of BDE-209 in indoor air samples was 4150 pg/m^3 with a median concentration of 3.8 pg/m^3 (n = 47) [26].

In outdoor air samples, BFRs were detected at low levels compared with those in indoors. For each of BDE-47, BDE-99 and BDE-100, concentrations in indoor air were 100 times higher than

the outdoor in the UK [17]. In the USA, ΣPBDE concentrations ranged between 10 and 85 pg/m^3, with BDE-47 predominant [27]. In China, concentrations of Σtri-hepta-PBDEs ranged between 87.6 and 1941 pg/m^3, with BDE-47 and BDE-99 predominant [28].

Recently, in addition to PBDEs, more attention has been paid to NBFRs. Low concentrations of NBFRs were detected in air samples. In Sweden, BEH-TEBP and DBDPE in indoor air ranged <35–150 pg/m^3 and < 90–250 pg/m^3 with detection frequencies of 15 and 8% for BEH-TEBP and DBDPE respectively [29]. In China, only EH-TBB and DBDPE were detected, at very low concentrations [30].

2.2.2. Levels of PBDEs and NBFRs in surface water

As a source of fresh water, lakes are important. In the UK, an average concentrations of tri-hexa-BDEs in nine English lakes was 61.9 pg/L. Spatial variation was found between lakes, however, no correlation was detected between PBDE concentrations and population density. In addition, no evidence a decline in concentrations during the sampling period [31]. Another study [32] in the USA, from 18 stations on the five Great Lakes' water, reported that the average concentrations of Σtri-deca-BDEs (112 pg/L) were dominated by BDE-47 and BDE-99 with average concentrations of 26.8 and 26.4 pg/L respectively followed by BDE-209 (9.5 pg/L). Average concentrations of BEH-TEBP, EH-TBB and other NBFRs were 10.4, 5.6 and <1.1 pg/L, respectively [32]. In sea water from the European Arctic, concentration of Σ_{10}PBDEs (tri-deca) in dissolved water and suspended phases of seawater ranged from 0.03 to 0.64 pg/L, with BDE-47 and BDE-99 predominant [33].

2.2.3. Levels of PBDEs and NBFRs in sediment and soil

PBDE congener profiles in sediments are dominated by higher brominated congeners such as BDE-209 and DBDPE. This is different from profiles in biota samples, which are dominated by lower brominated congeners, such as BDE-47 and BDE-99 [34]. In marine sediments, BFRs were detected in Canada [35], San Francisco Bay, USA [36], Gulf of Lion, France [37], Northern Arabian Gulf [38], East Java Province, Indonesia [39], Goseong Bay, Korea [40], South China [41], and the Scheldt estuary, the Netherlands [42]. With the exception of the Scheldt estuary, the Netherlands (where sediment concentrations ranged 14–22 ng/g dw for tri-hepta-BDEs and 240–1650 ng/g dw for BDE-209) and south China (for which sediment concentrations fell between 30 and 5700 ng/g dw for BDE-209); concentrations of PBDEs in other countries were very low. In surficial sediments sampled along cruise transects from the Bering Sea to the central Arctic Ocean, Σ_{24}PBDEs (without BDE-209) in the marine sediments ranged from <MDL to 67.8 pg/g dw, with an average concentration of 9.8 ± 11.9 pg/g dw [43]. The study pointed that the Σ_{24}PBDE concentrations show a reduction from 2008 to 2012. In river sediment cores from China, PBDE concentrations ranged between 1.3 and 1800 ng/g dwt with the highest levels found at 4–6 cm depth [44].

Soil represents a major sink for many volatile organic pollutants operating during atmospheric transport. In Birmingham, UK, average concentrations of BDE-209 and Σtri-hepta-BDEs in soil samples were 11 and 3.6 ng/g, respectively [45]. These concentrations were higher in sites

closest to Birmingham city centre [45]. In an e-waste recycling area in South China, PBDE and NBFR concentrations in rhizosphere soils and non-rhizosphere soils were 13.9–351 ng/g for PBDEs and 11.6–70.8 ng/g for NBFRs. BDE-209 and DBDPE were predominant compounds [46]. Another study in China emphasised that DBDPE and BDE-209 were the predominant compounds in the forest soil samples. The concentrations of DBDPE and BDE-209 ranged between 25-18,000 pg/g and <dl -5900 pg/g respectively. In the same study, the distribution of BEH-TEBP and most PBDEs were significantly correlated with population density. In addition, the correlation between PBDEs and their replacement products indicates similar environmental behaviour [47]. Possible debromination of BDE-209 to lower brominated congeners in soils and sediments is a major concern [48].

2.2.4. Levels of PBDEs and NBFRs in sewage sludge

Wastewater treatment plants may not be effective in removing PBDEs. About 52–80% and 21–45% PBDEs remained in effluent and dewatered sludge, respectively, post-sewage treatment [49]. On the other hand, both lower brominated PBDEs and BDE-209 could be successfully removed from contaminated sludge under aerobic conditions [50]. In Korea, concentrations of ΣPBDE in sludge ranged from 298 to 48,000 ng/g dry weight, and among 10 NBFRs, DBDPE and BTBPE were only detected in sludge samples. DBDPE and BTBPE concentrations ranged from <dl-3100 to <dl-21.0, with average concentrations of 237 and 1.57 ng/g dwt for DBDPE and BTBPE, respectively [40]. In Spain, the occurrence of eight PBDEs and NBFRs (EH-TBB, BTBPE, BEH-TEBP and DBDPE) was evaluated in wastewater from wastewater treatment plants. With the exception of BEH-TEBP, no PBDEs or NBFRs were detected in unfiltered influent samples. However, 279–2299 ng/g dwt of flame retardants were detected in primary sludge [51].

From 12 countries around the world, the highest levels of DBDPE in slug samples from wastewater treatment plants were found in Germany (216 ng/g dwt) compared with Europe (81 ng/g dwt) and North America (31 ng/g dwt). The highest concentrations of Deca-BDE were found in the UK and the USA with values of 12,000 ng/g dwt and 19,000 ng/g dwt, respectively [52]. In waste biological sludge and treated bio solids from wastewater treatment plants in Canada, BDE-209, BDE-99 and BDE-47 were the predominant compounds with concentrations of 230–82,000, 530–8800 and 420–6000 ng/g, for BDE-209, -99 and -47 respectively [53].

2.2.5. Levels of PBDEs and NBFRs in biota and food

During the last decade, in addition to PBDEs, their replacement of NBFRs has been shown to accumulate in biota. NBFR levels in seven animal species from the Arctic, specifically one fish species, three seabirds, and three mammalian species were investigated. BTBPE and DBDPE were not detected in any of these species, while EH-TBB was found in all species and BEH-TEBP in only five. Concentrations of EH-TBB ranged between 378 and 3460 pg/g wet wt, while those of BEH-TEBP ranged from 573 to 1799 in whole fish, liver, egg and plasma [54]. For PBDEs, Eulaers et al. [55] reported that PBDE concentrations in muscle, liver, adipose, preen gland and feathers in Barn Owls were 7.46–903 ng/g lw in 2008–2009, which were lower

than in those collected in 2003–2004 (46–11,000 ng/g lw). The authors tentatively ascribed the decline to the 2004 European ban of Penta- and Octa-BDE mixtures. By comparison, NBFRs were found to be poorly bioaccumulated (2.3%) [55].

PBDEs and NBFRs have been detected in human food, animal feed and baby food. In the UK, concentrations of Σ_{17}PBDEs in food samples ranged between 0.02 and 8.91 ng/g whole weight, and, in animal feed, samples ranged between 0.11 and 9.63 ng/g whole weight. The highest PBDE concentrations were detected in fish, processed foods and fish feeds [56]. In home produced eggs from e-waste sites in China, EH-TBB and BEH-TEBP were found in low concentrations in 50% of chicken egg samples, ranged between <dl-1.82 and 1.17–2.6 ng/g for EH-TBB and BEH-TEBP, respectively [57]. In the three categories of baby food (formula, cereal, and puree) from USA and Chinese stores, median concentrations of ΣPBDEs (sum of BDE-17, -28, -47, -49, -99, -100, -153, -183, and -209) were 21 and 36 pg/g for American and Chinese baby foods, respectively [58].

2.2.6. Levels of PBDE and NBFR in human tissues

As discussed above, numerous studies have shown the presence of PBDEs and NBFRs in many media pertinent for human exposure via inhalation, ingestion and dermal routes. Due to their persistent and bioaccumulative properties, PBDEs and NBFRs have been found in human milk, serum, hair and nail samples. EH-TBB, BEH-TEBP, BTBPE, DBDPE, BDE-209 and BDE-153 in paired human serum (n = 102) and breast milk (n = 105) samples from Canada were investigated. Only EH-TBB and BDE-153 (lower brominated degree and more bioaccumulative) had detection frequencies higher than 55% in both serum and human milk samples, while detection frequencies for other BFRs were lower than 30%. Concentrations in serum and human milk were 1.6 and 0.41 ng/g lw for EH-TBB, and 1.5 and 4.4 ng/g lw for BDE-153, respectively [59]. In the UK, the average concentrations of Σtri-hexa-BDE and BDE-209 in human milk were 5.95 and 0.31 ng/g lw respectively. Concentrations of BDE congeners were BDE-47 > BDE-153 > BDE-99 [60]. BDE-47, −99, −100, and −183 were detected in most human hair samples from Hong Kong [61]. Concentrations of PBDEs in human hair samples in females were higher than males [62]. For NBFRs, EH-TBB and BEH-TEBP were detected in hair and nail samples at concentrations between 20 and 240 and 11 and 350 ng/g in hair samples and <17–80 ng/g and <9–71 ng/g in nail samples for EH-TBB and BEH-TEBP respectively [63].

2.2.7. Levels of PBDE and NBFR in indoor dust

As semi-volatile organic compounds (SVOCs) and additive flame retardants, PBDEs and NBFRs can be released from the products via volatilisation into surrounding air, depending on their V_P. Such volatilised pollutants may then undergo deposition to both suspended and settled indoor dust, with the relative partitioning between these two phases governed by the K_{OA} of the BFRs [13].

A large number of investigations around the world have reported high concentrations of BFRs in indoor dust. The highest levels of PBDEs were reported in US dust samples with

Country (media) [reference]	Median/range—indoor air (pg/m^3)				
	BDEs	**EH-TBB**	**BEH-TEBP**	**BTBPE**	**DBDPE**
USA [21]	760				
Germany [18]	37.8				
Sweden [20]	330				
Australia [25]	19				
China [23]	628				
UK [17]	128				
Sweden [29]			<35		<90
China [30]		7.2			40
Indoor dust (ng/g)					
Germany [78]	979.1	<3.0	343	<10	146
USA [79]		133	142	30	201
Canada [80]		120	99	30	
Pakistan [70]	143.8				
UK [64]	2862				
Kuwait [70]	339.4				
Iraq [72]	631.5	5.3	64.2	14.1	125
Egypt [71]	53.07	0.81	0.12	0.24	
Pakistan [81]		0.03	3.5	3.15	14
Surface water (pg/L)					
European Arctic [33]	0.03–0.64				
USA, Great Lakes [32]	117–623				
UK, lakes [31]	9.2–171.5				
Sediment and soil (pg/g dw)					
Arabian Gulf [38]	0.06–0.44				
Netherlands [42]	14,000–22,000				
China Marin sediment) [41]	30,000–5,700,000				
China (river sediment) [44]	1300–1800				
South China (soil) [46]	13,900–351,000				
China (forest soils) [47]	<dl-5900 (BDE-209)	<dl-1400	4–643		25–1800
Sewage sludge (ng/g dw)					
Korea [40]	298–48,000			<dl-21.0	<dl-3100
Spain [51]	279–2299 (BFRs)				
Canada (biological slug) [53]	230–82,000 (BDE-209)				

Country (media) [reference]	Median/range—indoor air (pg/m^3)				
	BDEs	**EH-TBB**	**BEH-TEBP**	**BTBPE**	**DBDPE**
Biota, food and human tissues (ng/g)					
The Arctic (fish and seabirds) [54]		0.378–3.460	0.573–1.799		
Belgium (Barn Owls) [55]	7.46–903				
UK (food samples) [56]	0.02–8.91				
UK (animal feed) [56]	0.11–9.63				
China (Egg) [57]		<dl-1.82	1.17–2.6		
Canada (serum) [59]	1.5(BDE-153)	1.6			
Canada (human milk) [59]	4.4 (BDE-153)	0.41			
UK (human milk) [60]	6.26				
Hong Kong (human hair) [61]	0.86–5.24 (BDE-47)				

Table 3. Concentrations of PBDEs and NBFRs in air, water, sediment, soil, indoor dust and human tissues from different countries around the world.

median concentrations of ΣPBDEs ranging between 1910 and 21,000 ng/g [21, 63]. The UK displayed the second highest PBDE indoor levels with concentrations ranging between 2900 and 10,000 ng/g [64]. For other parts of the world, ΣPBDE median concentrations were: 950 ng/g in Canada [65], 386 ng/g in Germany [18], 510 ng/g in Sweden [20], 1941 ng/g in China [61] and 1200 ng/g in Australia [66]. In the Middle East, the first study in Kuwait in 2006 reported a median concentration of ΣPBDEs of 90.6 ng/g [67], these levels increased in 2011 to a median concentration of 356 ng/g [68]. In Egypt, Iraq and Pakistan, ΣPBDE median concentrations were 46 [69], 635 [70] and 143 ng/g [68], respectively. Similar to the distribution of PBDE congeners in indoor dust from UK and China, BDE-209 was the major BFR detected in indoor dust from the Middle East. The PBDE congener profiles have changed, and Penta-BDE levels were about one-third those measured in previous studies in 2006 [71, 72].

Recently, studies have increasingly measured NBFRs in indoor dust. EH-TBB, BEH-TEBP, BTBPE and DBDPE represented the highest NBFR concentrations in house dust in the USA [73], with a distribution profile of EH-TBB > BEH-TEBP > DBDPE > BTBPE. The median concentrations were 337, 186, 22.3 and 82.8 for EH-TBB, BEH-TEBP, BTBPE and DBDPE respectively [74]. In Europe, NBFR concentrations and profiles differ from those in the USA. The major compounds in European indoor dust are DBDPE and BEH-TEBP, with EH-TBB and BTBPE present at lower levels. In the UK (classroom dust), median concentrations were 25, 96, 9 and 98 for EH-TBB, BEH-TEBP, BTBPE and DBDPE, respectively [75]. Meanwhile, in Sweden, median concentrations of EH-TBB, BEH-TEBP, BTBPE and DBDPE were 51, 47, 320, 2.6, 61, 6.3, and 150 ng/g, respectively [76].

In China, in addition to the elevated concentrations of PBDEs, high concentrations of NBFRs were detected in floor house dust as well. ΣPBDEs ranged between 685 and 67,500 ng/g, and ΣNBFRs ranged between 1460 and 50,010 ng/g in indoor dust from e-waste sites, with BDE-209 and DBDPE the major BFRs. DBDPE was predominant (nd—16,000 ng/g) followed by

BEH-TEBP (nd—1600), BTBPE (0.2–220 ng/g) and EH-TBB (nd—6300 ng/g) [77]. In addition to the mentioned studies, **Table 3** summarises concentrations of PBDEs and NBFRs in air, water, sediment, soil, indoor dust and human tissues from different countries around the world.

3. Conclusion

Depending on their physiochemical properties, PBDEs and NBFRs show diverse behaviour in various environmental media and the possibility of human exposure. Low molecular weight compounds (less brominated degree) possess lower vapour pressures and higher log K_{OA}. This implies a high tendency of such chemicals to the gas phase of indoor air and consequently the exposure will occur via inhalation pathway. On the other hand, water solubility and octanol/water partition coefficient (K_{OW}) are important properties to assess the tendency of higher brominated compounds to organic carbon in sediment, soils, and indoor dust, in which the main exposure will occur via ingestion. This is different from profiles in biota samples which are dominated by lower brominated compounds such as BDE-47 and EH-TBB. The highest levels of PBDEs and NBFRs were reported in US, China and UK indoor dust samples, which were dominated by BDE-209, DBDPE and BEH-TEBP with a decline in PBDE levels and rise in NBFRs.

Author details

Layla Salih Al-Omran

Address all correspondence to: laylaalomran@yahoo.com

Department of Chemistry, College of Science, University of Basrah, Basrah, Iraq

References

[1] Danish EPA. Danish Ministry of Environment, Environmental Protection Agency. Fire Safety Requirements and Alternatives to Brominated Flame-Retardants. 2016. No. 1822. Available from: http://www2.mst.dk/Udgiv/publications/[Accessed: January 20, 2018]

[2] Alaee M. An overview of commercially used brominated flame retardants, their applications, their use patterns in different countries/regions and possible modes of release. Environment International. 2003;**29**(6):683-689. DOI: 10.1016/S0160-4120(03)00121-1

[3] UNEP. Stockholm Convention on POPs. Risk Management Evaluation for Commercial Octabromodiphenyl ether. 2008. Available from: http://chm.pops.int/portals/0/repository/poprc4/unep-pops-poprc.4-6.english.pdf [Accessed: December 15, 2017]

[4] Covaci A, Harrad S, Abdallah MA, Ali N, Law RJ, Herzke D, de Wit CA. Novel brominated flame retardants: A review of their analysis, environmental fate and behaviour. Environment International. 2011;**37**(2):532-556. DOI: 10.1016/j.envint.2010.11.007

[5] USEPA. US Environmental Protection Agency. An Alternatives Assessment for the Flame Retardant Decabromodiphenyl Ether (deca BDE). 2014. Available from: https://www.epa.gov/sites/production/files/2014-05/documents/decabde_final [Accessed: February 16, 2018]

[6] Birnbaum LS, Staskal DF. Brominated flame retardants: Cause for concern? Environmental Health Perspectives. 2004;**112**(1):9-17. DOI: 10.1289/ehp.6559

[7] USEPA. US Environmental Protection Agency. 2010. An Exposure Assessment of Polybrominated Diphenyl Ethers. Available from: http://www.epa.gov/ncea [Accessed: August 22, 2017]

[8] de Wit CA, Kierkegaard A, Ricklund N, Sellström U. Emerging Brominated Flame Retardants in the Environment. In: Eljarrat E, Barceló D, editors. Brominated Flame Retardants. The Handbook of Environmental Chemistry. Vol. 16. Berlin, Heidelberg: Springer; 2010. DOI: doi.org/10.1007/698_2010_73

[9] Tittlemier SA, Halldorson T, Stern GA, Tomy GT. Vapor pressures, aqueous solubilities, and Henry's law constants of some brominated flame retardants. Environmental Toxicology and Chemistry. 2002;**21**(9):1804-1810

[10] ATSDR. Agency for Toxic Substances and Disease Registry. Toxicological Profile for Polybrominated Biphenyls and Polybrominated Diphenyl Ethers. 2004. Available from: http://www.atsdr.cdc.gov/toxprofiles/tp68 [Accessed: March 19, 2018]

[11] EFSA, European Food Safety Authority. Scientific opinion on emerging and novel brominated flame retardants (BFRs) in food. European Food Safety Authority Journal. 2012;**10**(10):2908. DOI: 10.2903/j.efsa.2012.2908

[12] Domínguez AA, Law RJ, Herzke D, de Boer J. Bioaccumulation of Brominated Flame Retardants. In: Eljarrat E, Barceló D, editors. Brominated Flame Retardants. The Handbook of Environmental Chemistry. Vol. 16. Berlin, Heidelberg: Springer; 2010. DOI: doi.org/10.1007/698_2010_95

[13] Li X, Chen J, Zhang L, Qiao X, Huang L. The fragment constant method for predicting octanol–air partition coefficients of persistent organic pollutants at different temperatures. Journal of Physical and Chemical Reference Data. 2006;**35**(3):1365-1384. DOI: 10.1063/1.2203356

[14] Weschler CJ, Nazaroff WW. SVOC partitioning between the gas phase and settled dust indoors. Atmospheric Environment. 2010;**44**(30):3609-3620. DOI: 10.1016/j.atmosenv.2010.06.029

[15] Segev O, Kushmaro A, Brenner A. Environmental impact of flame retardants (persistence and biodegradability). International Journal of Environmental Research and Public Health. 2009;**6**(2):478-491. DOI: 10.3390/ijerph6020478

[16] Law RJ, Herzke D. Current Levels and Trends of Brominated Flame Retardants in the Environment: Brominated Flame Retardants in the Environment. In: Eljarrat E, Barceló D, editors. The Handbook of Environmental Chemistry. Vol. 16. Berlin, Heidelberg: Springer; 2010. DOI: 10.1016/j.chemosphere.2005.12.007

[17] Harrad S, Wijesekera R, Hunter S, Halliwell C, Baker R. Preliminary assessment of UK human dietary and inhalation exposure to polybrominated diphenyl ethers. Environmental Science and Technology. 2004;**38**(8):2345-2350. DOI: 10.1021/es0301121

[18] Fromme H, Körner W, Shahin N, Wanner A, Albrecht M, Boehmer S, Parlar H, Mayer R, Liebl B, Bolte G. Human exposure to polybrominated diphenyl ethers (PBDE), as evidenced by data from a duplicate diet study, indoor air, house dust, and biomonitoring in Germany. Environment International. 2009;**35**(8):1125-1135. DOI: 10.1016/j.envint.2009.07.003

[19] Vorkamp K, Thomsen M, Frederiksen M, Pedersen M, Knudsen LE. Polybrominated diphenyl ethers (PBDEs) in the indoor environment and associations with prenatal exposure. Environment International. 2011;**37**(1):1-10. DOI: 10.1016/j.envint.2010.06.001

[20] Thuresson K, Björklund JA, de Wit CA. Tri-decabrominated diphenyl ethers and hexabromocyclododecane in indoor air and dust from Stockholm microenvironments 1: Levels and profiles. Science of the Total Environment. 2012;**414**:713-721. DOI: 10.1016/j.scitotenv.2011.11.016

[21] Johnson-Restrepo B, Kannan K. An assessment of sources and pathways of human exposure to polybrominated diphenyl ethers in the United States. Chemosphere. 2009; **76**(4):542-548. DOI: 10.1016/j.chemosphere.2009.02.068

[22] Wilford BH, Shoeib M, Harner T, Zhu J, Jones KC. Polybrominated diphenyl ethers in indoor dust in Ottawa, Canada: Implications for sources and exposure. Environmental Science and Technology. 2005;**39**(18):7027-7035. DOI: 10.1021/es050759g

[23] Chen L, Mai B, Xu Z, Peng X, Han J, Ran Y, Sheng G, Fu J. In-and outdoor sources of polybrominated diphenyl ethers and their human inhalation exposure in Guangzhou, China. Atmospheric Environment. 2008;**42**(1):78-86. DOI: 10.1016/j.atmosenv.2007.09.010

[24] Takigami H, Suzuki G, Hirai Y, Sakai SI. Brominated flame retardants and other polyhalogenated compounds in indoor air and dust from two houses in Japan. Chemosphere. 2009;**76**(2):270-277. DOI: 10.1016/j.chemosphere.2009.03.006

[25] Toms LML, Hearn L, Kennedy K, Harden F, Bartkow M, Temme C, Mueller JF. Concentrations of polybrominated diphenyl ethers (PBDEs) in matched samples of human milk, dust and indoor air. Environment International. 2009;**35**(6):864-869. DOI: 10.1016/j.envint.2009.03.001

[26] Cequier E, Ionas AC, Covaci A, Marcé RM, Becher G, Thomsen C. Occurrence of a broad range of legacy and emerging flame retardants in indoor environments in Norway. Environmental Science and Technology. 2014;**48**(12):6827-6835. DOI: 10.1021/es500516u

[27] Hoh E, Zhu L, Hites RA. Novel flame retardants, 1,2-bis(2,4,6-tribromophenoxy)ethane and 2,3,4,5,6-pentabromoethylbenzene, in United States' environmental samples. Environmental Science and Technology. 2005;**39**(8):2472-2477. DOI: 10.1021/es048508f

[28] Chen LG, Mai BX, Bi XH, Chen SJ, Wang XM, Ran Y, Luo XJ, Sheng GY, Fu JM, Zeng EY. Concentration levels, compositional profiles, and gas-particle partitioning of polybrominated diphenyl ethers in the atmosphere of an urban city in South China. Environmental Science and Technology. 2006;**40**(4):1190-1196. DOI: 10.1021/es052123v

[29] Newton S, Sellström U, de Wit CA. Emerging flame retardants, PBDEs, and HBCDDs in indoor and outdoor media in Stockholm, Sweden. Environmental Science and Technology. 2015;**49**(5):2912-2920. DOI: 10.1021/es505946e

[30] Newton S, Sellström U, Harrad S, Yu G, de Wit CA. Comparisons of indoor active and passive air sampling methods for emerging and legacy halogenated flame retardants in Beijing, China offices. Emerging Contaminants. 2016;**2**(2):80-88. DOI: 10.1016/j.emcon.2016.02.001

[31] Yang C, Harrad S, Abdallah MAE, Desborough J, Rose NL, Turner SD, Davidson TA, Goldsmith B. Polybrominated diphenyl ethers (PBDEs) in English freshwater lakes, 2008-2012. Chemosphere. 2014;**110**:41-47. DOI: 10.1016/j.chemosphere.2014.03.028

[32] Venier M, Dove A, Romanak K, Backus S, Hites R. Flame retardants and legacy chemicals in Great Lakes' water. Environmental Science and Technology. 2014;**48**(16):9563-9572. DOI: 10.1021/es501509r

[33] Möller A, Xie Z, Sturm R, Ebinghaus R. Polybrominated diphenyl ethers (PBDEs) and alternative brominated flame retardants in air and seawater of the European Arctic. Environmental Pollution. 2011;**159**(6):1577-1583. DOI: 10.1016/j.envpol.2011.02.054

[34] Lee HJ, Kim GB. An overview of polybrominated diphenyl ethers (PBDEs) in the marine environment. Ocean Science Journal. 2015;**50**(2):119-142. DOI: 10.1007/s12601-015-0010-8

[35] Grant PBC, Johannessen SC, Macdonald RW, Yunker MB, Sanborn M, Dangerfield N, Wright C, Ross PS. Environmental fractionation of PCBs and PBDEs during particle transport as recorded by sediments in coastal waters. Environmental Toxicology and Chemistry. 2011;**30**(7):1522-1532. DOI: 10.1002/etc.542

[36] Klosterhaus SL, Stapleton HM, La Guardia MJ, Greig DJ. Brominated and chlorinated flame retardants in San Francisco Bay sediments and wildlife. Environment International. 2012;**47**:56-65. DOI: 10.1016/j.envint.2012.06.005

[37] Salvadó JA, Grimalt JO, López JF, de Madron XD, Heussner S, Canals M. Transformation of PBDE mixtures during sediment transport and resuspension in marine environments (Gulf of Lion, NW Mediterranean Sea). Environmental Pollution. 2012;**168**:87-95. DOI: 10.1016/j.envpol.2012.04.019

[38] Gevao B, Boyle EA, Aba AA, Carrasco GG, Ghadban AN, Al-Shamroukh D, Alshemmari H, Bahloul M. Polybrominated diphenyl ether concentrations in sediments from the

Northern Arabian Gulf: Spatial and temporal trends. Science of the Total Environment. 2014;**491**:148-153. DOI: 10.1016/j.scitotenv.2013.12.122

[39] Ilyas M, Sudaryanto A, Setiawan IE, Riyadi AS, Isobe T, Takahashi S, Tanabe S. Characterization of polychlorinated biphenyls and brominated flame retardants in sediments from riverine and coastal waters of Surabaya, Indonesia. Marine Pollution Bulletin. 2011;**62**(1):89-98. DOI: 10.1016/j.marpolbul.2010.09.006

[40] Lee S, Song GJ, Kannan K, Moon HB. Occurrence of PBDEs and other alternative brominated flame retardants in sludge from wastewater treatment plants in Korea. Science of the Total Environment. 2014;**470-471**:1422-1429. DOI: 10.1016/j.scitotenv.2013.07.118

[41] Zhang XL, Luo XJ, Chen SJ, Wu JP, Mai BX. Spatial distribution and vertical profile of polybrominated diphenyl ethers, tetrabromobisphenol A, and decabromodiphenylethane in river sediment from an industrialized region of South China. Environmental Pollution. 2009;**157**(6):1917-1923. DOI: 10.1016/j.envpol.2009.01.016

[42] Verslycke TA, Vethaak AD, Arijs K, Janssen CR. Flame retardants, surfactants and organotins in sediment and mysid shrimp of the Scheldt estuary (The Netherlands). Environmental Pollution. 2005;**136**(1):19-31. DOI: 10.1016/j.envpol.2004.12.008

[43] Ma Y, Halsall CJ, Crosse JD, Graf C, Cai M, He J, Gao G, Jones K. Persistent organic pollutants in ocean sediments from the North Pacific to the Arctic Ocean. Journal of Geophysical Research: Oceans. 2015;**120**(4):2723-2735. DOI: 10.1002/2014JC010651

[44] Jin J, Liu W, Wang Y, Tang XY. Levels and distribution of polybrominated diphenyl ethers in plant, shellfish and sediment samples from Laizhou Bay in China. Chemosphere. 2008;**71**(6):1043-1050. DOI: 10.1016/j.chemosphere.2007.11.041

[45] Drage DS, Newton S, de Wit CA, Harrad S. Concentrations of legacy and emerging flame retardants in air and soil on a transect in the UK West Midlands. Chemosphere. 2016;**148**:195-203. DOI: 10.1016/j.chemosphere.2016.01.034

[46] Wang S, Wang Y, Song M, Luo C, Li J, Zhang G. Distributions and compositions of old and emerging flame retardants in the rhizosphere and non-rhizosphere soil in an e-waste contaminated area of South China. Environmental Pollution. 2016;**208**(Pt B):619-625. DOI: 10.1016/j.envpol.2015.10.038

[47] Zheng Q, Nizzetto L, Li J, Mulder MD, Sáňka O, Lammel G, Bing H, Liu X, Jiang Y, Luo C, Zhang G. Spatial distribution of old and emerging flame retardants in Chinese forest soils: Sources, trends and processes. Environmental Science and Technology. 2015;**49**(5):2904-2911. DOI: 10.1021/es505876k

[48] Law RJ, Covaci A, Harrad S, Herzke D, Abdallah MAE, Fernie K, Toms L-ML, Takigami H. Levels and trends of PBDEs and HBCDs in the global environment: Status at the end of 2012. Environment International. 2014;**65**:147-158. DOI: 10.1016/j.envint.2014.01.006

[49] Deng D, Chen H, Tam NFY. Temporal and spatial contamination of polybrominated diphenyl ethers (PBDEs) in wastewater treatment plants in Hong Kong. Science of the Total Environment. 2015;**502**:133-142. DOI: 10.1016/j.scitotenv.2014.08.090

[50] Stiborova H, Vrkoslavova J, Lovecka P, Pulkrabova J, Hradkova P, Hajslova J, Demnerova K. Aerobic biodegradation of selected polybrominated diphenyl ethers (PBDEs) in wastewater sewage sludge. Chemosphere. 2015;**118**:315-321. DOI: 10.1016/j.chemosphere.2014.09.048

[51] Cristale J, Lacorte S. PBDEs versus NBFR in wastewater treatment plants: Occurrence and partitioning in water and sludge. AIMS Environmental Science. 2015;**2**(3):533-546. DOI: 10.3934/environsci.2015.3.533

[52] Ricklund N, Kierkegaard A, McLachlan MS. An international survey of decabromodiphenyl ethane (deBDethane) and decabromodiphenyl ether (decaBDE) in sewage sludge samples. Chemosphere. 2008;**73**(11):1799-1804. DOI: 10.1016/j.chemosphere.2008.08.047

[53] Kim M, Guerra P, Theocharides M, Barclay K, Smyth SA, Alaee M. Polybrominated diphenyl ethers in sewage sludge and treated biosolids: Effect factors and mass balance. Water Research. 2013;**47**(17):6496-6505. DOI: 10.1016/j.watres.2013.08.022

[54] Sagerup K, Herzke D, Harju M, Evenset A, Christensen GN, Routti H, Fuglei E, Aars J, Strom H, Gabrielsen GW. New brominated flame retardants in Arctic biota. Statlig Program for forurensningsovervåking. 2010. Available from: http://www.miljodirektoratet.no/old/klif/publikasjoner/2630/ta2630 [Accessed: February 29, 2018]

[55] Eulaers I, Jaspers VLB, Pinxten R, Covaci A, Eens M. Legacy and current-use brominated flame retardants in the Barn Owl. Science of the Total Environment. 2014;**472**:454-462. DOI: 10.1016/j.scitotenv.2013.11.054

[56] Fernandes AR, Mortimer D, Rose M, Smith F, Panton S, Garcia-Lopez M. Bromine content and brominated flame retardants in food and animal feed from the UK. Chemosphere. 2016;**150**:472-478. DOI: 10.1016/j.chemosphere.2015.12.042

[57] Zheng X, Xu F, Luo X, Mai B, Covaci A. Phosphate flame retardants and novel brominated flame retardants in home-produced eggs from an e-waste recycling region in China. Chemosphere. 2016;**150**:545-550. DOI: 10.1016/j.chemosphere.2015.09.098

[58] Liu LY, Salamova A, Hites RA. Halogenated flame retardants in baby food from the United States and from China and the estimated dietary intakes by infants. Environmental Science and Technology. 2014;**48**(16):9812-9818. DOI: 10.1021/es502743q

[59] Zhou SN, Buchar A, Siddique S, Takser L, Abdelouahab N, Zhu J. Measurements of selected brominated flame retardants in nursing women: Implications for human exposure. Environmental Science and Technology. 2014;**48**(15):8873-8880. DOI: 10.1021/es5016839

[60] Abdallah MAE, Harrad S. Polybrominated diphenyl ethers in UK human milk: Implications for infant exposure and relationship to external exposure. Environment International. 2014;**63**:130-136. DOI: 10.1016/j.envint.2013.11.009

[61] Kang Y, Wang HS, Cheung KC, Wong MH. Polybrominated diphenyl ethers (PBDEs) in indoor dust and human hair. Atmospheric Environment. 2011;**45**(14):2386-2393. DOI: 10.1016/j.atmosenv.2011.02.019

[62] Tang L, Lei B, Xu G, Ma J, Lei JQ, Jin SQ, Hu GY, Wu MH. Polybrominated diphenyl ethers in human hair from the college environment: Comparison with indoor dust. Bulletin of Environmental Contamination and Toxicology. 2013;**91**(4):377-381. DOI: 10.1007/s00128-013-1056-x

[63] Liu LY, Salamova A, He K, Hites RA. Analysis of polybrominated diphenyl ethers and emerging halogenated and organophosphate flame retardants in human hair and nails. Journal of Chromatography A. 2015;**1406**:251-257. DOI: 10.1016/j.chroma.2015.06.003

[64] Harrad S, Ibarra C, Abdallah MAE, Boon R, Neels H, Covaci A. Concentrations of brominated flame retardants in dust from United Kingdom cars, homes, and offices: Causes of variability and implications for human exposure. Environment International. 2008;**34**(8):1170-1175. DOI: 10.1016/j.envint.2008.05.001

[65] Harrad S, Abdallah MAE, Covaci A. Causes of variability in concentrations and diastereomer patterns of hexabromocyclododecanes in indoor dust. Environment International. 2009;**35**(3):573-579. DOI: 10.1016/j.envint.2008.10.005

[66] Sjödin A, Päpke O, McGahee E, Focant JF, Jones RS, Pless-Mulloli T, Toms LML, Herrmann T, Müller J, Needham LL. Concentration of polybrominated diphenyl ethers (PBDEs) in household dust from various countries. Chemosphere. 2008;**73**(1):S131-S136. DOI: 10.1016/j.chemosphere.2007.08.075

[67] Gevao B, Al-Bahloul M, Al-Ghadban AN, Al-Omair A, Ali L, Zafar J, Helaleh M. House dust as a source of human exposure to polybrominated diphenyl ethers in Kuwait. Chemosphere. 2006;**64**(4):603-608. DOI: 10.1016/j.chemosphere.2005.11.055

[68] Ali N, Ali L, Mehdi T, Dirtu AC, Al-Shammari F, Neels H, Covaci A. Levels and profiles of organochlorines and flame retardants in car and house dust from Kuwait and Pakistan: Implication for human exposure via dust ingestion. Environment International. 2013;**55**:62-70. DOI: 10.1016/j.envint.2013.02.001

[69] Hassan Y, Shoeib T. Levels of polybrominated diphenyl ethers and novel flame retardants in microenvironment dust from Egypt: An assessment of human exposure. Science of the Total Environment. 2015;**505**:47-55. DOI: 10.1016/j.scitotenv.2014.09.080

[70] Al-Omran LS, Harrad S. Polybrominated diphenyl ethers and "novel" brominated flame retardants in floor and elevated surface house dust from Iraq: Implications for human exposure assessment. Emerging Contaminants. 2016;**2**(1):7e13. DOI: 10.1016/j.emcon.2015.10.001

[71] Schreder ED, La Guardia MJ. Flame retardant transfers from U.S. households (dust and laundry wastewater) to the aquatic environment. Environmental Science and Technology. 2014;**48**(19):11575-11583. DOI: 10.1021/es502227h

[72] Stapleton HM, Misenheimer J, Hoffman K, Webster TF. Flame retardant associations between children's handwipes and house dust. Chemosphere. 2014;**116**:54-60. DOI: 10.1016/j.chemosphere.2013.12.100

[73] Brown FR, Whitehead TP, Park JS, Metayer C, Petreas MX. Levels of non-polybrominated diphenyl ether brominated flame retardants in residential house dust samples and fire station dust samples in California. Environmental Research. 2014;**135**:9-14. DOI: 10.1016/j.envres.2014.08.022

[74] La Guardia MJ, Hale RC. Halogenated flame-retardant concentrations in settled dust, respirable and inhalable particulates and polyurethane foam at gymnastic training facilities and residences. Environment International. 2015;**79**:106-114. DOI: 10.1016/j.envint.2015.02.014

[75] Ali N, Harrad S, Goosey E, Neels H, Covaci A. "Novel" brominated flame retardants in Belgian and UK indoor dust: Implications for human exposure. Chemosphere. 2011; **83**(10):1360-1365. DOI: 10.1016/j.chemosphere.2011.02.078

[76] Sahlström LMO, Sellström U, de Wit CA, Lignell S, Darnerud PO. Estimated intakes of brominated flame retardants via diet and dust compared to internal concentrations in a Swedish mother–toddler cohort. International Journal of Hygiene and Environmental Health. 2015;**218**(4):422-432. DOI: 10.1016/j.ijheh.2015.03.011

[77] Zheng X, Xu F, Chen K, Zeng Y, Luo X, Chen S, Mai B, Covaci A. Flame retardants and organochlorines in indoor dust from several e-waste recycling sites in South China: Composition variations and implications for human exposure. Environment International. 2015;**78**:1-7. DOI: 10.1016/j.envint.2015.02.006

[78] Fromme H, Hilger B, Kopp E, Miserok M, Volkel W. Polybrominated diphenyl ethers (PBDEs), hexabromocyclododecane (HBCD) and "novel" brominated flame retardants in house dust in Germany. Environment International. 2014;**64**:61-68. DOI: 10.1016/j.envint.2013.11.017

[79] Stapleton HM, Allen JG, Kelly SM, Konstantinov A, Klosterhaus S, Watkins D, McClean MD, Webster TF. Alternate and new brominated flame retardants detected in U.S. house dust. Environmental Science and Technology. 2008;**42**(18):6910-6916. DOI: 10.1021/es801070p

[80] Shoeib M, Harner T, Webster GM, Sverko E, Cheng Y. Legacy and current-use flame retardants in house dust from Vancouver, Canada. Environmental Pollution. 2012;**169**:175-182. DOI: 10.1016/j.envpol.2012.01.043

[81] Ali N, Harrad S, Muenhor D, Neels H, Covaci A. Analytical characteristics and determination of major novel brominated flame retardants (NBFRs) in indoor dust. Analytical and Bioanalytical Chemistry. 2011;**400**(9):3073-3083. DOI: 10.1007/s00216-011-4966-7

Section 3

Fire Retardant Polymer Nanocomposite

Chapter 3

Flame Retardant Polymer Nanocomposites and Interfaces

Yuan Xue, Yichen Guo* and Miriam H. Rafailovich

Additional information is available at the end of the chapter

http://dx.doi.org/10.5772/intechopen.79548

Abstract

The flame retardant efficiency of polymer nanocomposites is highly dependent on the dispersion of the nano-fillers within the polymer matrix. In order to control the filler dispersion, it is very essential to explore the interfacial compatibility between fillers and matrices, which provides a guide for the flame retardant nanocomposites compounding. In this short review, we mainly focus on the thermoplastic polymers and their interactions with the surfaces of the flame retardant fillers. Other physical properties of those nanocomposites such as mechanical properties, gas permeability, rheological performance and thermal conductivity are also briefly reviewed along with the flame retardancy, since they are all dispersion related.

Keywords: polymer nanocomposites, filler dispersion, interfacial compatibility, flame retardancy, mechanical properties

1. Introduction

In past decades, polymeric materials have been extensively used in construction, transportation, and electronic devices due to the high performance and cost-effectiveness [1]. However, most of the polymeric materials were intrinsically combustible, which caused the fire hazard. The necessity to improve the flame retardancy of polymeric materials was urgent, so that people started to incorporate flame retardants into polymers to produce flame retardant polymer composites. The commercial used flame retardants mainly included endothermic additives, halogenated additives, phosphorus additives, expandable graphite and melamine derivatives. However, using a single component flame retardant to make the polymer reach the desired flame retardant performance required high loading of additives, which can cause

the deterioration of the mechanical properties of the polymer matrix. In order to enhance the flame retardant efficiency of additives, synergistic flame retardant systems were developed [2–6]. These systems contained two or more additives. Some additives were not flame retardant themselves, but can effectively synergize the performance with other flame retardants, thereby minimizing the total loading of the additives within the polymer matrices. The most common combinations, such as antimony oxides [7]/halogens [8], metal hydroxides [9–11]/ zinc borate [12], and intumescent phosphates [13, 14] have already been widely used in various polymers and successfully commercialized. Recently, people started to use nano-scale additives to make polymer nanocomposites and expect further enhancement of the flame retardant performance. The practice of mixing nanoparticles with polymers to make polymer nanocomposites can be traced back to nineteenth century [15, 16]. Those composite materials inherited the properties of the nanoparticles and showed significant enhancement in performance compared to their polymeric matrices. However, the mechanisms for the reinforcement of the polymeric matrices by nanoparticles were not adequately understood until 1990s. This rise of polymer nanocomposites research benefitted from the growing availability of nanoparticles and the emergence of instrumentation to probe the nano-scale structure of materials [17]. Furthermore, powerful computers allowed for the development of theoretical models which together with experiments were used to develop the guiding principles for engineering new nanocomposites with desirable properties. These models highlighted the critical role of surface and interfacial energies between the fillers and the polymer matrix and as well as the role particle morphology. Consequently, research of flame retardant polymer nanocomposites has been widely reported from both academic and industrial laboratories [18, 19].

In this review, we will mainly focus on the thermoplastic polymer based nanocomposites. Comparing to the thermoset polymer nanocomposites, thermoplastic polymer nanocomposites are easy to process and formulate in manufacturing, which makes them a very diverse and manageable composite system. This review describes the mechanisms of interaction between singular or binary thermoplastic polymer matrices with the commonly used nanoparticles: montmorillonite clay, graphene, nature nanotubes and fibers. The effect of nanoparticles influence on flame retardant efficiency was discussed, as well as the change in physical properties, such as impact resistance, ductility, gas permeability and rheology performance.

2. Singular polymer matrix

2.1. Montmorillonite clays

Montmorillonite is one of the most commonly used fillers in materials application. It could be dispersed in a polymer matrix to form polymer-clay nanocomposite. Okamoto et al. have shown that the organically modified montmorillonite clay could improve the thermal mechanical and gas barrier effect of poly (lactic acid) (PLA) [20]. By using wide-angle X-ray diffraction and transmission electron microscopy, they found that with the differences in clay modification, four different types of clay-polymer morphology were formed: intercalated,

intercalated-and-flocculated, exfoliated and coexistence of intercalated and exfoliated. The intercalated structure achieved great mechanical property improvement, and the near exfoliated composite has the highest gas barrier effect. However, the mechanism of the surface interaction was not well developed. Also, to improve the degree of exfoliation of clay platelets, cation exchange with quaternary ammonium chloride salts was commonly used for clay modification. The development of this method was held back due to the toxicity of these salts [21].

Recently, Guo et al. developed a much efficient way to determine the affinity between large aspect ratio nanoparticles and the polymer matrix by simply measuring the Young's contact angle [22]. The relative affinity between PLA and Closite Na^+ clay/Closite 30B (C-30B) clay were studied. They also used resorcinol di(phenyl phosphate) (RDP) adsorption to modify the Closite Na^+ clay (C-Na^+), which has been proven to perform better than using organoclays alone in conventional polymer systems [23]. The chemical formula of RDP is shown in **Figure 1**. With the nonpolar moieties of phenol groups and polar moieties of phosphoric acids groups, RDP could be used as a surfactant [24]. It has also been proven to react with polymers at high temperatures to form chars, which renders its ability to work as a flame retardant additive [25, 26]. In this research, a monolayer of these clay particles were formed on Si wafer using Langmuir–Blodgett (LB) technique. A 5 mg PLA pellet was melted on top of each clay monolayer and the Young's contact angles at the polymer/clay surface/air interface were measured. The procedure is illustrated in **Figure 2**. Then with the combination of the interfacial energy equation and the equation for work of adhesion (W_a), the relationship between W_a and Young's contact angle (A) was developed as below:

$$W_a = \gamma_l(1 + \cos A)$$

whereγ_l is the surface tension of liquid phase, which is PLA in this case. By substituting the measured contact angle and calculate the individual W_a between PLA and each clay (listed in **Figure 2**), they found that comparing to the original MMT clay C-Na^+, the synthesized C-30B clay and the C-RDP clay were more compatible to the PLA matrix. Further small angle scattering (SAXS) and TEM results, shown in **Figure 3**, confirmed that there is no change on the interlayer spacing of C-Na^+ clay and they formed tactoids inside the polymer matrix.

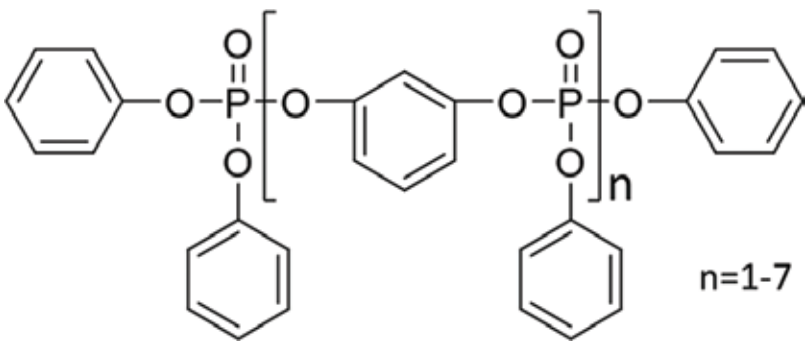

Figure 1. The chemical formula of RDP.

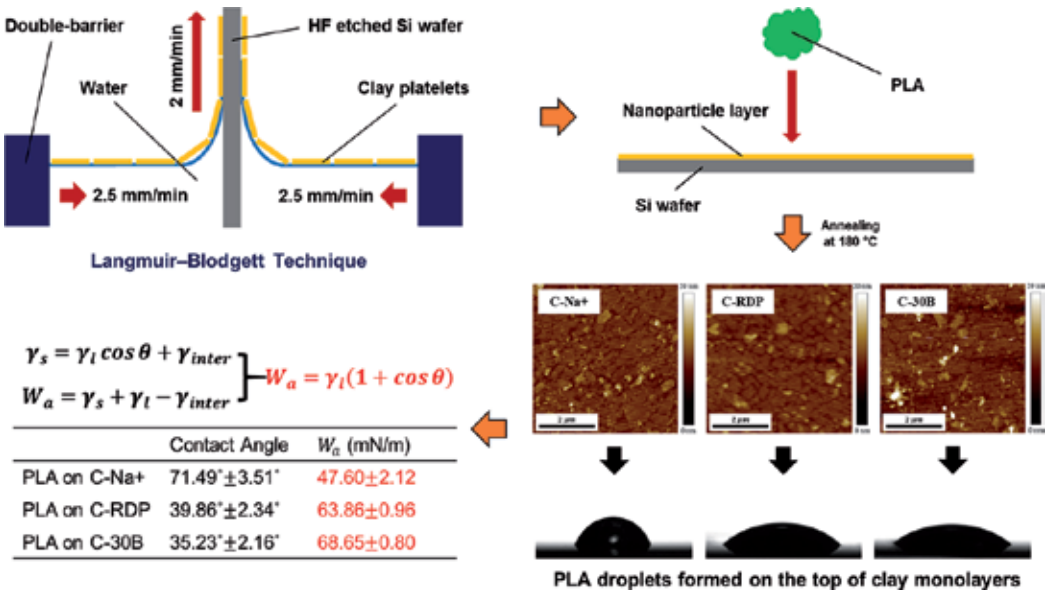

	Contact Angle	W_a (mN/m)
PLA on C-Na+	71.49°±3.51°	47.60±2.12
PLA on C-RDP	39.86°±2.34°	63.86±0.96
PLA on C-30B	35.23°±2.16°	68.65±0.80

Figure 2. An illustration of creating monolayer of nanoparticle by LB technique, and a list of measure contact angle of PLA on each type of clay with calculated work of adhesion. Adapted from Ref. [22]. Copyright (2018) with permission from Elsevier.

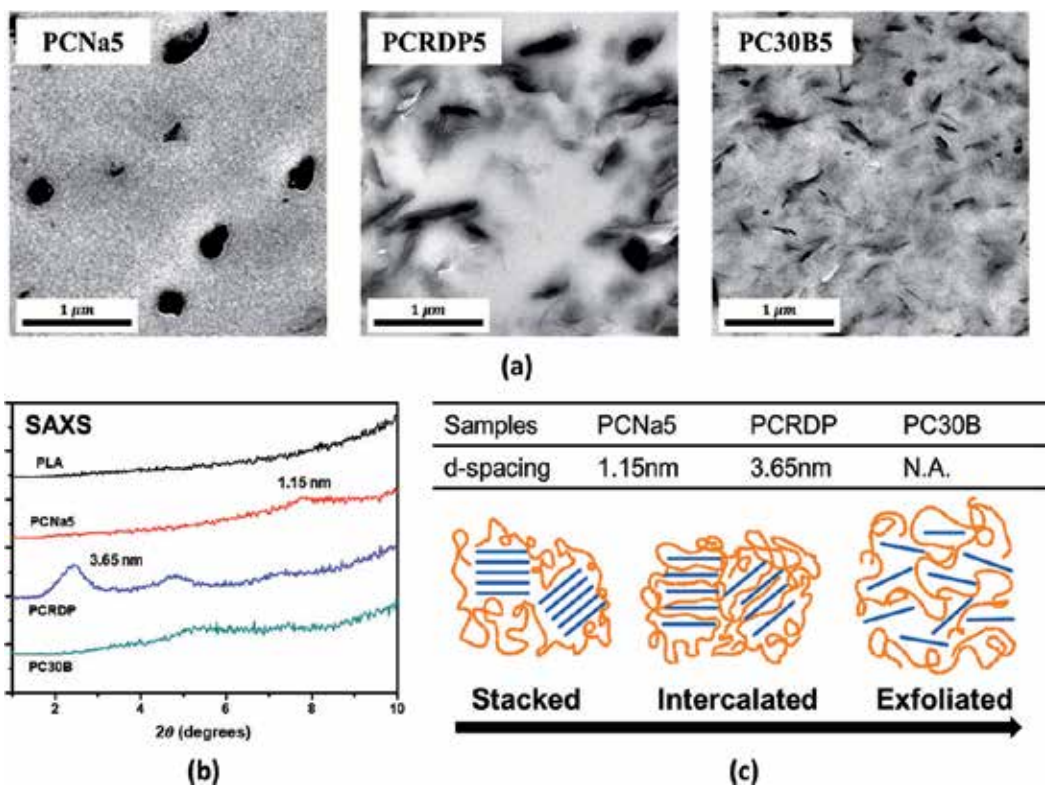

Figure 3. TEM imaging and X-ray pattern of PLA/clay composites: (a) TEM images of PLA/C-Na^+ blend (PCNa5), PLA/C-RDP blend (PCRDP5) and PLA/C-30B blend (PC30B5); (b) small angle X-ray scattering patterns of pure PLA and composites with clays. Adapted from Ref. [22]. Copyright (2018) with permission from Elsevier.

The interlayer spacing for C-RDP increased from 2.04 to 3.65 nm, which indicates the polymer chains intercalated with the clay platelets. In the case for C-30B, the SAXS pattern only showed a weak secondary (002) peak which proved that the C-30B platelets were exfoliated. These results are in good agreement with the previous W_a measurement, which concludes that the work of adhesion between the clay platelets and polymer needs to increase to achieve particle exfoliation inside polymer matrix.

Since C-30B are mostly exfoliated in the PLA matrix, Guo et al. continued to study its possible effect on improving the performance of flame retardant agent [4]. As a biodegradable polymeric material with good mechanical and processing properties, PLA has been extensively studied over recent years and has been used as a substitution for conventional polymers [27, 28]. In order to expand its usage into electron devices and automobile industry, the high flammability of PLA must be resolved. Melamine polyphosphate (MPP) was used in this study, which is a halogen-free flame retardant agent [29]. When used alone, 28 wt.% of MPP is needed to achieve the V0 grade in UL-94 vertical burning test. TEM images in **Figure 4(a)** showed that the MPP formed droplet shaped domains with a diameter around 500 nm. According to Araki et al., when large aspect ratio particles were used to compatible a binary system, the domain size is controlled by balancing between the reduction of system enthalpy and the increase of bending energy due to particle curvature [30], and the minimum domain size should be similar to the radius of particle platelets. When 1 wt.% of C-30B is added to the system, the MPP were better dispersed and the domain size were reduced to around 150 nm, which is similar to the radius of C-30B platelets. And only 17 wt.% of MPP is needed to obtain the V0 grade, as

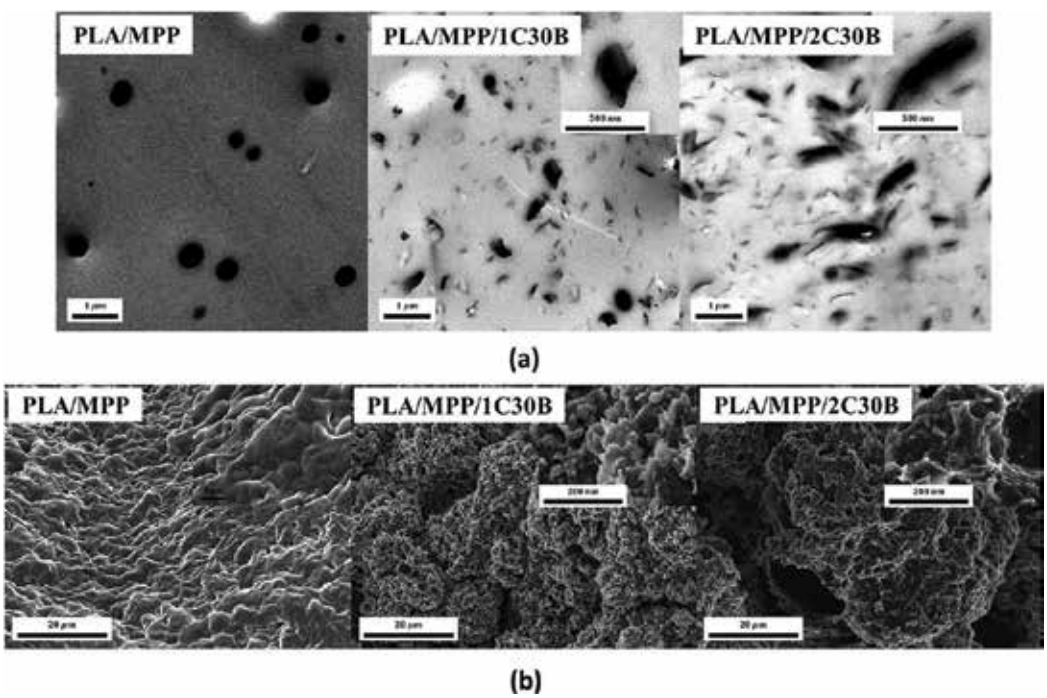

Figure 4. TEM and SEM images of PLA/MPP/C-30B blends: (a) TEM images taken on cross-sections of PLA composites; (b) SEM images on the char residue after cone calorimetry test. Adapted from Ref. [4]. Copyright (2018) with permission from Elsevier.

Sample	Avg. heat release rate (kW/m^2)	Peak heat release rate (kW/m^2)	Total heat release (MJ/m^2)
100PLA	6–1120	1.1–29.0	80–920
PLA/MPP	117.5	12.6	359
PLA/MPP/1C-30B	239.7	17.3	441
PLA/MPP/2C-30B	133.3	13.4	348

Table 1. Cone calorimetry results of PLA/MPP/C-30B blends. Adapted from Ref. [4]. Copyright (2018) with permission from Elsevier.

oppose to the previous 28%. However, further increase C-30B concentration to 2% resulted in enlarged and elongated MPP domain, which is to reduce the energy penalty brought by bending clay particles. And C-30B starts to form aggregates on the elongated MPP domain surface, which blocked the contact of polyphosphate to the PLA molecules. In the cone calorimetry test (listed in **Table 1**), the better dispersed MPP/1%C-30B system has lower average heat release rate (aHRR), peak heat release rate (pHRR) and total heat release (THR) than MPP with 2% C-30B. Examination of char residue also agree with this result. Intumescent char layers were found for both samples with only MPP and MPP/1% C-30B. As shown in **Figure 4(b)**, the char layer of sample with only MPP is continuous and has a winkled structure due to the gas inflating during heating and releasing after cooling. Similar winkled structure was found on the char layer of sample containing MPP/1% C-30B, where the winkle was formed by dense polymer/clay aggregates. In contrast, the char layer of sample with MPP/2% C-30B was loose and powdery, which is composed of large polymer/clay agglomerates and has numerous micro-cracks. This result confirmed their theory that when clay platelets were exfoliated and act as a dispersant, the MPP is better dispersed which could increase the flame retardant efficiency. The exfoliated clay platelets also provide large surface area to interact with both polymer chain and MPP, improving the formation of the intumescent char. Yet the window of improvement is limited because further increasing clay content would result in clay aggregating on the polymer/FR interface and harming the FR performance.

2.2. Graphene

Having a similar platelet structure to clay, graphene is also a large aspect ratio nanoparticle and has gained great attention in many research areas due to its superior thermal conductivity, heat sink effect and great mechanical performance [31–33]. Given the large surface area and heat adsorption of graphene, Xue et al. developed a three component flame retardant ethylene vinyl acetate (EVA) composite as a replacement of polyvinyl chloride (PVC) for cable sheathing [6]. The three component FR system consists of aluminum hydroxide (ATH), molybdenum disulfide (MoS_2) and graphene nanoplatelets (GNPs). When ATH was used alone, it could absorb heat and release water vapor during combustion, which could dilute the oxygen surround the sample surface. However, due to the poor compatibility between ATH and EVA, ATH would form large aggregates in the polymer matrix, which decreased the interfacial area for ATH to react and therefore decreasing its efficiency, as shown in the TEM

http://dx.doi.org/10.5772/intechopen.79548

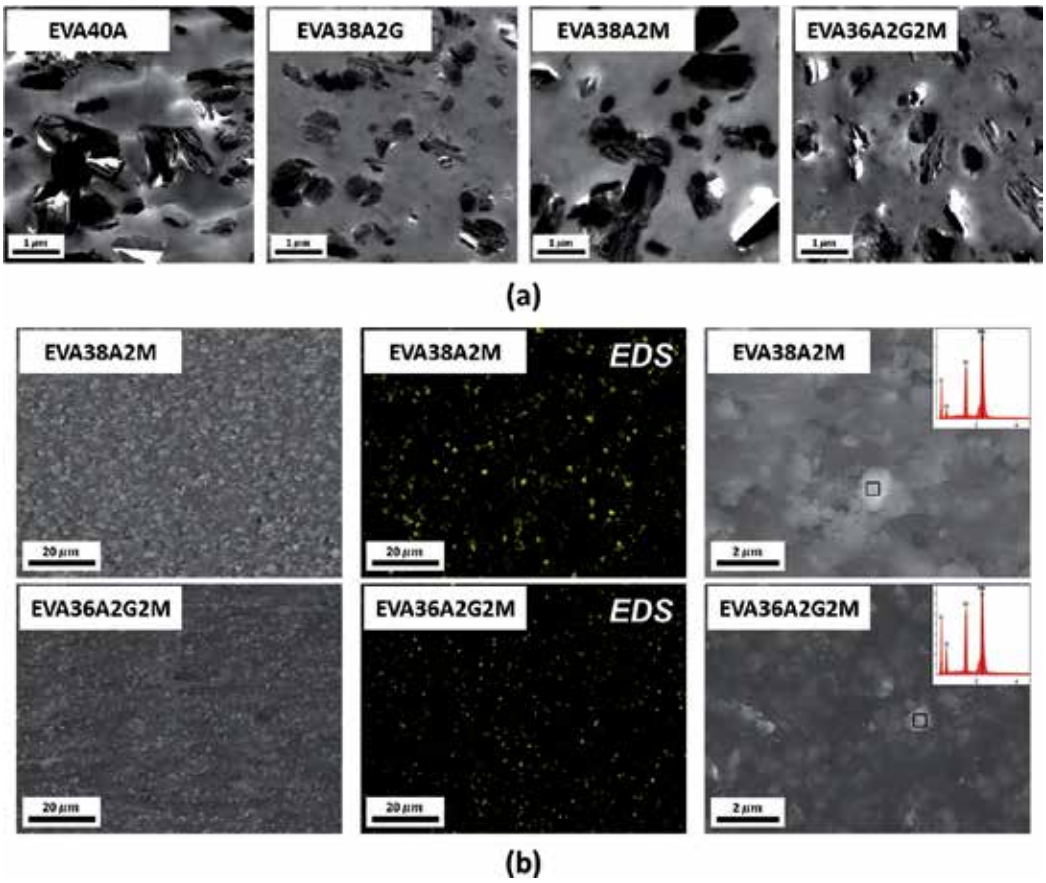

Figure 5. (a) TEM images taken on cross-sections of EVA based composites; (b) SEM and EDS mapping of EVA based composites. Annotations of abbreviations used: A—ATH, M—MoS_2 G—GNPs and numbers stands for weight ratio. Adapted from Ref. [6]. Copyright (2018) with permission from Elsevier.

images in **Figure 5(a)**. As a result, 50–60 wt.% of ATH is needed to achieve the V0 grade in UL-94 test, which will greatly decrease the ductility of EVA. When substituting 2 wt.% of ATH to MoS_2, the PHRR was reduced but a sharp peak is still observed on the heat release curve, as seen in **Figure 6**. This is because MoS_2 have formed tactoids in EVA matrix, which decreased their surface area and reducing its ability to form protective char layer. On the other hand, when further substituting 2 wt.% of ATH to GNPs, a better dispersion was observed for both ATH and MoS_2 and the heat release curve was flattened. TEM images showed that the domain size of ATH is greatly reduced and EDS mapping (**Figure 5(b)**) showed that MoS_2 was partially exfoliated. This is contributed to the large surface area of graphene platelets, which could react at the polymer/filler interface and reducing the interfacial tension. Thus, as shown in **Scheme 1**, when the EVA composite with the three-component FR system was subject to high heat flux or flame, the ATH has a higher efficiency on absorbing heat and releasing water vapor due to the improved dispersion. The exfoliated MoS_2 and GNPs will form protective char layer on the sample surface, which could reduce the peak heat release rate and flatten

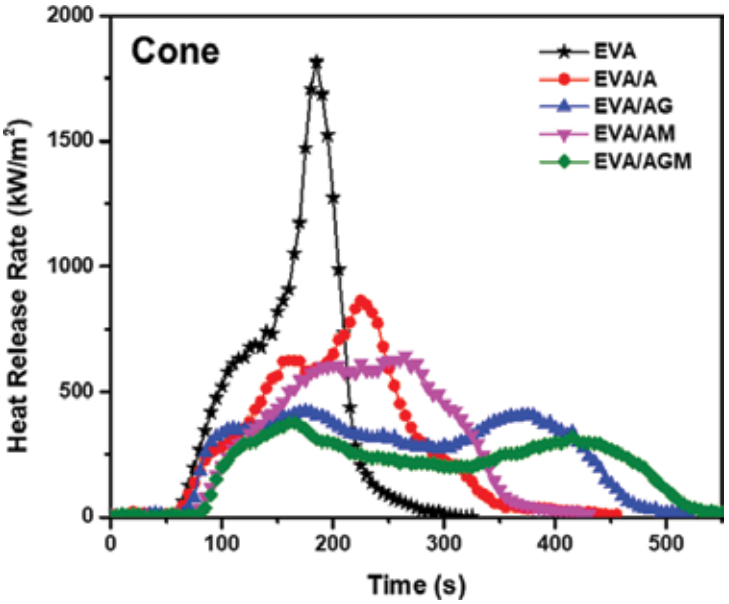

Figure 6. Cone calorimetry results of EVA composites. Reproduced from Ref. [6]. Copyright (2018) with permission from Elsevier.

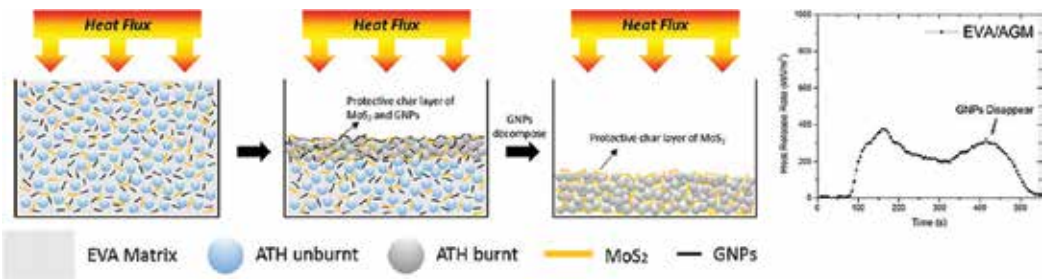

Scheme 1. The decomposition process of EVA/ATH/MoS_2/GNPs composite. Adapted from Ref. [6]. Copyright (2018) with permission from Elsevier.

the heat release curve. The GNPs will start to decompose at around 635°C, but the MoS_2 layer will continue to control the heat release. As a result, this EVA-ATH-MoS_2-GNPs composite has a PHRR of 377 kW/m^2, which is a huge reduction comparing to that of pure EVA, which is 1815 kW/m^2.

2.3. Natural nanotubes and fibers

Nanotubes such as carbon nanotube, Halloysite nanotube (HNTs), and cellulose fibers have gained increasing attentions in recent years to replace filler that have high environmental persistence [34–36]. They could also render the polymer composite to have increased mechanical properties [37]. When applied in the flame retardant composites, surface modification is commonly used to increase the flame retardancy. As previous mentioned, resorcinol bis (diphenyl

http://dx.doi.org/10.5772/intechopen.79548

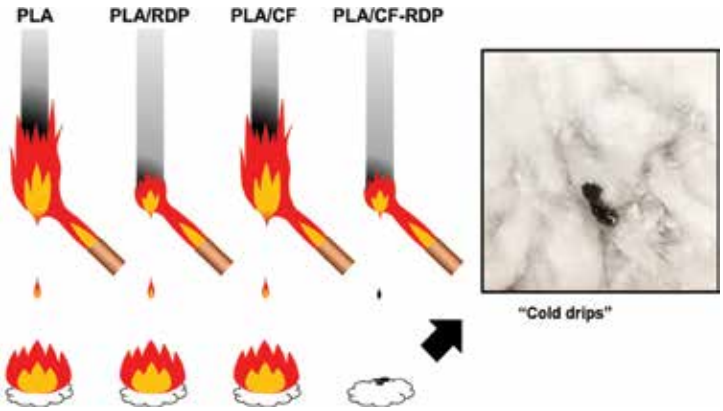

Scheme 2. An illustration of the UL-94 test process of PLA based composites. CF stands for cellulose fiber. Adapted from Ref. [5]. Copyright (2018) with permission from Elsevier.

phosphate) (RDP) is a liquid form flame retardant, which could be adsorbed on to fillers with hydroxyl groups. In the previously mentioned study [22], Guo et al. have also compared the change of work of adhesion between PLA and HNTs, with and without the RDP coating. They found that RDP coated HNTs had a higher work of adhesion to PLA than pure HNTs, which indicated that PLA wetted the RDP coating, and RDP could successfully improve the dispersion of HNTs. Thus, they used the same methodology to develop a new flame retardant PLA composite using RDP coated cellulose [5]. When subjected to flame, pure PLA burns easily with heavy dripping that could ignite the cotton on the bottom in a UL-94 test. An illustration of the burning proves is shown in **Scheme 2**. When 2 wt.% of RDP is added to the polymer, the sample could self-extinguish in 2 s, but it also induced heavy dripping due to the fact that RDP is also a liquid plasticizer. When 6 wt.% cellulose was used alone, the dripping was greatly reduced but the sample kept on burning for more than 30 s. Although neither RDP nor cellulose could make the composite pass the V0 criteria, they could significantly improve one of the factors that would lead to V0 grade. Naturally, the idea of combining the two occurred and the addition of only 8 wt.% RDP coated cellulose (CF-RDP) is needed for

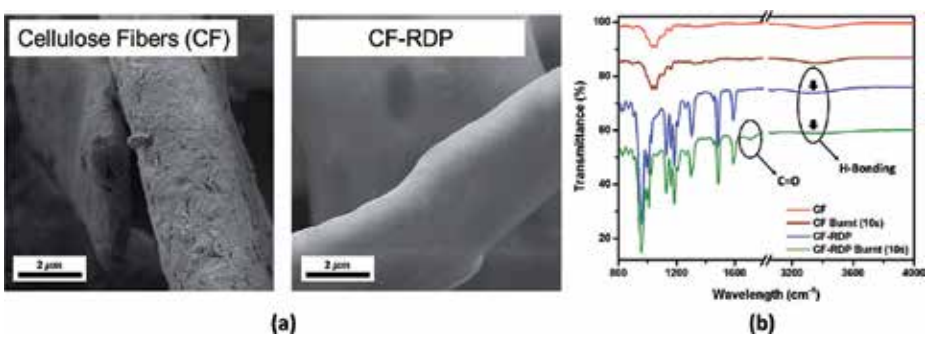

Figure 7. SEM image and FTIR spectra of cellulose fibers: (a) SEM images taken on neat cellulose fiber with and without RDP coating; (b) FTIR spectra of neat cellulose fiber and RDP-cellulose before and after 10s burning. Adapted from Ref. [5]. Copyright (2018) with permission from Elsevier.

the PLA composite to self-extinguish in 2 s and only slight dripping was observed, which is also relatively cold and did not ignite the cotton on the bottom. Further SEM imaging and FTIR tests showed that RDP completely wets the cellulose surface though the hydrogen bond between RDP and cellulose, as shown in **Figure 7**. Cellulose also immobilized RDP which help retained its ability of plasticizing and surface blooming. When PLA/CF-RDP decomposes during combustion, CF-RDP will dehydrate, where it releases water vapor and lower the temperature by absorbing heat. The dehydration of CF-RDP is confirmed by the intensity reduction of the H-bonding on the FTIR spectra.

3. Binary polymer system

Melt blending two different polymers together is one of the simplest way to produce a new material with combined properties. Yet most polymers tend to phase separate due to the large unfavorable enthalpy [38–40]. Although the block or graft copolymers could easily solve the problem, the synthesizing procedure is often system specific and expensive for industrial applications [41]. Thus, research on numerous possible compatibilizers have been done over several decades [42–45]. As briefly mentioned before, Araki et al. have developed a theory for explaining the effect of clay in compatibilizing polymer blends [30]. Two types of polymer blends were studied: polystyrene/poly(methyl methacrylate) (PS/PMMA) blend stands for when only one polymer has a favorable interaction with clay; polycarbonate/poly(styrene-co-acrylonitrile) (PC/SAN) blend stands for when both polymers have similar affinity to clay platelets. In both situations, the organoclays have successfully reduced the domain size and phase separation, and the clay platelets appeared to be adsorbed onto the polymer interface and aligned following the contour of the domain. The compatibilizing effect would generally increase with increasing clay concentration. When the domain size is reduced with better compatibility, more interface area is created to contain the increased clay content. However, the clay platelets would start to bend when the domain size is smaller than the clay radius. This would result in increasing the bending energy, as opposed to reducing the system free energy. Thus, the compatibilizing effect of clay could only work to the extend where the minimum domain size is reached. And the minimum domain size is approximately equal to the linear dimension of the filler.

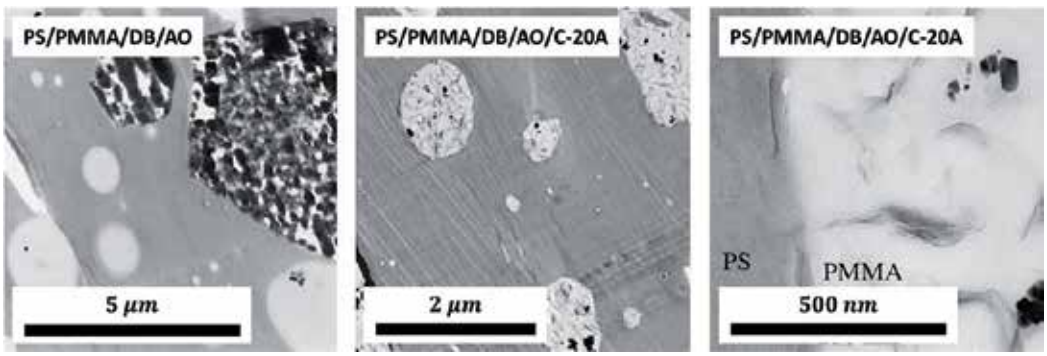

Figure 8. TEM images taken on cross-sections of PS/PMMA composites. Adapted from Ref. [2]. Copyright (2018) with permission from Elsevier.

Based on this theory, Park et al. studied the effect of clay's effect on improving flame retardant efficiency in binary polymer systems [2]. For the PS/PMMA/Microfine AO_3 (AO)/decabromodiphenyl ether (DB) blend, addition of Cloisite 20A clay (C-20A) could significantly improve the dispersion of DB and AO, shown in **Figure 8**, which result in passing the UL-94 V0 grade. C-20A clay was exfoliated in the polymer blend, and the FR agents were attached to the clay surface. Hence, the dispersion of FR agent was also improved and resulted in higher FR efficiency. However, for PC/SAN/DB/AO blend, adding C-20A did not enhance the flame retardant performance. They argue that for this blend, the attraction between clay and FR agent is larger than that between clay and the polymer blend. Thus clay has a lower degree of exfoliation and did not enhance the FR agent's dispersion. Later on, they have also discussed the effect of RDP coating [23]. RDP coated clay was added to both PS/PMMA blend and PC/SAN24 blend and two different morphologies were observed. The RDP coated clay would segregate in the PMMA domain in PS/PMMA blend, whereas it was segregated on the polymer interface in PC/SAC24 blend. This difference is attributed to the interfacial tension difference between RDP with each polymer component, and the interfacial tension of the polymer interface. In PS/PMMA blend, the interfacial tensile of RDP/PS and RDP/PMMA were both larger than that of PS/PMMA interface. In this case, the addition of RDP-clay could not reduce the overall interfacial energy. As a contrast, the interfacial energy of PC/SAN24 interface is higher than that of PC/RDP-clay. Hence, the system interfacial energy would decrease with RDP-clay segregated on the PC/SAN24 interface. Further examination on the flammability of PC/SAN24 blend with RDP-clay also showed that during combustion, the RDP-clay worked against the phase separation and stabilized the polymer blend. RDP helped reducing the brittleness of the protective char layer, which in turn reduced the heat release rate and mass loss rate.

4. Physical properties

4.1. Impact resistance

It was well known that for singular polymer matrix, the particle size and particle/polymer surface interaction have a great influence on the composite's mechanical properties [46]. By comparing between C-Na^+, C-RDP clay and C-30B clay, Guo et al. [22] concludes that the mechanical properties, such as impact strength and tensile strength, will decrease with increasing degree of exfoliation of the clay particles. This is due to the fact that the magnitude of the internal stress, which generated at the tip of the particle and could form micro-cracks, is in direct proportion to the particle aspect ratio. Given that the aspect ratio of exfoliated clay platelets could be several magnitudes larger than that of clay tactoids, it is easier for the micro-cracks to enlarge and propagate under external stress in the exfoliated polymer/clay blend. Moreover, a similar result was also found in binary polymer blends with clay [47]. When C-Na^+, C-RDP clay and C-30B clay were added to a biodegradable PLA/poly(butylene adipate-*co*-butylene terephthalate) (PBAT) blend, C-30B performs best in reducing the domain size and increasing compatibility between two polymers, as can be seen in **Figure 9**. However, the PLA/PBAT blend with clays showed a rapid and huge reduction on the impact strength even with low clay concentration, as seen in **Figure 10**. This phenomenon is explained by the theory that the clay platelets formed a strong barrier at the polymer interface, which blocked inter-diffusion between two polymers, and as a consequence, the two polymer phases were easily separated under stress.

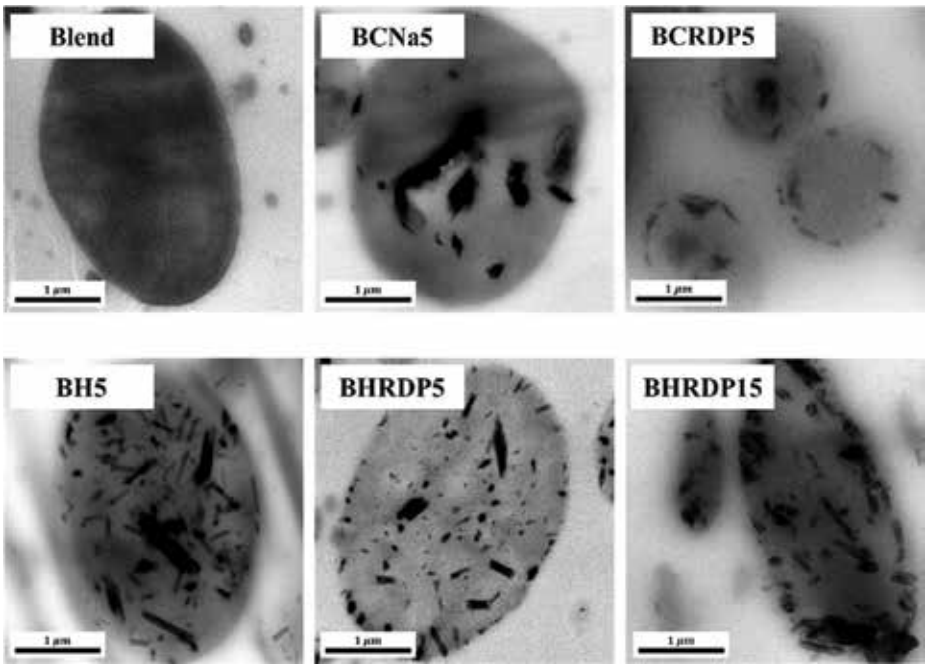

Figure 9. TEM images taken on cross-sections of PLA/PBAT based composites: (Blend) PLA/PBAT; (BCNa5) PLA/PBAT/5 wt.% of C-Na[2]; (BCRDP5) PLA/PBAT/5 wt.% of C-RDP; (BH5) PLA/PBAT/5 wt.% of HNTs; (BHRDP5) PLA/PBAT/5 wt.% of H-RDP; (BHRDP15) PLA/PBAT/15 wt.% of H-RDP. Adapted with permission from Ref. [47]. Copyright (2018) American Chemical Society.

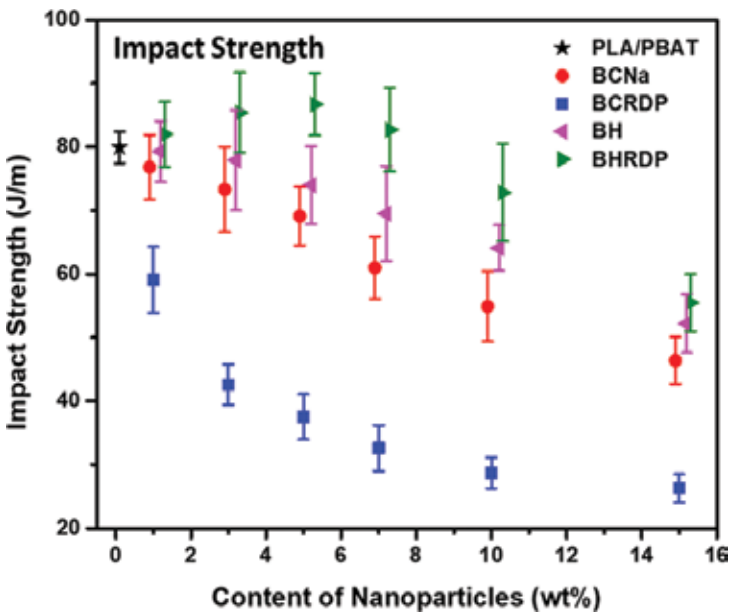

Figure 10. Impact strength of PLA/PBAT based blends. Adapted with permission from Ref. [47]. Copyright (2018) American Chemical Society.

To resolve the problem of the mechanical properties reduction, they discovered that tubular nanoparticles, such as Hollysite nanotubes, would lie perpendicular to the PLA/PBAT polymer interface instead of parallel as the clay, shown in **Figure 9**. Moreover, with this vertical orientation of HNTs particle, a "stitching" effect was observed where the impact strength first increase with the increasing HNTs concentration. The difference of particle orientation between nanotubes and clays is due to the fact that nanotubes are longer and more rigid than clay platelets. Hence, a much larger bending energy is required for nanotubes to lie along the domain curvature. As a result, the system energy is lower when nanotubes lie vertical to the polymer interface. In this way, nanotubes could enhance the interfacial diffusion and reinforce the binary polymer blend.

4.2. Ductility

For polymers that are highly flammable, high loading of flame retardant filler is generally need to render self-extinguish of the composite [48–50], which will significantly reduce the ductility of the material, making the composite hard to process. In the previous discussed three component flame retardant EVA composite [6], EVA/ATH/MoS_2/graphene, the total FR filler loading was reduced from 60 to 40 wt.%, which maintained the elasticity of pure EVA and increased the tensile modulus and tensile strength to equivalent with that of PVC, as summarized in **Table 2**. With careful examination of the individual effect of each component, they discovered that addition of MoS_2 to the EVA/ATH blend decreased the tensile modulus, strength and elongation, while addition of graphene significantly increased these mechanical properties. In the V0 blend containing all three components, the ultimate tensile strength is even higher than the EVA/ATH/graphene blend, which has the highest tensile modulus and elongation at break. This is achieved through the second quasi-elastic response, which is an indication of nanoparticles reinforcing the matrix against scission and polymer chain disentanglement. Thus, the addition of graphene platelets improved the overall FR particle dispersion which provide a larger surface area for polymer chain absorption, while MoS_2 did not have the dispersant effect which lead to reduction of its specific surface area.

Ductility is also an important property which determines the extruding conditions when the polymers are processed. In particular, the recent popularity of FDM printing requires that the ductility of the blends needs to be preserved and allow them to be drawn into uniform

Sample	Young's modulus (MPa)	Tensile strength (MPa)	Elongation at break (%)	Impact toughness (J/cm^3)	UL-94 grade
PVC	6–1120 (avg. 38.8)	1.1–29.0 (avg. 15.6)	80–920 (avg. 308)	N.A.	V-0
EVA/ATH	117.5 ± 8.6	12.6 ± 1.1	359 ± 28	39.3	V-2
EVA/ATH/MoS_2	163.5 ± 9.3	14.1 ± 1.0	306 ± 26	35.0	V-2
EVA/ATH/GNPs	261.6 ± 15.5	19.7 ± 1.6	455 ± 51	72.9	NG
EVA/ATH/MoS_2/GNPs	258.4 ± 12.2	21.5 ± 1.5	448 ± 43	70.7	V-0

Table 2. Tensile properties and impact toughness of EVA based blends. Reproduced from Ref. [6]. Copyright (2018) with permission from Elsevier.

filaments and withstand further drawing through the printer nozzles [51]. As mentioned in previous section [4], the addition of C-30B to PLA/MPP successfully improved the dispersion of MPP which provides a higher flame retardant efficiency. Through comparing the impact strength, the addition of MPP embrittles the PLA composite, while adding C-30B and MPP together restored the impact strength to the same level of pure PLA and even slight higher. Examination of the fracture surface showed that the MPP tactoids would delaminate from the PLA matrix under impact stress. With C-30B localized at the PLA/MMP interface, the micro-cracks brought by MPP tactoids were restricted by the rigid C-30B platelets. Therefore, the impact energy dissipation was improved and the PLA/MPP/C-30B blend was successfully drawn into filaments. The printed PLA/MPP/C-30B sample also achieved V0 grade in the UL-94 test. **Figure 11** summarized the comparison of cone calorimetry test result and mechanical properties between molded and printed PLA/MPP/C-30B sample. The cone calorimetry data of printed sample was similar to the molded one. The impact strength, Young's modulus, tensile strength and elongation of the printed sample was slightly lower than the molded sample, but the difference was within one statistical deviation. This is due to the incomplete fusion between the filaments during printing. Never the less, the printing process does not have a significant influence on the composite performance.

4.3. Gas permeability

Gas permeability is a very important factor for polymer materials used in packaging. Many studies have been established that layered particles have a great effect in enhancing the gas barrier effect [52, 53]. As part of their study on comparing between clay platelets and nanotubes, Guo et al. [22] derived individual equations to calculate the oxygen permeability for blends containing clay or nanotubes:

$$\frac{P}{P_o} = \frac{1-\varnothing}{1+\frac{\alpha}{2}\varnothing} \text{(for clay)} \tag{1}$$

$$\frac{P}{P_o} = \frac{1-\varnothing}{1+\frac{\pi^2-8}{16}\varnothing} \text{(for nanotubes)} \tag{2}$$

where, P is gas permeability of polymer with particle, and P_o is gas permeability of polymer without particle. $\varnothing$ is the volume fraction of nanoparticles.α is the aspect ratio of clay platelets. From the equations we could see that the aspect ratio of platelets particle could directly influence the

PLA/MPP/C30B	t_1	t_2	Dripping	Grade	LOI
Molded	1s	2s	N	V0	28.5
Printed	1s	4s	N	V0	28.5

(a)

PLA/MPP/C30B	Impact (J/m)	Modulus (GPa)	Tensile (MPa)	Elongation (%)
Molded	31.1±3.0	4.05±0.14	80.4±4.1	2.61±0.18
Printed	27.4±2.8	3.91±0.22	70.0±3.8	2.32±0.21

(b)

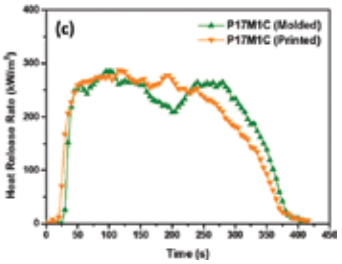

Figure 11. Comparison between molded and 3D printed PLA/MPP/C-30B blend: (a) UL-94 test results; (b) mechanical properties; (c) cone calorimetry test result. Adapted from Ref. [4]. Copyright (2018) with permission from Elsevier.

http://dx.doi.org/10.5772/intechopen.79548

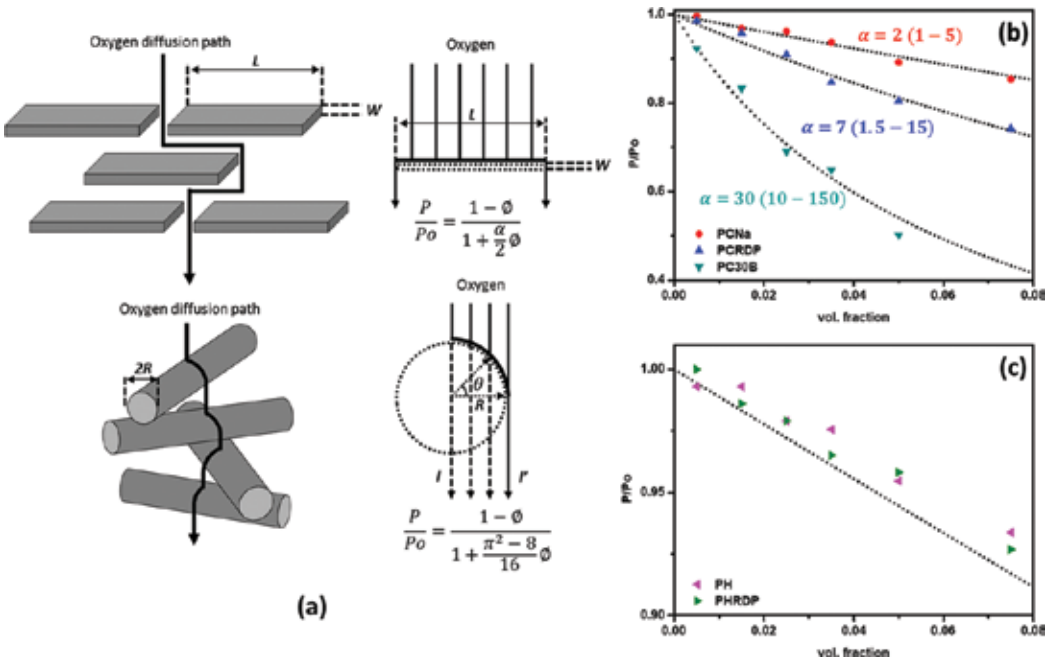

Figure 12. Gas permeability results of PLA based blends: (a) an illustration of oxygen pathway in PLA blends with clay or nanotubes; (b) comparison between calculated (dotted line) and measured values of gas permeability of PLA/clay blends; (c) comparison between calculated (dotted line) and measured values of gas permeability of PLA/nanotubes blends. Adapted from Ref. [22]. Copyright (2018) with permission from Elsevier.

gas permeability, whereas for tubular particles the gas permeability is independent on its dimension. **Figure 12** shows the comparison between the measured gas permeability and the calculated value, and a scheme of the possible pathway in PLA blends with clay or nanotubes. For clay particles, when calculating the gas permeability with the dimension of single clay platelets, the calculated result is higher than the measured result. By back calculating the α value from the measured gas permeability, the values are equivalent to the aspect ratio of the tactoids, instead of dimension of the clay platelets. Therefore, the gas permeability of polymer/clay blend is directly affected by the work of adhesion (W_a) between the polymer and the clay surface. When W_a increases, the clay platelets have a higher degree of exfoliation in the polymer matrix, which result in a smaller tactoid aspect ratio and produces low gas permeability result. On the other hand, the measured gas permeability data for polymer/HNTs blend and polymer/H-RDP blend showed only slight decreasing with increasing nanotubes concentration. This result is in good agreement with the previous equation. Moreover, there is not much difference between the gas permeability data of polymer/HNTs and polymer/H-RDP, which is in agreement with the slight difference on their W_a. In conclusion, clay platelets have a higher barrier effect than nanotubes due to their structure difference, and the barrier effect will increase with increasing degree of exfoliation.

4.4. Thermal conductivity

In addition to its compatibilizing effect and char promotion effect, the high thermal conductivity of graphene has drawn a great attention as well. Kai et al. melt blended graphene with polypropylene (PP) [54]. PP blends with carbon black and Cu microparticles, which also have

Sample	Particle concentration (wt.%)	Thermal conductivity (W/mK)
PP	100/0	0.23
PP/Cu	80/20	0.29
PP/carbon black	80/20	0.36
PP/GNPs	80/20	0.57
	70/30	1.12
	60/40	2.02
	50/50	2.31

Table 3. Thermal conductivity of PP based composites. Reproduced from Ref. [55] with open access.

high thermal conductivity, were also prepared. They found that at the same filler loading, the thermal conductivity of PP/graphene blend is two times higher than that of pure PP, as seen in **Table 3**, whereas the addition of carbon black or Cu only slightly increased the thermal conductivity. This effect is contributed to the large aspect ratio of graphene. The large surface area of graphene provides a better coupling between polymer chains and graphene. Comparing to the spherical structure of carbon black and Cu, it is easier for graphene platelets to form an efficient heat transfer path inside the polymer matrix. They also measured the thermal conductivity of PP/graphene at different graphene loading, and found that the thermal conductivity increased linearly with graphene concentration up to 50% graphene loading. Zhang et al. have stated that up to approximately 30 vol.% of filler, the thermal conductivity will first increase linearly with filler loading due to the increase in the contact area between filler and the polymer matrix [55]. Then the slop of this linear relationship will decrease because the filler starts to agglomerate within the polymer matrix and the conductive pathway was destructed. Thus, the linear relationship found by Kai et al. indicated that graphene platelets were uniformly distributed in the PP matrix. At 40% graphene loading, the thermal conductivity of PP/graphene blend is 2.0 W/mK, which is the same with flue gas in a metal heat exchanger. This result opens up the possibility of PP/graphene blends used in the application of heat exchanger which is also corrosion resistance and easy to process.

4.5. Rheology

In general, since the addition of fillers will restrict polymer chain movement, they will reinforce the polymer matrix in the rheological response. The efficiency of the reinforcement is related to the interaction between the filler and the polymer matrix. Through the comparison between the G′ dependency on frequency of PLA blend with C-Na^+, C-RDP and C-30B, Guo et al. [22] discovered that PLA/C-30B has the lowest slop at low frequency, and it is related to the fact that C-30B has the highest degree of exfoliation comparing to C-Na^+ and C-RDP, shown in **Figure 13**. PLA blends with HNTs and H-RDP have the similar result to PLA/C-30B, which indicates the nanotubes are very effective in restrict the polymer chain motion. Moreover, the PLA/H-RDP blend have a better performance than PLA/HNTs blend, which is due to the higher affinity (W_a) between the PLA and particles induced by RDP coating. When

http://dx.doi.org/10.5772/intechopen.79548

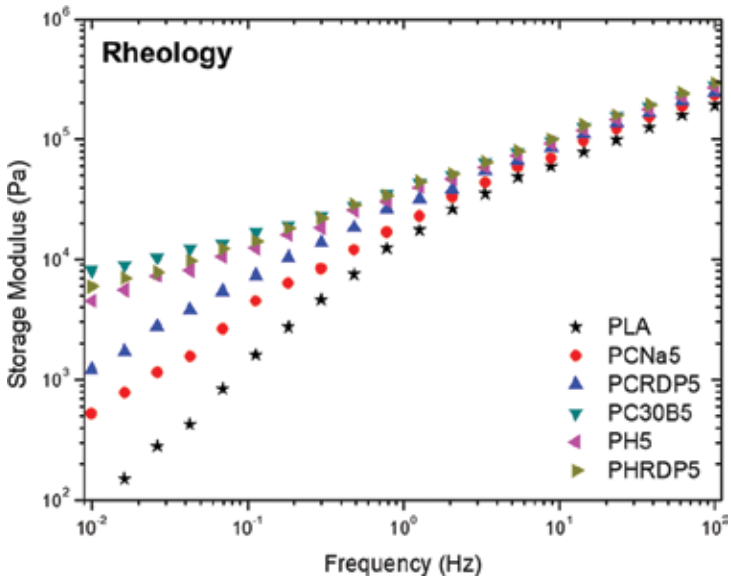

Figure 13. Rheology performance of PLA based composites. Adapted from Ref. [22]. Copyright (2018) with permission from Elsevier.

utilized in flame retardant composites, using RDP alone will decrease the G′, which results in swelling the polymer chain and reducing the strength, and also caused heavily dripping during UL-94 test [5]. By adding cellulose to the PLA matrix, the G′ was increased at low frequency, which resulted in prevent deformation and reduce dripping during combustion. Replacing cellulose by RDP coated cellulose, the G′ further increased slightly showing that the RDP coating would increase the interaction between the polymer and the cellulose fiber. Hence, the RDP coated cellulose has a higher efficiency in prevent deformation upon heating and prevent dripping during combustion.

For binary polymer systems, the morphology of the polymer phase separation and filler location play a significant role in the rheological response. In previous section, Guo, et al. [47, 56] showed that the addition of C-30B and C-RDP could effectively increase the compatibility between PLA and PBAT, while reducing the impact strength due to the strong barrier effect at the polymer interface. HNTs and H-RDP were not as effective at reducing the domain size and increasing the polymer compatibility, but the impact strength was enhanced with the "stitching" effect of nanotubes. The rheological response of PLA/PBAT blends were plotted in **Figure 14**, they found that the G′ of PLA/PBAT/C-30B and PLA/PBAT/C-RDP were both three magnitudes higher than PLA/PBAT control blend. This is attributed to the strong interaction between clay platelets and the polymers. However, at higher strain amplitude, both PLA/PBAT/C-30B and PLA/PBAT/C-RDP sample showed a G′ peak. This is identified as a stick slip motion caused by polymer chain confinement due to clay platelets blocking the polymer chain entanglement. On the G′ curve of PLA/PBAT/H-RDP blend, no peak was observed. This is also attributed to the nanotubes stay perpendicular to the polymer interface, and therefore the entanglement between two polymers was not affected.

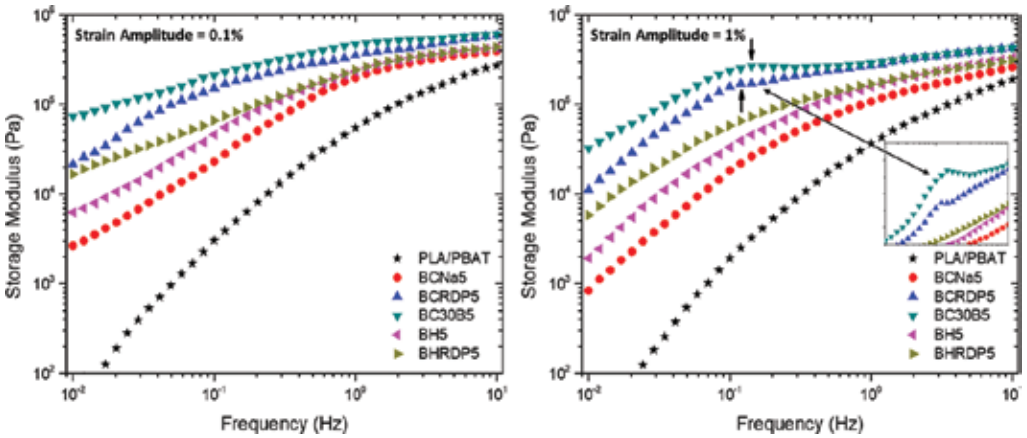

Figure 14. Rheology response of PLA/PBAT blends with clays or nanotubes. Adapted with permission from Ref. [47]. Copyright (2018) American Chemical Society.

5. Conclusion

We first reviewed the interaction between three widely used nanoparticles and singular polymer matrix. As being reported, the affinity between the nanoparticle and polymer could be determined by measuring the Young's contact angle and calculating the work of adhesion (W_a). With a higher W_a, the nanoparticle will generally achieve a higher degree of exfoliation inside the polymer matrix. In a polymer composite where flame retardant particles tend to form agglomerates, the high exfoliated nanoparticle could act as a dispersant. They will segregate at the polymer/FR particle interface and increase the interaction between these two. As a result, the dispersion of the flame retardant particle is improved, as well as a higher flame retardant efficiency, which will render the polymer composite pass the V0 rating in UL-94 test at a lower filler content. We also looked at the surface interaction of nanoparticles in binary polymer systems, they perform in a similar mechanism as in the singular polymer system, where the dispersion of the flame retardant additive is improved and the phase separation is reduced. Moreover, the addition of the nanoparticles has a significant influence on the mechanical properties of the polymer composite. In a singular polymer matrix, when clay platelets were added, the impact strength will decrease with increasing degree of clay exfoliation, due to the high magnitude of internal stress created at the tip of exfoliated clay platelets. In binary polymer blends, the addition of clay will also decrease the impact resistance by localizing at the polymer interface and blocking the polymer chain entanglement across the interface. Tubular nanoparticle, on the other hand, will lie perpendicular to the polymer interface, which will enhance the impact and tensile properties by a "stitching" effect. Rheology performance was affected in the similar way as the impact and tensile properties. Clay has also been proved to have a higher improvement on the gas barrier effect than tubular particles. Large aspect ratio particles with high thermal conductivity, such as graphene, could also be used in applications for developing corrosion-resistant polymer composites for heat exchangers. In sum, the usage of nanoparticles could greatly increase the flame retardant efficiency by improving the filler dispersion in the polymer matrix, as well as other physical properties.

Author details

Yuan Xue, Yichen Guo* and Miriam H. Rafailovich

*Address all correspondence to: guoichen@gmail.com

Department of Materials Science and Engineering, Stony Brook University, New York, USA

References

[1] Lubin G. Handbook of Composites. Springer Science & Business Media; 2013

[2] Pack S et al. Mode-of-action of self-extinguishing polymer blends containing organoclays. Polymer Degradation and Stability. 2009;**94**(3):306-326

[3] Si M et al. Self-extinguishing polymer/organoclay nanocomposites. Polymer Degradation and Stability. 2007;**92**(1):86-93

[4] Guo Y et al. Engineering flame retardant biodegradable polymer nanocomposites and their application in 3D printing. Polymer Degradation and Stability. 2017;**137**:205-215

[5] Guo Y et al. Incorporation of cellulose with adsorbed phosphates into poly (lactic acid) for enhanced mechanical and flame retardant properties. Polymer Degradation and Stability. 2017;**144**:24-32

[6] Guo Y et al. Capitalizing on the molybdenum disulfide/graphene synergy to produce mechanical enhanced flame retardant ethylene-vinyl acetate composites with low aluminum hydroxide loading. Polymer Degradation and Stability. 2017;**144**:155-166

[7] Li N et al. Influence of antimony oxide on flammability of polypropylene/intumescent flame retardant system. Polymer Degradation and Stability. 2012;**97**(9):1737-1744

[8] Alaee M et al. An overview of commercially used brominated flame retardants, their applications, their use patterns in different countries/regions and possible modes of release. Environment International. 2003;**29**(6):683-689

[9] Sain M et al. Flame retardant and mechanical properties of natural fibre–PP composites containing magnesium hydroxide. Polymer Degradation and Stability. 2004;**83**(2):363-367

[10] Wang D-Y et al. Preparation and burning behaviors of flame retarding biodegradable poly (lactic acid) nanocomposite based on zinc aluminum layered double hydroxide. Polymer Degradation and Stability. 2010;**95**(12):2474-2480

[11] Zhang S et al. Intercalation of phosphotungstic acid into layered double hydroxides by reconstruction method and its application in intumescent flame retardant poly (lactic acid) composites. Polymer Degradation and Stability. 2018;**147**:142-150

[12] Wang X et al. Controllable fabrication of zinc borate hierarchical nanostructure on brucite surface for enhanced mechanical properties and flame retardant behaviors. ACS Applied Materials & Interfaces. 2014;**6**(10):7223-7235

[13] Chen S et al. Intumescent flame-retardant and self-healing superhydrophobic coatings on cotton fabric. ACS Nano. 2015;**9**(4):4070-4076

[14] Zhu C et al. Synthesis and application of a mono-component intumescent flame retardant for polypropylene. Polymer Degradation and Stability. 2018;**151**:144-151

[15] Baekeland LH. Bakelite, a new composition of matter: Its synthesis, constitution, and uses. Scientific American, Suppl. 1909;**68**:322

[16] Goodyear C. Dinglers Polytechnisches Journal. 1856;**139**:376

[17] Balazs AC, Emrick T, Russell TP. Nanoparticle polymer composites: Where two small worlds meet. Science. 2006;**314**(5802):1107-1110

[18] Morgan AB, Wilkie CA. Practical Issues and Future Trends in Polymer Nanocomposite Flammability Research. New York, NY, USA: John Wiley & Sons; 2007

[19] Laoutid F et al. New prospects in flame retardant polymer materials: from fundamentals to nanocomposites. Materials Science and Engineering: R: Reports. 2009;**63**(3):100-125

[20] Ray SS et al. New polylactide/layered silicate nanocomposite: Nanoscale control over multiple properties. Macromolecular Rapid Communications. 2002;**23**(16):943-947

[21] <MSDS - Quaternary Ammonium Chloride.pdf>.

[22] Guo Y et al. Effects of clay platelets and natural nanotubes on mechanical properties and gas permeability of poly(lactic acid) nanocomposites. Polymer. 2016;**83**:246-259

[23] Pack S et al. Role of surface interactions in the synergizing polymer/clay flame retardant properties. Macromolecules. 2010;**43**(12):5338-5351

[24] Modro AM, Modro TA. The phosphoryl and the carbonyl group as hydrogen bond acceptors. Canadian Journal of Chemistry. 1999;**77**(5-6):890-894

[25] Jang BN, Wilkie CA. The effects of triphenylphosphate and recorcinolbis(diphenylp hosphate) on the thermal degradation of polycarbonate in air. Thermochimica Acta. 2005;**433**(1):1-12

[26] Granzow A. Flame retardation by phosphorus compounds. Accounts of Chemical Research. 1978;**11**(5):177-183

[27] Gross RA, Kalra B. Biodegradable polymers for the environment. Science. 2002;**297**(5582): 803-807

[28] Bourbigot S, Fontaine G. Flame retardancy of polylactide: An overview. Polymer Chemistry. 2010;**1**(9):1413-1422

[29] Fontaine G, Bourbigot S. Intumescent polylactide: A nonflammable material. Journal of Applied Polymer Science. 2009;**113**(6):3860-3865

[30] Si M et al. Compatibilizing bulk polymer blends by using organoclays. Macromolecules. 2006;**39**(14):4793-4801

[31] Lee C et al. Measurement of the elastic properties and intrinsic strength of monolayer graphene. Science. 2008;**321**(5887):385-388

[32] Stankovich S et al. Graphene-based composite materials. Nature. 2006;**442**(7100):282

[33] Feng X et al. Studies on synthesis of electrochemically exfoliated functionalized graphene and polylactic acid/ferric phytate functionalized graphene nanocomposites as new fire hazard suppression materials. ACS Applied Materials & Interfaces. 2016;**8**(38):25552-25562

[34] Sinha Ray S et al. New polylactide/layered silicate nanocomposites. 1. Preparation, characterization, and properties. Macromolecules. 2002;**35**(8):3104-3110

[35] Jonoobi M et al. Mechanical properties of cellulose nanofiber (CNF) reinforced polylactic acid (PLA) prepared by twin screw extrusion. Composites Science and Technology. 2010;**70**(12):1742-1747

[36] Iwatake A, Nogi M, Yano H. Cellulose nanofiber-reinforced polylactic acid. Composites Science and Technology. 2008;**68**(9):2103-2106

[37] Lu Y et al. Improved mechanical properties of polylactide nanocomposites-reinforced with cellulose nanofibrils through interfacial engineering via amine-functionalization. Carbohydrate Polymers. 2015;**131**:208-217

[38] Bates FS. Polymer-polymer phase behavior. Science. 1991;**251**(4996):898-905

[39] Van de Witte P et al. Phase separation processes in polymer solutions in relation to membrane formation. Journal of Membrane Science. 1996;**117**(1-2):1-31

[40] Nishi T, Wang T, Kwei T. Thermally induced phase separation behavior of compatible polymer mixtures. Macromolecules. 1975;**8**(2):227-234

[41] Paul DR, Bucknall CB. Polymer Blends. Wiley; 2000

[42] Tanaka H, Lovinger AJ, Davis DD. Pattern evolution caused by dynamic coupling between wetting and phase separation in binary liquid mixture containing glass particles. Physical Review Letters. 1994;**72**(16):2581

[43] Ginzburg VV et al. Simulation of hard particles in a phase-separating binary mixture. Physical Review Letters. 1999;**82**(20):4026

[44] Zhou Y et al. Nanorods with different surface properties in directing the compatibilization behavior and the morphological transition of immiscible polymer blends in both shear and shear-free conditions. Macromolecules. 2018;**51**(8):3135-3148

[45] Cho KY et al. Highly enhanced electromechanical properties of PVDF-TrFE/SWCNT nanocomposites using an efficient polymer compatibilizer. Composites Science and Technology. 2018;**157**:21-29

[46] Fu S-Y et al. Effects of particle size, particle/matrix interface adhesion and particle loading on mechanical properties of particulate–polymer composites. Composites Part B: Engineering. 2008;**39**(6):933-961

[47] Guo Y et al. Enhancing the mechanical properties of biodegradable polymer blends using tubular nanoparticle stitching of the interfaces. ACS Applied Materials & Interfaces. 2016;**8**(27):17565-17573

[48] Hoffendahl C et al. The combination of aluminum trihydroxide (ATH) and melamine borate (MB) as fire retardant additives for elastomeric ethylene vinyl acetate (EVA). Polymer Degradation and Stability. 2015;**115**:77-88

[49] Yen Y-Y, Wang H-T, Guo W-J. Synergistic flame retardant effect of metal hydroxide and nanoclay in EVA composites. Polymer Degradation and Stability. 2012;**97**(6):863-869

[50] Cavodeau F et al. Fire retardancy of ethylene-vinyl acetate composites—Evaluation of synergistic effects between ATH and diatomite fillers. Polymer Degradation and Stability. 2016;**129**:246-259

[51] Krishnaswamy RK. Analysis of ductile and brittle failures from creep rupture testing of high-density polyethylene (HDPE) pipes. Polymer. 2005;**46**(25):11664-11672

[52] Sinha Ray S et al. Polylactide-layered silicate nanocomposite: A novel biodegradable material. Nano Letters. 2002;**2**(10):1093-1096

[53] Tenn N et al. Effect of nanoclay hydration on barrier properties of PLA/montmorillonite based nanocomposites. The Journal of Physical Chemistry C. 2013;**117**(23):12117-12135

[54] Yang K et al. The thermo-mechanical response of PP nanocomposites at high graphene loading. Nano. 2015;**1**(3):126-137

[55] Zhang S et al. The effects of particle size and content on the thermal conductivity and mechanical properties of Al_2O_3/high density polyethylene (HDPE) composites. Express Polymer Letters. 2011;**5**(7):581-590

[56] Guo Y et al. Enhancing impact resistance of polymer blends via self-assembled nanoscale interfacial structures. Macromolecules. 2018;**51**(11):3897-3910

Section 4

Computational analysis

Chapter 4

Stochastic Finite Element Modelling of Char Forming Filler Addition and Alignment – Effects on Heat Conduction into Polymer Condensed Phase

Hamidreza Ahmadi Moghaddam and Pierre Mertiny

Additional information is available at the end of the chapter

http://dx.doi.org/10.5772/intechopen.82878

Abstract

Micro- and nano-filler particles have been considered as char-forming flame retardants for polymers. It has been shown that suitable particles may operate in the condensed phase to prevent or delay the escape of fuel into the gas phase. Good flame retardancy performance may be achieved in composites with comparatively low filler loadings. However, many candidate filler materials, such as rod-like and plate-like carbon allotrope fillers with high aspect ratio, will effectively enhance the composite's thermal conductivity, and hence, may greatly increase heat input into the condensed phase. Moreover, anisotropy in terms of thermal conductivity must be considered when rod-like and plate-like particles are aligned, for example as a result of manufacturing processes. The presented study investigates these effects, i.e., thermal conductivity enhancement due to filler addition and alignment, using a modeling framework based on Monte Carlo simulation that was developed for predicting effective composite properties considering filler-matrix and particle-to-particle interfacial effects. A stochastic finite element analysis was performed to model rod-shaped carbon particles embedded in a polymer matrix. The chosen analysis is demonstrated to be an effective means for elucidating the effect of filler addition and alignment on the heat conduction into polymer materials containing fillers as char-forming flame retardants.

Keywords: filler modified polymer composites, char-forming flame retardants, thermal conductivity, stochastic finite element analysis, Monte Carlo simulation

1. Introduction

The advent of engineered nanoparticles with high aspect ratio, such as graphene and carbon nanotubes (CNT), and their availability in quantities relevant for industrial production, has greatly expanded opportunities to modify polymers to meet demanding requirements in a broad range of applications. Such nano-additives have been shown to improve polymer mechanical (e.g., stiffness, strength and fracture properties) as well as physical characteristics (e.g., electrical and thermal conductivity), see e.g., [1–6]. The same holds true in the context of flame retardancy. Among the three commonly considered flame retardant approaches—i.e., gas phase flame retardants, endothermic flame retardants, and char-forming flame retardants —nanofillers are typically active via the latter mechanism. Nanofillers operate in the polymer condensed phase where they may provide thermal insulation and a mass transport barrier that mitigates the release of fuel into the gas phase. Nanocomposites with suitable filler morphology and loading were observed to form a coherent filler network layer covering sample surfaces, which significantly reduced peak heat release and radiant heat flux [7]. In addition to the char-forming mechanism, nanofillers were found to reduce the melt flow of polymers. High aspect ratio nano-additives were reported to form jammed network structures causing melt to behave rheologically like a gel, thus inhibiting dripping of flammable material [8].

While the potential of nano-fillers to enhance flame retardancy through increased barrier properties impeding heat flux and fuel release, and altered rheological properties inhibiting flammable drips, has widely been acknowledged in the technical literature, the influence of filler addition on increased thermal conductivity and thus heat transfer into the polymer still requires further study [1]. Carbon-based fillers possess thermal conductivities that exceed those of polymers by several orders of magnitude. For example, thermal conductivity ranging from 2000 to 5000 W m^{-1} K^{-1} has been reported for CNT and graphene while values for typical polymers are between 0.1 and 0.3 W m^{-1} K^{-1} [9, 10]. Assessing and understanding thermal conduction in nanocomposites with high aspect ratio fillers is particular complex due to the inherent propensity of filler contact, alignment and agglomeration.

Besides randomly oriented and dispersed particles, polymer nanocomposites with purposely aligned particulate fillers have been created, which resulted in improved performance in a variety of applications. Nanocomposites with aligned particles have been used for the design of sensors [11–13] and high-strength modified polymers that require particle alignment in order to achieve specific anisotropic properties [14–16]. Carbon nanotubes, as a 'one-dimensional' high aspect ratio carbon allotrope, are especially suited to create nanocomposites with anisotropic properties, e.g., in terms of heat transfer properties [17–22].

Determining the mechanical and physical properties using experimental methods is typically a time-consuming and costly approach. Analytical methods, on the other hand, are highly efficient for predicting effective material properties of particulate composites [23]. However, analytical methods lack accuracy when predicting properties, especially for higher filler volume fraction modified polymers. Considering these limitations, and in light of a rapidly growing number of applications involving particulate composites, experimental and analytical approaches are not sufficient to address the demands imposed by a vast field of available filler

http://dx.doi.org/10.5772/intechopen.82878

materials and fabrication parameters. Hence, alternative methods for assessing and designing filler modified composites need to be developed [24–26].

Stochastic analysis is one of the most reliable and recognized methods for analyzing complex problems involving many input and output parameters in the field of reliability analysis. This method can predict accurate outcomes using statistical principles. Stochastic analysis can be used in a variety of applications, e.g., financial forecasting and modeling, where numerous input and output variables need to be considered. Recently, a numerical modeling framework was developed based stochastic analysis to simulate the effective material properties of filler modified composites [27]. Specifically, a stochastic finite element analysis (SFEA) approach was employed that enabled the prediction of the effective thermal conductivity of randomly distributed and disperses spherical particles embedded in a polymer matrix. In the present contribution, aforementioned SFEA approach was adopted to predict the effective thermal conductivity of a polymer matrix containing randomly oriented or aligned rod-shaped filler particles. The particle geometry was adapted to mimic CNT. The study described herein investigates the effect of filler addition and alignment on heat transfer into polymer composites in the context of fire-retardant materials.

2. Stochastic finite element analysis framework

The nature of stochastic analysis, and thus the presented modeling approach, requires performing numerous iterations in order to calculate the effective thermal conductivity of a polymer matrix containing a rod-shaped filler. The SFEA algorithm described in [27] was adopted and employed for the present study. This algorithm provides a framework for connecting a customized stochastic analysis with a parametric finite element analysis (FEA). In this manner, the process of applying uncertainty to input variables, and creating and solving FEA models is automated. The modeling framework, which uses several scripting languages, is briefly summarized in the present section. The interested reader is referred to [27] for additional details on the modeling approach. **Figure 1** depicts a flowchart outlining the main domain, i.e., the elemental structure and connections, of the framework's various modules.

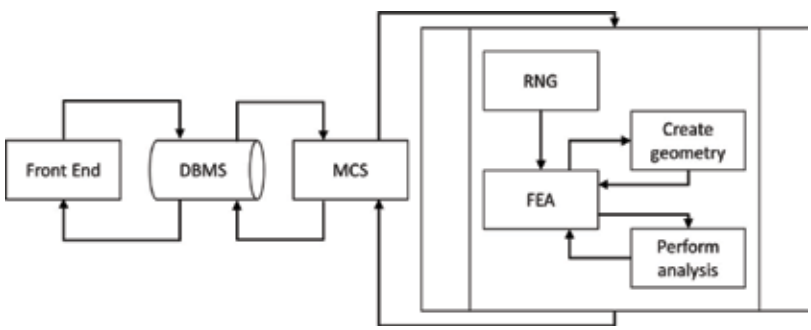

Figure 1. Stochastic finite element analysis framework [27].

The main domain was developed in Visual Basic for Applications scripting language (VBA; Microsoft, Redmond, Washington, USA). Input parameters are provided via the 'Front End' module. The set of required input parameters comprises (i) the modeling domain that is defined by the size of the considered cubic representative volume element (RVE); (ii) a set of filler volume fractions that are to be analyzed; (iii) the material properties for the filler and matrix; (iv) the filler particle size distribution; (v) information on boundary effects, i.e., particle-to-particle and particle-to-matrix interfacial thermal resistance (ITR) as well as a threshold gap size that defines direct contact between particles and particles to the RVE boundary; (vi) details for the FEA mesh generation; and (vii) details regarding the model output acceptance criteria required for statistical analyses, i.e., standard deviation and variance. The input parameters are transferred to a database with an appropriate management system ('DBMS'), which holds and communicates input and computed data between the various modules.

The Monte Carlo simulation (MCS) module, also developed using VBA scripting language, performs two subprocesses, i.e., the random number generator (RNG) and the FEA modeling. Using the algorithm depicted in **Figure 2**, the MCS module retrieves needed input parameters from the database, performs iteratively the SFEA, computes statistical data (standard deviation and variance) after each iteration, and finally stores results back into the database. The MCS module repeats the modeling subprocess until the acceptance criteria defined in the database are satisfied. Once results converge according to the criteria specified, the MCS module determines the effective thermal conductivity (by calculating an average value). The MCS module repeats the above processes until all specified filler volume fractions are analyzed.

The RNG module was developed in the numerical computing environment MATLAB (MathWorks, Natick, Massachusetts, USA), which has pseudorandom number generating capabilities. This module retrieves the input data defining the RVE size and the particle size distribution from the database. The RNG module sequentially creates sets of random numbers for anchor points in Cartesian coordinates as well as vectors required for generating the

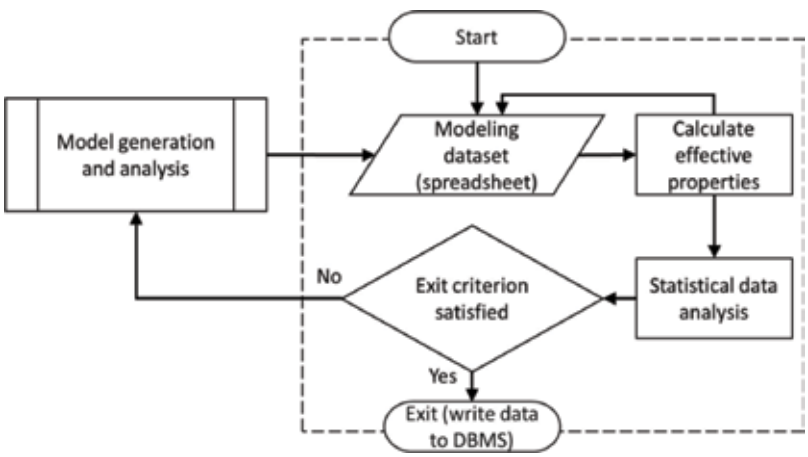

Figure 2. Monte Carlo simulation (MCS) module algorithm [27].

http://dx.doi.org/10.5772/intechopen.82878

position and orientation of rod-shaped filler particle geometries, respectively. The RNG module also performs a collision detection using a geometrical model to avoid particles interfering with each other as well as with the RVE surfaces. When detecting interference, the RNG rejects the most recently generated particle. In the geometrical model, the rod-shaped particle geometry is represented by a series of spheres (see **Figure 3**). The distance between each sphere associated with the most recent rod-shaped particle and all preexisting sphere geometries in the RVE, and the RVE boundaries, is evaluated to discern a particle collision. While representing rod-shaped particles using a series of spheres is only an approximation, it provides an expedient means for performing the collision detection algorithm. For the analyses presented herein, as series of 200 spheres was used to represent rod-shaped particles for interference detection.

The process performed by the RNG module can be controlled to yield both randomly oriented and aligned rod-shaped particles within the RVE. In the case of aligned particles, constraints are imposed on the vector indicating particle orientation. As shown in **Figure 4**, after generating the set of random numbers for each particle, these data are stored in the database in a tabulated format for later use by the FEA module. The RNG module iteration is terminated when the required filler volume fraction is reached.

It should be mentioned that the RNG module also has the ability of creating particles that conform to a given size distribution (whilst, this feature was not utilized in the present study). The interested reader is referred to [27] for details on the algorithm that produces particles obeying a certain size distribution, and the effect that different size-ordered particle addition has on computational performance.

The FEA module was developed as a fully customizable parametric FEA platform in ANSYS Workbench (Version 19, ANSYS Inc., Canonsburg, PA, USA) using IronPython scripting language, which enabled applying uncertainties to input parameters required for performing the FEA simulation. This platform consists of a model generation environment, i.e., ANSYS DesignModeler, and a model solution environment, i.e., ANSYS Mechanical, which enable creating the parametric geometry and the finite element model, respectively. JAVA scripting language was used to automate the process of reading input data from the database (i.e., RVE dimensions and particle anchor points and orientation vectors) and creating particle geometries in the model generation environment. The three-dimensional geometry thus created is transferred to the model solution environment for further analysis. Similar to the model generation environment, the model solution environment also uses JAVA scripting language to automate the FEA process. The model solution environment retrieves further inputs parameters

Figure 3. Schematic of series of spheres representing rod-shaped particles.

from the database, including material properties, information on boundary effects and conditions, and mesh generation parameters, and then constructs the finite element model for each model iteration. After performing the analysis, the FEA results are saved to the database in tabulated format for further statistical analysis. **Figure 5** illustrated the algorithm for the FEA module.

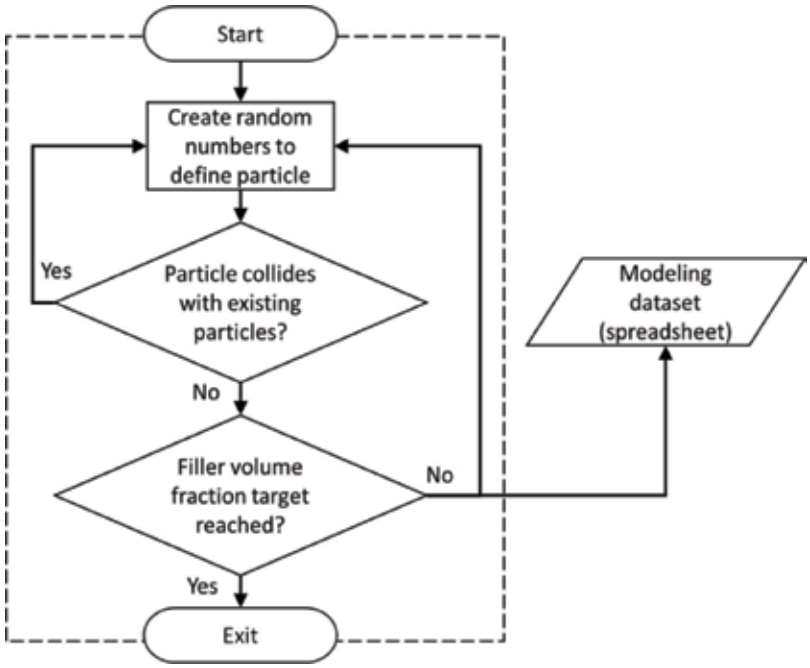

Figure 4. Random number generator algorithm [27].

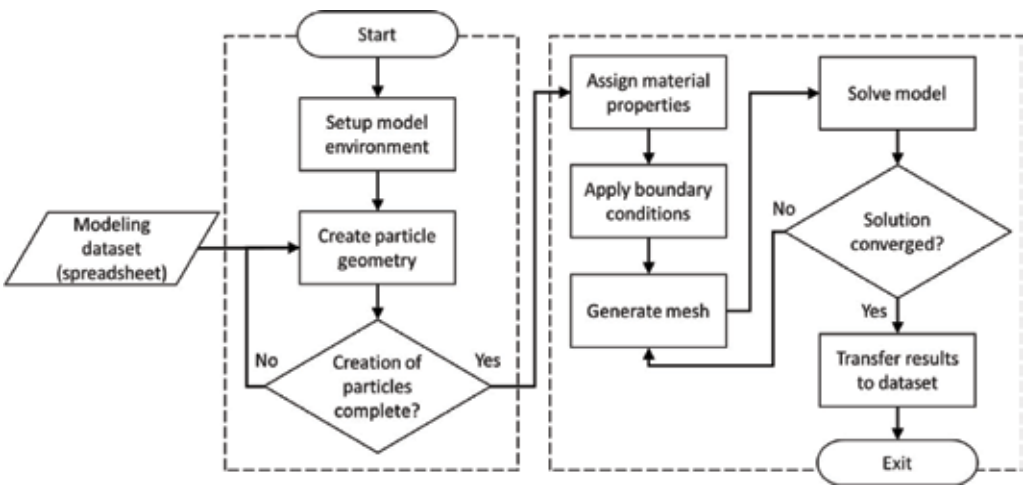

Figure 5. FEA module algorithm [27].

http://dx.doi.org/10.5772/intechopen.82878

3. Steady-state numerical modeling

The developed SFEA framework was employed to estimate the effective thermal conductivity under steady-state conditions of filler modified composites with randomly and aligned rod-shaped particles embedded in a polymer matrix. The rod-shaped particles mimic CNT embedded in epoxy polymer in order to elucidate the effect of filler addition and alignment in the context of fire-retardant materials. **Table 1** shows the CNT longitudinal and lateral thermal properties and volumetric mass density, which were adopted from [9, 28, 29]. The mean particle diameter was set to 2.85 nm with a constant particle aspect ratio of 56, i.e., only a single particle size was utilized in this study to limit the parameter space affecting the results. The RVE size was set 200 nm.

Since CNT have anisotropic thermal properties it is not possible to define their thermal conductivity using global coordinates. Hence, an algorithm was developed in JAVA scripting language that provides dedicated local Cartesian coordinates for each rod-shaped particle. As depicted in **Figure 6**, the local coordinates (x,y,z) have their origin at one end of a particle with the x-direction aligning with the particle's longitudinal axis. For the case of aligned particles the components describing the vector for each particle's major axis (x) were constrained to

Material	Epoxy	CNT
Density [kg m^{-3}]	1250	1600
Thermal conductivity, longitudinal [W m^{-1} K^{-1}]	0.25	3500
Thermal conductivity, lateral [W m^{-1} K^{-1}]	0.25	1.5

Table 1. Volumetric mass density and thermal conductivity of polymer and CNT [9, 28, 29].

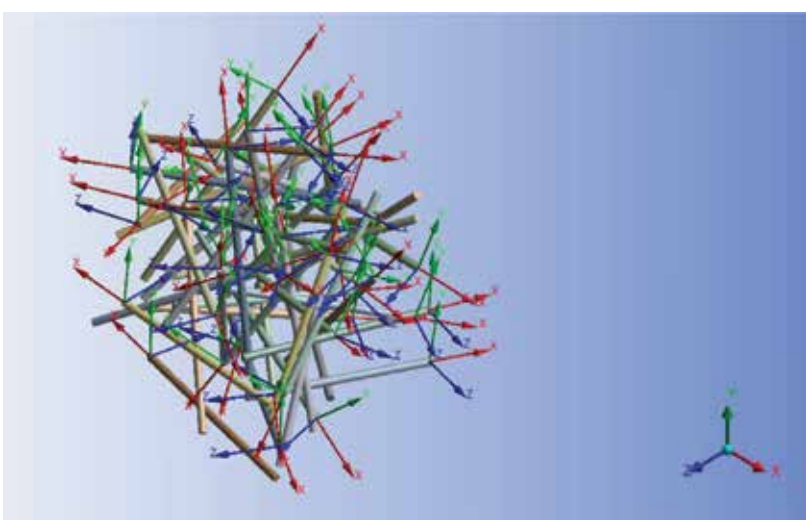

Figure 6. Illustration of local coordinate systems for rod-shaped particles.

remain within upper and lower bounds. For the present analyses, these constraints correspond to a maximum possible angle of approximately 8.5° between a particle's major axis (x) and the global (RVE) X-direction.

Three-dimensional ten-node quadratic tetrahedral thermal solid elements, i.e., SOLID87, were used to generate the finite element mesh for both the particles and matrix. This element type, which provides one degree of freedom (temperature), is recommended for meshing irregular geometries. The latter characteristic is desirable in the present context, given that the rod-shaped particles constitute geometries that typically are difficult to mesh. As an example, **Figure 7** depicts the meshing generated for the matrix (left-hand side) and randomly distributed and aligned rod-shaped particles occupying the RVE devoid matrix (right-hand side).

As demonstrated in [27], it is essential to model the ITR between particles and the matrix as well as between particles that are in contact with each other in order to achieve a model that realistically captures effective thermal conductivities for different filler loadings. In this study the particle-to-matrix thermal contact conductance (TCC) was adopted from literature [30–32] as 10^8 W m^{-2} K^{-1}. Also, the direct particle-to-particle heat transfer threshold was set to approximately 1 nm. Note that implementing this threshold is necessary since the employed particle collision algorithm prevents true direct particle-to-particle contact. ITR and particle-to-particle thermal contact was implemented using three-dimensional 6-node quadratic surface-to-surface elements, i.e., CONTA174 and TARGE170. For details on the chosen approach to model contact phenomena the readers is referred to [27].

Thermal boundary conditions were applied to the RVE to perform the stead-state thermal analysis and calculate effective thermal conductivities. A temperature 22 and 32°C were defined on opposite sides of the RVE, respectively, with the remaining surfaces considered adiabatic. Note that for the case of aligned filler particles, the alignment direction is referred to as the

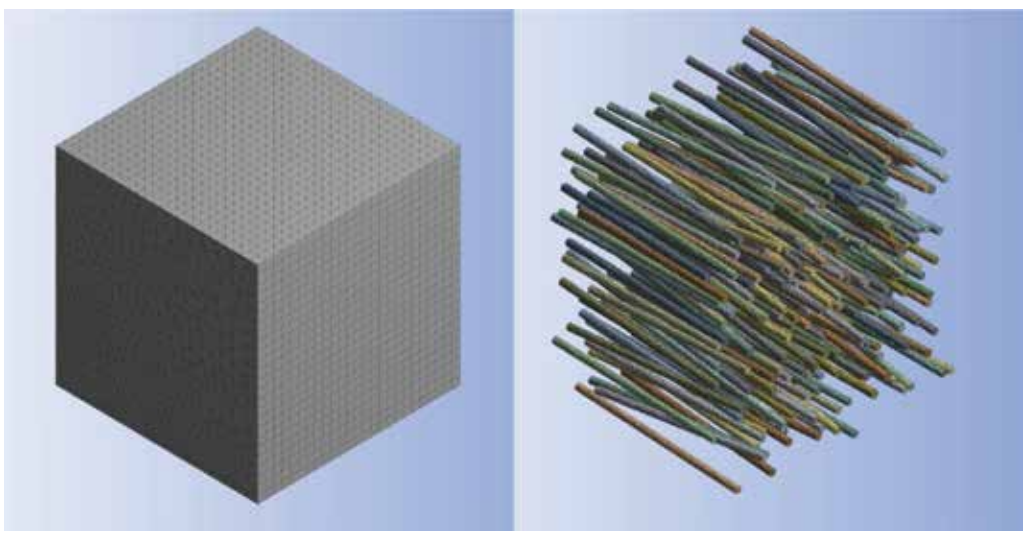

Figure 7. Finite element mesh of matrix (left) and aligned rod-shaped particles occupying the RVE devoid matrix (right).

http://dx.doi.org/10.5772/intechopen.82878

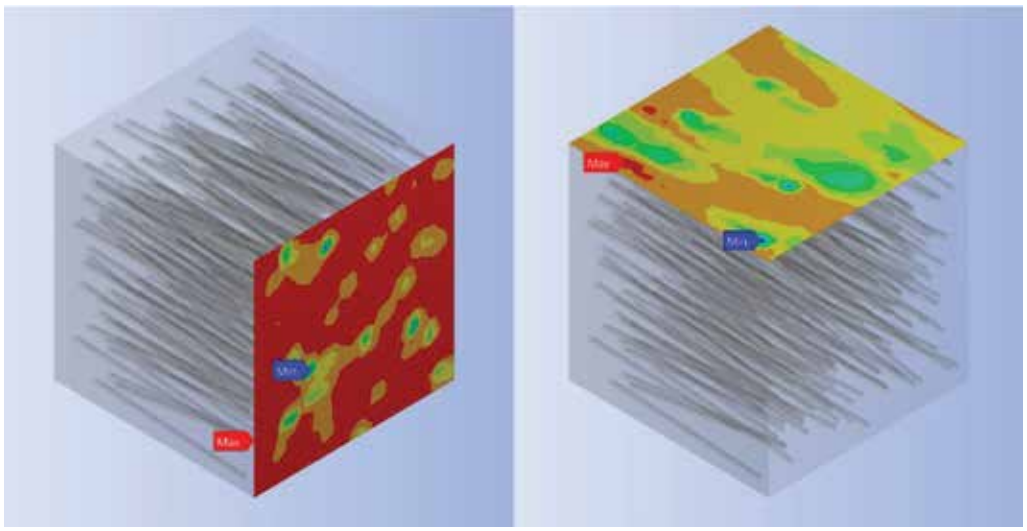

Figure 8. Illustration of longitudinal (left) and lateral (right) heat flux between opposing warm and cold RVE surfaces.

longitudinal direction, as opposed to the two lateral directions that are defined in a Cartesian coordinate system. Three sets of boundary conditions were also applied for randomly distributed filler particles for determining the effective thermal conductivities along the global Cartesian coordinate directions (X,Y,Z), thus enabling the assessment of isotropy. The applied boundary conditions create a temperature gradient and thus a heat flux between the warm and cold RVE surfaces, as illustrated in **Figure 8**. The thermal conductivity of nodes K_i located in the warm surface was determined using Eq. (1).

$$K_i = \frac{Q_i \times l}{T_2 - T_1} \tag{1}$$

where Q_i is the calculated numerical total heat flux at the ith node located on the warm side, l is the RVE length, and T_1 and T_2 correspond the temperature on the warm and cold surface, respectively. Consequently, Eq. (2) yields the effective thermal conductivity, K_{eff}.

$$K_{\text{eff}} = \frac{\sum_{i=1}^{n} K_i}{n} \tag{2}$$

where n is total number nodes on the warm surface of the RVE.

4. Results and discussion

The described modeling framework was employed to calculate effective thermal conductivities of composites with randomly distributed particles that were either aligned or had random

orientations. The studied filler volume fractions were 2.0, 4.0, 7.5 and 10%. Note that successful mesh generation becomes challenging for high filler aspect ratios, and hence, the particle aspect ratio was limited to 56 in the current study. While this value is comparatively low for CNT it does represent actual (multiwall) CNT structures as indicated in [33]. Moreover, modeling filler volume fractions exceeding 10% was found to demand excessive computational effort, and hence, analyses were limited to 10% filler volume fractions and below. Note that effective enhancement of flame retardant properties was ascertained in CNT-polymer composites that were significantly below the set 10% limit, see e.g., [7].

A convergence study was performed for a composite with randomly distributed and aligned particles at a filler volume fraction of 4.0%. To assess the sensitivity of the computed effective thermal conductivity to mesh refinement, numerical analyses were performed at different levels of mesh refinement. The results are depicted in **Figure 9**. It was observed that changing mesh density from ~266,000 nodes to ~376,000 nodes created a change in the effective thermal conductivity result of only less than 3.5%. Consequently, in order to maintain computational efforts within reasonable bounds, mesh generation was controlled to remain below 400,000 nodes.

Figure 10 shows an example of a model with randomly distributed and randomly oriented particles. Ideally, particle spacial distributions for this case should result in isotropic thermal

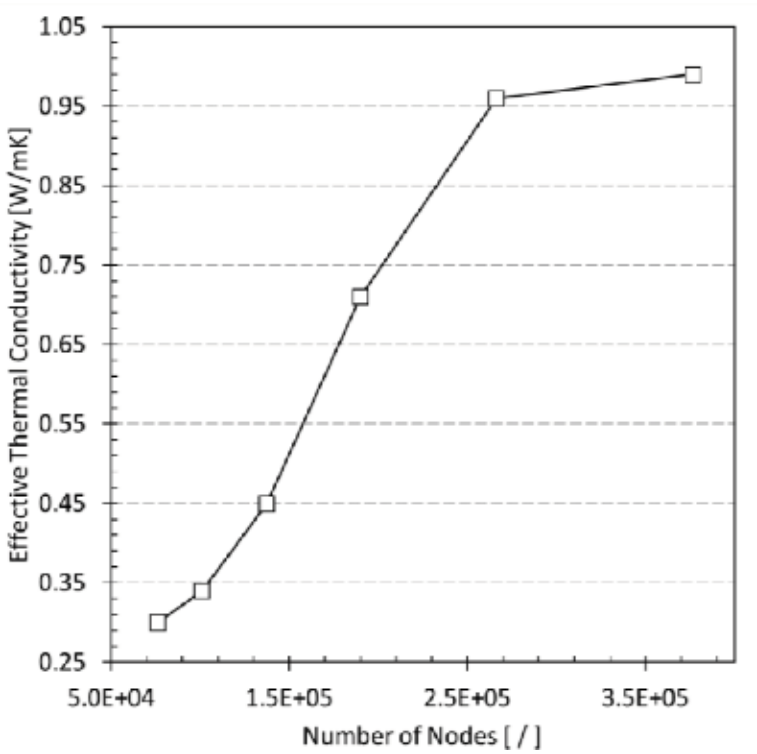

Figure 9. Convergence study for composites with 4% filler volume fraction.

http://dx.doi.org/10.5772/intechopen.82878

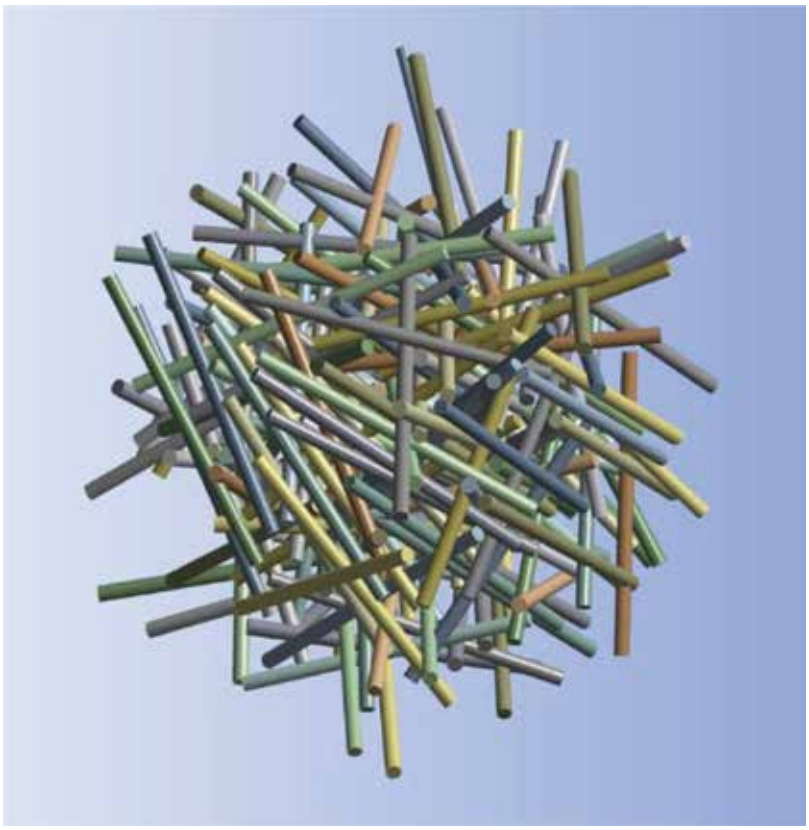

Figure 10. Example of randomly distributed and randomly oriented filler particles.

conductivity properties. To further investigate this hypothesis, a study was performed in which effective thermal conductivities were computed along the global RVE directions, i.e., *X*,*Y*,*Z* coordinates. This analysis was completed for the chosen set of filler volume fractions (2.0, 4.0, 7.5 and 10%). Corresponding effective thermal conductivity results for a single model are included in **Table 2**. The given data indicates that thermal conductivity values were

Filler volume fraction [%]	**2.0%**	**4.0%**	**7.5%**	**10%**
Thermal conductivity, X [W m^{-1} K^{-1}]	0.556	0.781	1.08	1.29
Thermal conductivity, Y [W m^{-1} K^{-1}]	0.525	0.676	1.14	1.26
Thermal conductivity, Z [W m^{-1} K^{-1}]	0.525	0.778	1.13	1.14
Average thermal conductivity [W m^{-1} K^{-1}]	0.536	0.745	1.12	1.23

Table 2. Average and directional thermal conductivities of composites with randomly distributed and randomly oriented filler particles.

essentially isotropic for models with lower filler loading (i.e., 2%) while for increasing filler volume fractions a mild level of anisotropy was sometimes observed. For that reason, the average effective thermal conductivity was computed from the three Cartesian coordinate directions and subsequently used for comparing composites with randomly oriented particles with aligned filler composites.

As explained previously, the MCS module of the modeling framework performs numerous iterations for each filler volume fraction and subsequently computes the effective thermal conductivity and stores these data in the database. The MCS module repeats this process until specified acceptance criteria are satisfied. For the presented study, the analysis process was terminated after 100 iterations for each of the set filler volume fractions. (Alternatively, a threshold for the unbiased standard deviation or variance could be defined as a termination criterion.) The effective thermal conductivity for a certain filler volume fraction was then computed from the mean of the results stored in the database. Statistical analyses were also performed on the data in order to assess the quality of the employed stochastic process. Data plots for specific volume fractions suggest that data is normally distributed, as shown in **Figure 11** by the normalized probability density of effective thermal conductivity data for the direction lateral to filler alignment in a composite with 4.0% filler volume fraction. Data were computed for normality tests for each volume fraction, including the data mean, median, skewness and

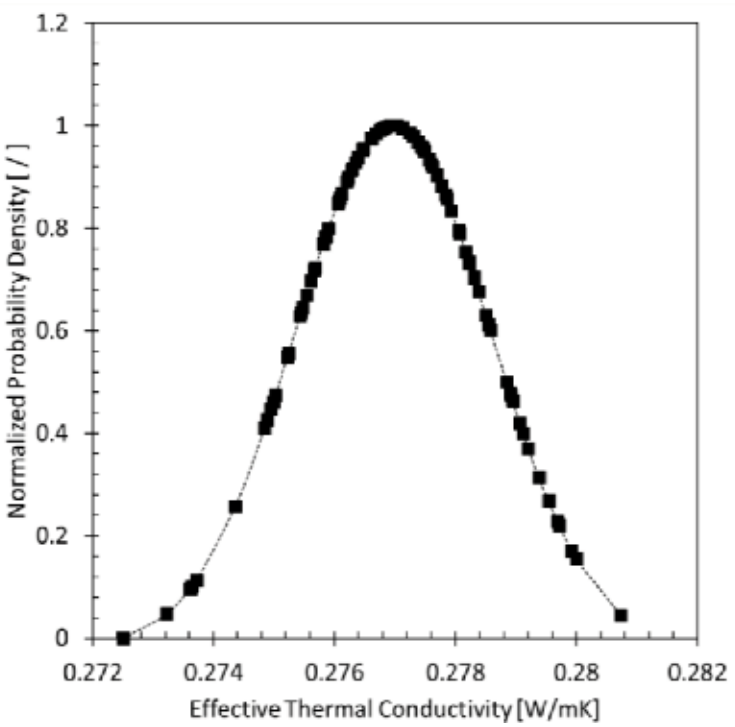

Figure 11. Normalized probability density of effective thermal conductivity data for the direction lateral to filler alignment and 4.0% filler volume fraction.

kurtosis. **Tables 3** and **4** list corresponding results for the longitudinal and lateral directions of composites with randomly distributed and aligned particles. These results indicate that the effective thermal conductivity data obey normal distributions, e.g., mean and median of effective thermal conductivity results were practically identical (differences are less than 0.04%). Similar to results presented in [27], appropriate randomness of computed data was thus ascertained. Graphs

Filler volume fraction [%]	**2.0**	**4.0**	**7.5**	**10.0**
Number of iterations [/]	100	100	100	100
Mean value [W m^{-1} K^{-1}]	0.775	1.027	1.318	1.489
Median value [W m^{-1} K^{-1}]	0.774	1.031	1.325	1.486
Standard deviation [W m^{-1} K^{-1}]	0.019	0.032	0.037	0.038
Variance [W m^{-1} K^{-1}]	3.7×10^{-4}	1.0×10^{-3}	1.3×10^{-3}	1.4×10^{-3}
Skewness [/]	1.197	−0.159	−0.672	0.083
Kurtosis [/]	−0.079	−0.539	0.607	0.128
95% confidence value [W m^{-1} K^{-1}]	0.0038	0.0064	0.0073	0.0076

Table 3. Results for longitudinal effective thermal conductivity and statistical analyses.

Filler volume fraction [%]	**2.0**	**4.0**	**7.5**	**10.0**
Number of iterations [/]	100	100	100	100
Mean value [W m^{-1} K^{-1}]	0.262	0.276	0.306	0.332
Median value [W m^{-1} K^{-1}]	0.262	0.276	0.306	0.331
Standard deviation [W m^{-1} K^{-1}]	0.001	0.001	0.003	0.004
Variance [W m^{-1} K^{-1}]	1.6×10^{-6}	2.6×10^{-6}	9.4×10^{-6}	2.3×10^{-5}
Skewness [/]	−0.819	−0.267	−0.180	0.216
Kurtosis [/]	2.410	0.031	−0.124	0.344
95% confidence value [W m^{-1} K^{-1}]	0.0002	0.0003	0.0006	0.0009

Table 4. Results for lateral effective thermal conductivity and statistical analyses.

showing normally distributed effective thermal conductivity data for the chosen filler volume fractions are plotted for the longitudinal and lateral case in **Figures 12** and **13**, respectively.

The effective thermal conductivity data calculated by SFEA framework can be considered continuous random variables, and hence, it is recommended to calculate the probability of occurrence of an explicit effective thermal conductivity within an identified interval. This calculation can be performed using Eq. (3).

$$P(a \le X \le b) = \int_a^b f(\chi) d\chi \tag{3}$$

where P is the probability of an event of explicit effective thermal conductivity within the interval a and b; X and $f(\chi)$ are correspondingly a continuous random variable and the probability distribution function. A cumulative distribution function (CDF) can be computed from Eq. (3) for each of the selected filler volume fractions. Corresponding CDF graphs are depicted in **Figures 14** and **15** for the longitudinal and lateral cases of aligned filler composites, respectively.

Finally, the modeling approach was used to achieve the objective of the study, that is, assessing the effect of filler addition and alignment on heat transfer into polymer composites in the context of fire-retardancy. **Figure 16** depicts average effective thermal conductivity results for different

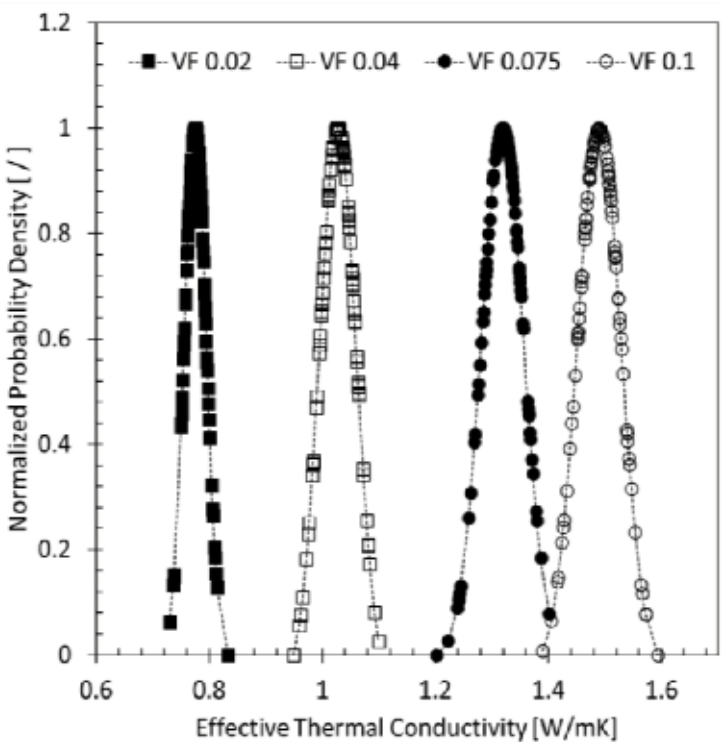

Figure 12. Normalized probability density of effective thermal conductivity data for the direction of filler alignment and different filler volume fractions (VF).

http://dx.doi.org/10.5772/intechopen.82878

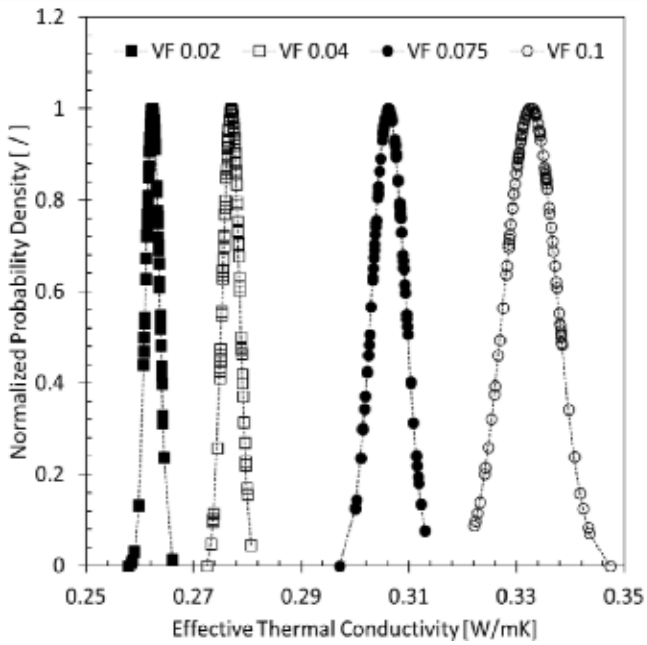

Figure 13. Normalized probability density of effective thermal conductivity data for the direction lateral to filler alignment and different filler volume fractions (VF).

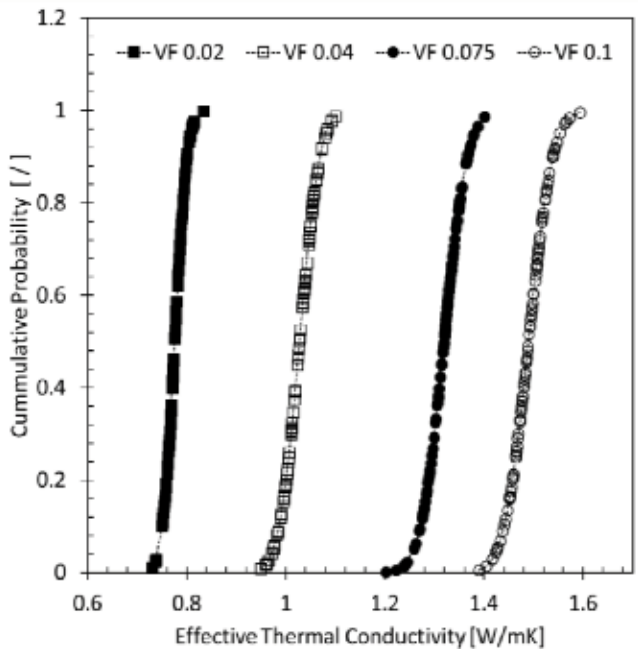

Figure 14. Cumulative density function of effective thermal conductivity data for the direction of filler alignment and different filler volume fractions (VF).

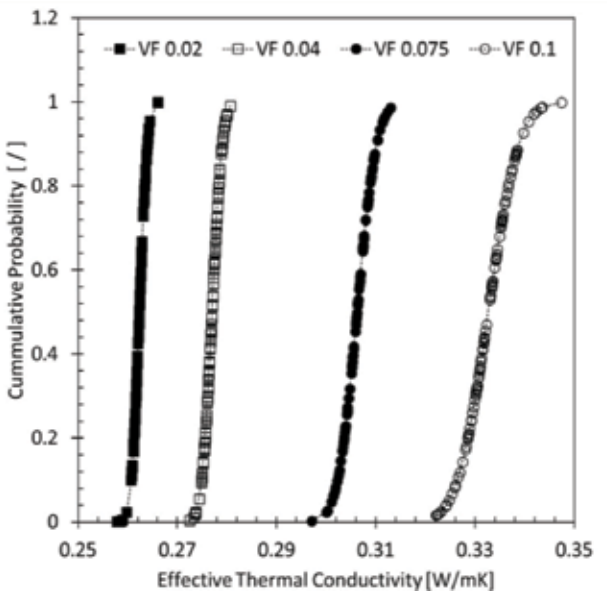

Figure 15. Cumulative density function of effective thermal conductivity data for the direction lateral to filler alignment and different filler volume fractions (VF).

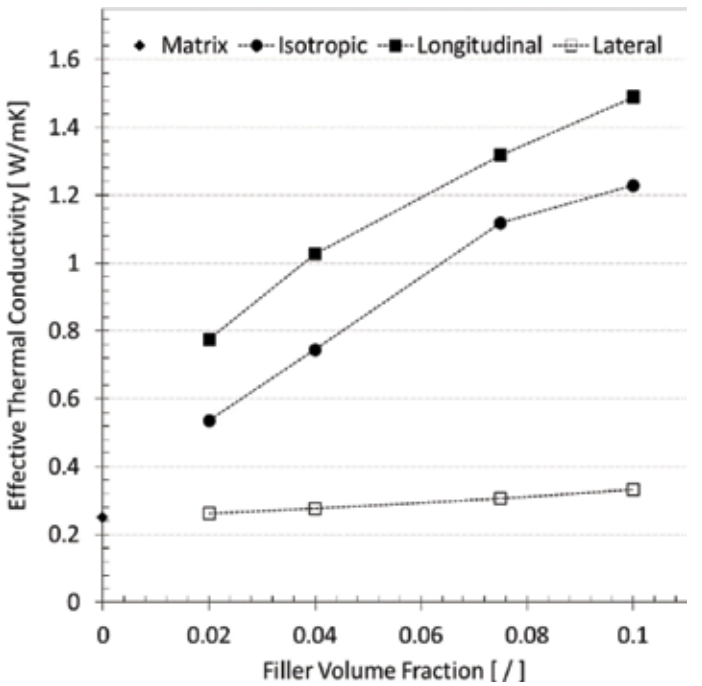

Figure 16. Effective thermal conductivity of randomly oriented and aligned rod-shaped particles embedded in epoxy polymer matrix.

http://dx.doi.org/10.5772/intechopen.82878

filler volume fractions for the cases of randomly oriented (isotropic) and aligned rod-shaped particles mimicking CNT. For the aligned filler morphologies, effective thermal conductivity results are shown for the direction of filler alignment (longitudinal) and the corresponding lateral direction. Despite the fact that the modeling approach employed generic material properties and simplifying assumptions for the CNT geometry, the data is in satisfactory agreement with data published in the technical literature (e.g., [32]). Experimentally characterized CNT-polymer composites involve a wide range of material properties and fabrication routes. Notwithstanding these differences, the modeled thermal conductivity in the order of 1.0 W m^{-1} K^{-1} for isotropic composites with filler loadings approaching 10% are shown to be realistic.

The relative increase in effective thermal conductivity for the different filler volume fractions is depicted in the graph in **Figure 17** for the cases of randomly oriented (isotropic) and aligned particles (longitudinal and lateral). These data clearly demonstrate that heat transfer into the polymer can greatly be reduced when filler particles are aligned parallel to the surface of a component. For example, while thermal conductivity in an isotropic and aligned filler composite was found to respectively increase almost sixfold and fivefold over the matrix for 10% filler loading, the lateral thermal conductivity in the aligned filler composite rose only by a factor of 1.3. In the context of fire-retardancy it can therefore be concluded that aligning CNT and other high aspect ratio carbon allotrope fillers parallel to the surface of a polymer component may provide an effective means for alleviating heat input into the material while enabling

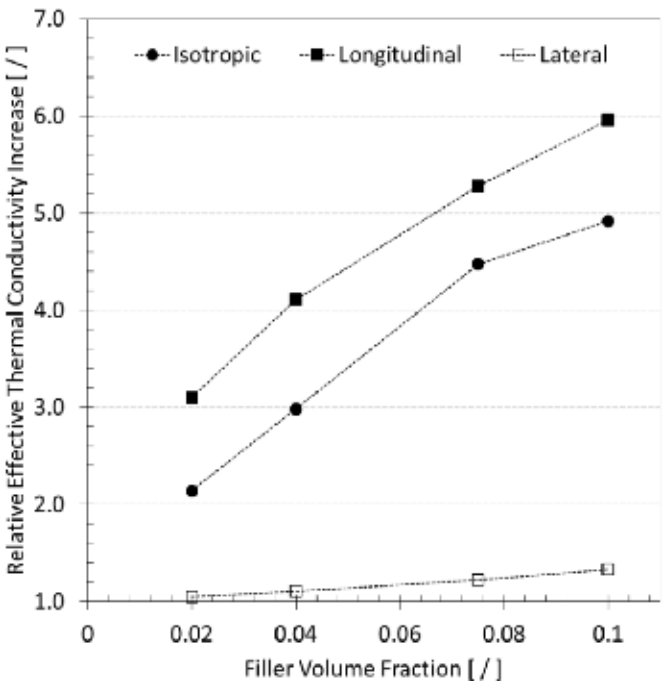

Figure 17. Relative increase in effective thermal conductivity of randomly oriented and aligned rod-shaped particles embedded in epoxy polymer matrix.

the desired mass transport barrier for mitigating fuel release into the gas phase, and reduced peak heat release and radiant heat flux.

5. Conclusions

A stochastic finite element analysis framework was employed to simulate the effective thermal conductivity of randomly distributed rod-shape particles mimicking carbon nanotubes embedded in a polymer matrix. Particles were either randomly oriented or aligned, creating isotropic or anisotropic thermal conductivity behavior, respectively. The modeling framework that is based on Monte Carlo simulation considers filler-matrix and particle-to-particle interfacial effects.

The numerical study indicated that the effective thermal conductivity is greatly enhanced for aligned filler composites in the alignment direction and isotropic filler modified composites. However, in the direction lateral to filler alignment the increase in thermal conductivity is only modest. Therefore, in order to limit heat input into the material, CNT and other high aspect ratio carbon allotrope fillers may be aligned parallel to the surface of a polymer component. In this manner, the flame-retardancy effectiveness of filler modified polymer composites can be improved, while providing a mass transport barrier that lessens the release of fuel into the gas phase, peak heat release and radiant heat flux, all of which were previously described in the technical literature.

Acknowledgements

The authors gratefully acknowledge Hi-Kalibre Equipment Ltd. for providing software and computing resources for this research. This work was further supported by the Natural Sciences and Engineering Research Council of Canada, Grant number: RGPIN-2016-04650.

Author details

Hamidreza Ahmadi Moghaddam and Pierre Mertiny*

*Address all correspondence to: pmertiny@ualberta.ca

Department of Mechanical Engineering, University of Alberta, Edmonton, Alberta, Canada

References

[1] Liu S, Chevalia VS, Xu Z, Hui D, Wang H. A review of extending performance of epoxy resins using carbon nanomaterials. Composites Part B: Engineering. 2018;**136**:197-214. DOI: 10.1016/j.compositesb.2017.08.020

[2] Mishra D, Mohapatra S, Satapathy A. A detailed investigation on thermal and microstructural properties of hexagonal boron nitride composites. Materials Today: Proceedings. 2018;**5**(9):19747-19753. DOI: 10.1016/j.matpr.2018.06.337

[3] Ansari R, Rouhi S, Ahmadi M. On the thermal conductivity of carbon nanotube/polypropylene nanocomposites by finite element method. Journal of Computational Applied Mechanics. 2018;**49**(1):70-85. DOI: 10.22059/jcamech.2017.243530.195

[4] Shi X, Hassanzadeh Aghdam MK, Ansari R. Effect of aluminum carbide interphase on the thermomechanical behavior of carbon nanotube/aluminum nanocomposites. Proceedings of the Institution of Mechanical Engineers, Part L: Journal of Materials: Design and Applications. 2018. DOI: 10.1177/1464420718794716

[5] Ahmadi M, Ansari R, Hassanzadeh Aghdam MK. Micromechanical analysis of elastic modulus of carbon nanotube-aluminum nanocomposites with random microstructures. Journal of Alloys and Compounds. 2019;**779**:433-439. DOI: 10.1016/j.jallcom.2018.11.326

[6] Ahmadi M, Ansari R, Rouhi S. Investigating the thermal conductivity of concrete/graphene nanocomposite by a multi-scale modeling approach. International Journal of Modern Physics B. 2018;**32**(14):15. Artical ID: 1850171. DOI: 10.1142/S0217979218501710

[7] Kashiwagi T, Grulke E, Hilding J, Groth K, Harris R, Butler K, et al. Thermal and flammability properties of polypropylene/carbon nanotube nanocomposites. Polymer. 2004;**45**: 4227-4239. DOI: 10.1016/j.polymer.2004.03.088

[8] Liu S, Yan H, Fang Z, Wang H. Effect of graphene nanosheets on morphology, thermal stability and flame retardancy of epoxy resin. Composites Science and Technology. 2014; **90**:40-47. DOI: 10.1016/j.compscitech.2013.10.012

[9] Pop E, Mann D, Wang Q, Goodson K, Dai H. Thermal conductance of an individual single-wall carbon nanotube above room temperature. Nano Letters. 2006;**6**(1):96-100. DOI: 10.1021/nl052145f

[10] Balandin AA, Ghosh S, Bao W, Calizo I, Teweldebrhan D, Miao F, et al. Superior thermal conductivity of single-layer graphene. Nano Letters. 2008;**8**:902-907. DOI: 10.1021/nl0731872

[11] Liu J, Liu J, Yang L, Chen X, Zhang M, Meng F, et al. Nanomaterial-assisted signal enhancement of hybridization for DNA biosensors: A review. Sensors. 2009;**9**(9):7343-7364. DOI: 10.3390/s90907343

[12] Balasubramanian K, Burghard M. Biosensors based on carbon nanotubes. Analytical and Bioanalytical Chemistry. 2006;**385**(3):452-468. DOI: 10.1007/s00216-006-0314-8

[13] Yan T, Wang Z, Wang YQ, Pan ZJ. Carbon/graphene composite nanofiber yarns for highly sensitive strain sensors. Materials & Design. 2018;**143**:214-223. DOI: 10.1016/j.matdes.2018.02.006

[14] Coleman JN, Khan U, Gun'ko YK. Mechanical reinforcement of polymers using carbon nanotubes. Advanced Materials. 2006;**18**(6):689-706. DOI: 10.1002/adma.200501851

[15] Moniruzzaman M, Winey KI. Polymer nanocomposites containing carbon nanotubes. Macromolecules. 2006;**39**(16):5194-5205. DOI: 10.1021/ma060733p

[16] Green MJ, Behabtu N, Pasquali M, Adams WW. Nano tubes as polymer. Polymer. 2009; **50**(21): 50:4979-4997. DOI: 10.1016/j.polymer.2009.07.044

[17] Harris PJF. Carbon nanotubes and related structures: New materials for the twenty-first century. American Journal of Physics. 2004;**72**(3):415. DOI: 10.1119/1.1645289

[18] Dai L. Carbon Nanotechnology: Recent Developments in Chemistry, Physics, Materials Science and Device Applications. 1st ed. Amsterdam: Elsevier; 2006. ISBN-13: 978-0-444-51855-2

[19] Wu Q, Zhu W, Zhang C, Liang Z, Wang B. Study of fire retardant behavior of carbon nanotube membranes and carbon nanofiber paper in carbon fiber reinforced epoxy composites. Carbon. 2010;**48**(6):1799-1806. DOI: 10.1016/j.carbon.2010.01.023

[20] Knight C, Filbert IP, Zeng C, Zhange C, Wang B. A highly efficient fire-retardant nanomaterial based on carbon nanotubes and magnesium hydroxide. Fire and Materials. 2013; **37**(2):91-99. DOI: 10.1002/fam.2115

[21] Xiong L, Liu K, Shuai J, Hou Z, Zhu L, Li W. Toward high strength and high electrical conductivity in super-aligned carbon nanotubes reinforced copper. Advance Engineering Materials. 2018;**20**(5):1700805. DOI: 10.1002/adem.201700805

[22] Xiong L, Shuai J, Liu K, Hou Z, Zhu L, Li W. Enhanced mechanical and electrical properties of super-aligned carbon nanotubes reinforced copper by severe plastic deformation. Composites Part B: Engineering. 2018;**160**:315-320. DOI: 10.1016/j.compositesb.2018.10.023

[23] Meincke O, Kaempfer D, Weickmann H, Friedrich C, Vathauer M, Warth H. Mechanical properties and electrical conductivity of carbon-nanotube filled polyamide-6 and its blends with acrylonitrile/butadiene/styrene. Polymer. 2004;**45**(3):739-748. DOI: 10.1016/j.polymer.2003.12.013

[24] Valavala PK, Odegard GM. Modeling techniques for determination of mechanical properties of polymer nanocomposites. Advances in Materials Science. 2005;**9**:34-44

[25] Odegard G, Clancy T, Gates T. Modeling of the mechanical properties of nanoparticle/polymer composites. Polymer. 2005;**46**(2):553-562. DOI: 10.1016/j.polymer.2004.11.022

[26] Liu YJ, Chen XL. Evaluations of the effective material properties of carbon nanotube-based composites using a nanoscale representative volume element. Mechanics of Materials. 2003;**35**(1–2):69-81. DOI: 10.1016/S0167-6636(02)00200-4

[27] Ahmadi Moghaddam H, Mertiny P. Stochastic finite element analysis framework for modelling thermal conductivity of particulate modified polymer composites. 2018;**11**:905-914. DOI: 10.1016/j.rinp.2018.10.045

[28] Sinha S, Barjami S, Iannacchione G, Schwab A, Muench G. Off-axis thermal properties of carbon nanotube films. Journal of Nanoparticle Research. 2005;**7**(6):651-657. DOI: 10.1007/s11051-005-8382-9

[29] Sugime H, Esconjauregui S, Yang J, D'Arsié L, Oliver RA, Bhardwaj S, et al. Low temperature growth of ultra-high mass density carbon nanotube forests on conductive supports. Applied Physics Letters. 2013;**103**(7):109901. DOI: 10.1063/1.4818619

[30] Huxtable ST, Cahill DG, Shenogin S, Xue L, Ozisik R, Barone P, et al. Interfacial heat flow in carbon nanotube suspensions. Nature Material. 2003;**2**(11):731-734. DOI: 10.1038/nmat996

[31] Shenogin S, Xue L, Ozisik R, Keblinski P, Cahill DG. Role of thermal boundary resistance on the heat flow in carbon-nanotube composites. Journal of Applied Physics. 2004;**95**: 8136-8144. DOI: 10.1063/1.1736328

[32] Han Z, Fina A. Thermal conductivity of carbon nanotubes and their polymer nanocomposites: A review. Progress in Polymer Science. 2011;**36**(7):914-944. DOI: 10.1016/j.progpolymsci.2010.11.004

[33] Xu DH, Wang ZG, Douglas JF. Influence of carbon nanotube aspect ratio on normal stress differences in isotactic polypropylene nanocomposite melts. Macromolecules. 2008;**41**(3): 815-825. DOI: 10.1021/ma702178e

Edited by Fahmina Zafar and Eram Sharmin

Flame retardants reduce the risk of fire by decreasing the combustion rate and flame propagation in the presence of fire, leading to the prevention and control of fire. *Flame Retardants* is divided into four sections: section 1 consists of the introduction, section 2 discusses properties, Section 3 comprises nanocomposites, and section 4 includes computational analysis. The book will be useful for scientists and researchers interested in the field of fire control.

Published in London, UK

IntechOpen

ISBN 978-1-83881-139-6